Master's thesis

NTNU
Norwegian University of Science and Technology
Faculty of Engineering
Department of Energy and Process Engineering

Johan Christian Rømcke

Performance Analysis of Prototype Residential CO2 Heat Pump

Master's thesis in Energy and Environmental Engineering

Supervisor: Armin Hafner

June 2020

NTNU
Norwegian University of
Science and Technology

Johan Christian Rømcke

Performance Analysis of Prototype Residential CO2 Heat Pump

Master's thesis in Energy and Environmental Engineering
Supervisor: Armin Hafner
June 2020

Norwegian University of Science and Technology
Faculty of Engineering
Department of Energy and Process Engineering

NTNU
Norwegian University of
Science and Technology

Preface

This master thesis represents the final work of my master's degree at the Norwegian University of Science and Technology, Department of Energy and Process Engineering. The master project has been conducted during the 10th semester, in the spring of 2020, constituting 30 ECTS credits.

This semester has been different and memorable in many ways. With the outbreak of the Corona virus in mid Mars, and the lockdown of society, a strange and challenging time for all of us emerged. As for this thesis, the situation led to some smaller delays in the practical part of the project. All things considered, I've been fortunate and have been able to carry out the work largely as planned.

There are several people who have contributed to this master project, that I would like to thank. First and foremost, a special thanks to my supervisor Prof. Armin Hafner for all guidance and valuable discussions. I would also like to thank Marcel Ulrich Ahrens for ideas and tips in the model building process. Lastly, a big thanks to Kenneth Sjølstad and Per Alsvik at Winns AS for assisting in the practical part of this project.

Abstract

Heat pumps are today rarely used for heating of domestic hot water (DHW) in Norwegian households. This is largely due to the limitations of conventional residential heat pumps, which cannot provide high enough temperatures in an effective and practical way. Heat pumps using the natural working fluid CO_2 can deliver hot water temperatures of 60-70 ^oC without compromising the coefficient of performance (COP). Commercialization of CO_2 heat pumps with the purpose DHW heating can potentially be a large energy saver for the Norwegian building sector. At NTNU-SINTEF a combined mode CO_2 heat pump, for both space- and DHW heating, was developed from 2000-2004. The heat pump has since undergone several altercations and has been the research topic of this master thesis. The purpose has been to analyse the system solutions, realistic energy/power capacity, dependability and instrumentation which enables optimized operation.

The master project has been conducted in bipartite fashion; A practical part with experimental testing and operation, and a theoretical part with computer model development. During the first phase of the experimental testing, the CO_2 heat pump was set up in a test rig at Winns AS. This phase consisted of troubleshooting, instrumentation and optimization. The heat pump was then moved to a residential location for operational testing. A dynamic computer model of the heat pump system was developed in the modelling software Dymola, supported by reference models developed in CoolPack and Simple One-Stage CO_2 Cycle. The goal was to have a valid model to use as a tool for system analysis.

As a mean to validate the model, a sensitivity analysis comparison of the real system and the model was conducted. The comparison showed a high degree of correlation between the model and the real system, which strongly supported the validity of the model and accordingly the simulation results from model analysis which followed.

The results from the simulations and the operational data from the residential location showed that the maximum capacity of the heat pump realistically is between 4,5 – 5 kW. The highest COP were achieved under combined mode heating, at 3,62. During DHW mode the maximum COP was 3,49. The lowest maximum COP was found under space heating mode, at 3,25. These findings emphasises the importance of sufficient CO_2 cooldown in order to achieve the highest possible COP. It was also found that optimum high-side pressure range for maximum space heating water (SHW) production was 80-85 bar. For maximum DHW production the optimum high-side pressure was higher, at 95-100 bar. To maximize the production of both DHW and SHW during combined mode heating, the pressure range 90-92 bar was found to be the optimum high-side pressure.

Sammendrag

Varmepumper er i dag i svært liten grad benyttet til oppvarming av tappevann i norske boliger. Dette handler i stor grad om at det ikke har hensiktsmessig latt seg gjøre med de konvensjonelle varmepumpene som bruker syntetiske arbeidsmedier. Varmepumper med det naturlige arbeidsmediet CO_2 kan levere varmtvannstemperaturer på 60-70 grader uten at det går på bekostning av ytelseskoeffisienten (COP). Kommersialisering av CO_2 varmepumper til dette formål potensielt kunne være svært energibesparende for det norske bygningssektoren. En CO_2 varmepumpe med kombinert tappevann- og romoppvarmings funksjon ble fra 2000 til 2004 utviklet ved NTNU-SINTEF. Varmepumpen har siden gjennomgått flere endringer, og har vært forskningsemnet for denne masteroppgaven. Hensikten har vært å analysere systemløsningene, realistisk energi/effektkapasitet, pålitelighet og instrumentering som muliggjør optimalisert drift.

Utførelsen av masterprosjektet har vært todelt; En praktisk del med eksperimentell testing og drift, og en teoretisk del med datamodellutvikling. I den første fasen av den eksperimentelle testingen ble CO_2 varmepumpen satt opp i en testrigg hos Winns AS. Denne fasen besto av feilsøking, instrumentering og optimalisering. Varmepumpen ble deretter flyttet til en bolig for operasjonell testing. En dynamisk datamodell av varmepumpesystemet ble utviklet i modelleringsprogramvaren Dymola, støttet av referansemodeller utviklet i CoolPack og Simple One-Stage CO2 Cycle. Målet var å ha en gyldig modell som kunne brukes som et verktøy for systemanalyse.

Som en metode for å validere modellen ble det utført en sammenligning av sensitivitetsanalyser for det virkelige systemet og modellen. Sammenligningen viste en høy grad av korrelasjon mellom modellen og det virkelige systemet, noe som sterkt støttet gyldigheten av modellen, og følgelig simuleringsresultatene fra den etterfølgende modellanalysen.

Resultatene fra simuleringene og driftsdataene fra boligen viste at den maksimale kapasiteten til varmepumpen realistisk er mellom 4,5 - 5 kW. Den høyeste COP ble oppnådd under kombinert modus, på 3,62. I tappevannsmodus var maksimal COP 3,49. Den laveste maksimale COP ble funnet i romoppvarmingsmodus, 3,25. Disse funnene understreker viktigheten av tilstrekkelig CO_2-nedkjøling for å oppnå høyest mulig COP. Det ble også funnet at det optimale høysidetrykkområdet for maksimal produksjon av vann til romvarme var 80-85 bar. For maksimal varmtvannsproduksjon var det optimale høysidetrykket høyere, 95-100 bar. For å maksimere produksjonen av både varmtvann og SHW under oppvarming av kombinert modus, ble trykkområdet 90-92 bar funnet å være det optimale høysidetrykket.

List of Content

Preface I
Abstract II
Sammendrag III
List of Figures VIII
List of Tables IX
List of Abbreviations X
1 Introduction 1
1.1 Background and Motivation 1
1.2 Problem Description 1
2 Theoretical Background 2
2.1 Heat Pump Fundamentals 2
2.1.1 The Reversed Carnot Cycle 3
2.1.2 The Ideal Vapour Compression Cycle 4
2.1.3 Realistic Vapour Compression Cycle 5
2.1.4 Compressor efficiency 6
2.2 Working Fluids 6
2.2.1 R134a (CH_2F-CF_3) 7
2.2.2 R410A (HFC Mixture) 7
2.2.3 R717(NH_3) 8
2.2.4 R744 (CO_2) 8
2.2.5 Comparison 9
2.3 CO_2 Refrigerant Cycle 10
2.3.1 Modified Lorentz Cycle 10
2.3.2 The Ideal Lorentzen Cycle 11
2.3.3 The Realistic Lorentzen Cycle 12
2.3.4 Temperature Characteristics 13
2.3.5 Pressure Characteristics 14
2.3.6 Optimum Heat Rejection Pressure 15
2.3.7 Internal Heat Exchanger 16
2.4 Residential CO_2 Heat Pump Configurations 17
2.4.1 Single Gas Cooler DHW System 17
2.4.2 Tripartite Gas Cooler Combined Heating System 18
2.5 Hydronic Heating Systems 18
2.5.1 System Designing 19
2.5.2 Heat Power Regulation 20

2.5.3 System Start-up Regulation 21
2.6 Geothermal Heat Source 22
2.6.1 Direct Systems 22
2.6.2 Indirect Systems 23
2.6.3 Thermal Response Test 23
2.6.4 Ground Conditions in Trondheim 24
3 System Description 25
3.1 CO_2 Heat Pump Structure 25
3.1.1 Compressor 26
3.1.2 Evaporator 26
3.1.3 Gas Coolers 26
3.1.3.1 DHW Preheating Gas Cooler 26
3.1.3.2 Space Heating Gas Cooler 26
3.1.3.3 DHW Reheating Gas Cooler 26
3.1.4 Suction Gas Heat Exchanger 26
3.1.5 Low Pressure Receiver 27
3.1.6 Sub Cooler 27
3.1.7 Expansion Valves 27
3.2 WINNS Test Rig 27
3.3 Hydronic System at Residential Location 28
3.3.1 Floor Heating System 28
3.3.2 DHW System 29
4 Methodology 30
4.1 Working Tools 30
4.1.1 Draw.io 30
4.1.2 CoolPack 30
4.1.3 Simple One Stage CO_2 Cycle (SOSCC) 30
4.1.4 Modelica Language 30
4.1.5 Dymola 31
4.1.6 IDA ICE 31
4.2 Model Development 31
4.2.1 Reference models 31
4.2.2 Dynamic Dymola Modelling 33
4.2.2.1 Evaporator 33
4.2.2.2 LPR and Compressor 34
4.2.2.3 Tripartite Gas Cooler Configuration 35
4.2.2.4 Closed DHW Circuit, Expansion Valve and Heat Ports 36

4.2.2.5 SGHX and Sub Cooler 36
4.2.2.6 System Completion with Control System 37
4.2.3 Residential Model 39
4.3 Experimental Phase 40
4.3.1 Initial Testing 41
4.3.2 Troubleshooting 41
4.3.3 Instrumentation and Equipment 43
4.3.3.1 RHEONIK Coriolis Flowmeter 43
4.3.3.2 Kamstrup MULTICAL 603 44
4.3.3.3 Kamstrup MULTICAL 403 44
4.3.4 Final Testing 45
4.3.5 Setup at Residential Location 45
4.3.5.1 Data Logging 46
4.3.5.2 Control Strategy 47
5 Results 49
5.1 Model Validation and Simulation Analysis 49
5.1.1 Comparison of Sensitivity Analysis 50
5.1.2 System Characterists and Performance 53
5.1.2.1 Optimum High-side Pressure Analysis 53
5.1.2.2 Hot Water Production 56
5.1.3 Simulations with IDA ICE Load Profiles 57
5.1.3.1 Combined Mode 58
5.1.3.2 DHW Heating Mode 59
5.1.3.3 Space Heating Mode 61
5.2 Operational Results 63
5.2.1 Refrigerant Side 63
5.2.2 Accumulator Tanks 66
5.2.2.1 Tank 1 66
5.2.2.2 Tank 2 67
5.2.2.3 Tank 3 67
5.2.2.4 Tank 4 68
6 Discussion 69
6.1 Validity of the Dymola Model 69
6.2 System Performance Analysis in Dymola 70
6.2.1 Optimum Pressure 70
6.2.2 Operating Modes 71
6.3 Experimental Testing and Operation 72

7 Conclusion 74
8 Further Work 76
References 77
Appendices 79

List of Figures

Figure 2.1: Simple heat pump principle sketch 3
Figure 2.2: T-s diagram of the reversed Carnot cycle 4
Figure 2.3: Simple Log P-h diagram illustrating the ideal vapour compression cycle 5
Figure 2.4: Log P-h diagram illustrating the real vapour compression cycle with its sub-processes 6
Figure 2.5: Graphic illustration of compressor volume, with the R717 compressor size as a reference (100%) [12] 10
Figure 2.6: T-s diagram illustrating the modified Lorentz cycle 11
Figure 2.7: T-s diagram illustrating the ideal Lorentzen cycle 12
Figure 2.8: T-s diagram illustrating the real Lorentzen cycle 12
Figure 2.9: Graph illustrating temperature behavior during a gas cooler heat exchange 13
Figure 2.10: T-h diagram with isobars for different pressure levels [15] 14
Figure 2.11: Graph illustrating the relationship between COP and pressure for different t_c [16] 15
Figure 2.12: Graph illustrating the relationship between COP and t_{sh} at different pressure levels [16] 16
Figure 2.13: Principle sketch of single gas cooler DHW system 17
Figure 2.14: Principle sketch of a combined mode system 18
Figure 2.15: Simple illustration of a one-pipe system (left) and two-pipe system (right) 19
Figure 2.16: Simplified characteristics chart 21
Figure 2.17: Flowchart illustrating the different GSHP configurations 22
Figure 2.18: Principle sketch of indirect system (left) and direct system (right) 23
Figure 3.1: Principle sketch of the CO2 heat pump 25
Figure 3.2: The Semi-hermetic double stage compressor [27] 27
Figure 3.3: Principle sketch of the test rig 28
Figure 3.4: Principle sketch of the hydronic floor heating system 29
Figure 3.5: Principle sketch of the DHW system 29
Figure 4.1: 90 bar reference model developed in CoolPack 32
Figure 4.2: Model of the evaporator in Dymola 33
Figure 4.3: Dymola model with evaporator, LPR and compressor 34
Figure 4.4: Dymola model with the tripartite gas cooler configuration 35
Figure 4.5: Dymola model with expansion valve and heat ports 36
Figure 4.6: The complete Dymola model with component labelling 37
Figure 4.7: 3D visualization of the residential model developed in IDA ICE 39
Figure 4.8: Load/User profile import in Dymola 40
Figure 4.9: The heat pump in the test rig during initial testing 41
Figure 4.10: Picture of the PLC monitor screen, with temperature sensors from RT001-RT016, during a test session. 42
Figure 4.11: The Rhoenik RHE08 remote unit during calibration 43
Figure 4.12: Display of the Kamstrup MULTICAL 603 44
Figure 4.13: The two MULTICAL 403 energy meters during mounting 44
Figure 4.14: The PLC screen during the final test session 45
Figure 4.15: The heat pump implemented at the residential location 46
Figure 4.16: P&ID of the residential heat pump system 48
Figure 5.1: Comparison of the compressor speed (Frequency) 50
Figure 5.2: Evaporator pressure level comparison 50
Figure 5.3: Level of suction gas superheat 51

Figure 5.4: Comparison of CO_2 refrigerant mass flow rate 51
Figure 5.5: High side pressure level compared 52
Figure 5.6: Compressor discharge CO_2 temperature 52
Figure 5.7: Gas cooler outlet temperature of CO_2 refrigerant 53
Figure 5.8: Gas cooler heat rejection [W] during variable high-side pressure 54
Figure 5.9: Graph showing the COP behavior during pressure increase 55
Figure 5.10: SGHX and Sub Cooler heat exchange [W] during pressure increase 55
Figure 5.11: Amount of DHW produced in a 24-hour period at different pressure setpoints 57
Figure 5.12: Amount of SHW produced during a 24-hour period at different pressure setpoints 57
Figure 5.13: The space heating demand vs gas cooler heat rejection 58
Figure 5.14: DHW demand vs gas cooler heat rejection 58
Figure 5.15: Achieved temperature vs setpoints of DHW and SHW 59
Figure 5.16: Total heat rejection of gas coolers vs DHW demand 60
Figure 5.17: Temperature profile of the DHW tank 60
Figure 5.18: COP seen in relationship with compressor frequency 61
Figure 5.19: IDA ICE load profile compared to the space heating GC 61
Figure 5.20: Temperature of the SHW tank 62
Figure 5.21: Compressor frequency vs COP 62
Figure 5.22: Outdoor temperature profile 63
Figure 5.23: Compressor frequency during the week of operation 64
Figure 5.24: Logged values for energy meters U3 and U4 64
Figure 5.25: CO_2 temperature through the gas coolers 65
Figure 5.26: Degree of superheat in the suction gas line 65
Figure 5.27: High- and low-side pressure 66
Figure 5.28: Overview of the accumulator tanks with sensors 66
Figure 5.29: Temperature profile for Tank 1 67
Figure 5.30: Temperature profile for Tank 2 67
Figure 5.31: Temperature profile for Tank 3 68
Figure 5.32: Temperature profile for Tank 4 68

List of Tables

Table 2-1: Overview of important parameters for the four working fluids 9
Table 2-2: Thermal properties of bedrock types 24
*Table 4-1: Evaporator specifications (*LinearEnthalpyDistribution) (**LinearTemperatureDistribution)* 34
Table 4-2: Overview of the gas cooler parameters 36
Table 4-3: SGHX and sub cooler specifications 37
Table 4-4: PI-Controller specifications 39
Table 5-1: Parameter comparison at three main pressure levels 56

List of Abbreviations

COP	Coefficient of Performance
CFC/HCFC	Chlorofluorocarbons/Hydrochlorofluorocarbons
HFC	Hydrofluorocarbons
HP	Heat Pump
CO_2	Carbon Dioxide
ODP/GWP	Ozone Depleting Potential/Global Warming Potential
Log P-h	Logarithmic Pressure-Enthalpy
SHW/SH	Space Heating Water/Space Heating
DHW	Domestic Hot Water
SGHX	Suction Gas Heat Exchanger
SOSCC	Simple One-Stage CO_2 Cycle
PI-Control	Proportional-Integral-Control
GC	Gas Cooler

1 Introduction

1.1 Background and Motivation

The Norwegian Government has set the goal to reduce greenhouse gas emissions in Norway with at least 40 % by 2030 [1]. The building sector accounts for nearly 40 % of the total energy consumption in Norway, while about 60% of the energy use in Norwegian households is used for heating [2]. In order to reach the emission and energy goals of the future, new technology needs to be developed and implemented. The heat pump is optimal for that purpose, as it typically provides 3-4 times more thermal energy than electrical energy consumed. In the buildings of the future, zero energy buildings and power houses, a highly efficient heat pump is crucial. In the refrigeration industry, there is a vast untapped potential for natural working fluids like carbon dioxide and ammonia. Heat pumps using CO_2 as working fluid can provide temperatures high enough for heating of domestic hot water, while still having a high performance efficiency. CO_2 heat pumps can very well be the heating technology of the future and contribute to reducing the energy consumption of the building sector.

1.2 Problem Description

The research topic of this master project is a prototype residential CO_2 heat pump developed and built at NTNU-SINTEF from 2000-2004. The heat pump has since undergone several altercations, such as new compressor and expansion valve. The goal of this master project is to investigate the current state of the heat pump, and evaluate the system solutions, realistic energy/power capacity, dependability and instrumentation which enables optimized operation.

The following sub-objectives for this thesis has been established:

- Review of relevant literature and theory regarding heat pumps, CO_2 working fluids and residential heating systems.
- Develop a robust, dynamic Dymola model of the CO_2 heat pump.
- Perform operational testing and optimization of the CO_2 heat pump.
- Analyse and evaluate the results from the simulations and the testing.
- Draft version of scientific paper (Attached in Appendix F)

2 Theoretical Background

This chapter aims to give the reader a basic understanding of the heat pump technology, what seperates CO_2 from other working fluids, and the basic theory of hydronic heating systems and ground source heat.

2.1 Heat Pump Fundamentals

The heat pump is a technology that uses thermodynamic principles to move thermal energy from one source to another. Historically it has been used for cooling purposes, and for that reason it's commonly known as a "refrigerating machine". The first functional refrigerating machine was built by Jacob Perkins in 1876, using ether as working fluid [3]. The theory in this thesis will focus on the heating application of refrigeration systems.

The main advantages with a heat pump are that it can move a greater amount of thermal energy between the sources, than electrical energy applied. There are four key components to a heat pump: Evaporator, compressor, condenser and expansion valve. These components are connected by a closed loop, in which a refrigerant (working fluid) is circulating in different phase states. This process, the vapour compression cycle, is often referred to as a reversed Carnot-cycle. The refrigerants usually have certain desirable thermodynamics properties such as high specific heat capacity and low boiling point. This makes it possible for the heat pump to harvest thermal energy from low temperature sources, such as the sea, bedrock or outdoor air. Waste heat from industrial processes or wastewater is also a good heat source for a heat pump. The basics of the process can be explained in four steps, using the main components:

1. Evaporator: This is where the energy from the heat source is collected. The refrigerant is at low temperature and pressure will start to evaporate. The latent energy required for the phase change is extracted through a heat exchange with the heat source.
2. Compressor: Fully evaporated, the refrigerant is compressed, causing high temperature and pressure. The compressor requires electrical input.
3. Condenser: The super-heated refrigerant reaches its saturation temperature and starts to condensate. During this process the heat is rejected to the heat sink.
4. Expansion valve: Fully condensed the refrigerant is expanded, and pressure is relieved. The cycle then starts over.

Figure 2.1 is a principle sketch showing the four key components of a heat pump.

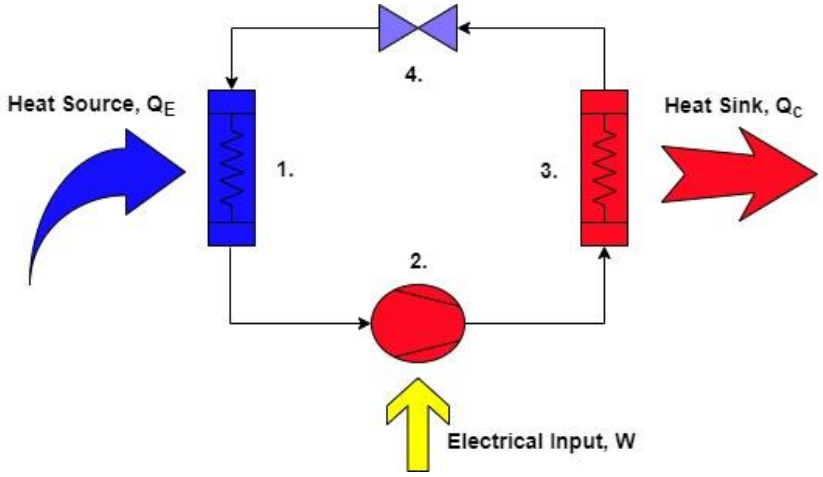

Figure 2.1: *Simple heat pump principle sketch*

2.1.1 The Reversed Carnot Cycle

The underlying thermodynamic process for heat pumps and refrigeration systems is a vapour compression cycle [4]. The most generalised cycle for a heat pump is the Carnot cycle, named after the French physicist Nicolas Sadi Carnot in 1824 [5]. The Carnot cycle is an ideal energy conversion cycle in which the input is heat and the output is work [5]. For a heat pump, the Carnot cycle is reversed and represents a theoretical ideal vapour compression cycle, shown in *Figure 2.2*. This cycle can be divided into the following sub-processes:

- **1-2** Isentropic compression from low temperature $\boldsymbol{T_C}$ to high temperature $\boldsymbol{T_H}$. Constant entropy ***S (dS=0)***
- **2-3** Isothermal heat rejection $\boldsymbol{Q_C}$ at constant temperature $\boldsymbol{T_H}$
- **3-4** Isentropic expansion from $\boldsymbol{T_H}$ to $\boldsymbol{T_C}$
- **4-1** Isothermal heat extraction $\boldsymbol{Q_E}$ at constant temperature $\boldsymbol{T}$

The total rejected heat $\boldsymbol{Q_C}$ at the condenser, by the First Law of Thermodynamics, is given by equation 2.1:

$$\dot{Q}_C = \dot{Q}_E + \dot{W} \qquad 2.1$$

The performance of this process is often referred to as the Carnot efficiency factor. The Carnot efficiency factor is in theory the ideal coefficient of performance (COP), which is a common way to evaluate the performance of a heat pump. The COP is the relationship between delivered heat at the condenser and the required electrical input at the compressor. The coefficient of performance is given by equation 2.2:

$$COP_{HP} = \frac{\dot{Q}_C}{\dot{W}} = \frac{T_H * \Delta S}{(T_H - T_C) * \Delta S} = \frac{T_H}{(T_H - T_C)} \quad 2.2$$

Figure 2.2 is a simple temperature-entropy (T-s) graph showing the sub-processes of the reversed Carnot cycle.

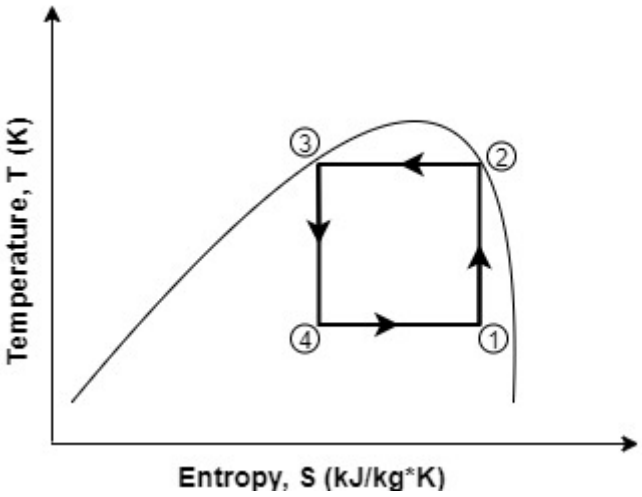

Figure 2.2: *T-s diagram of the reversed Carnot cycle*

2.1.2 The Ideal Vapour Compression Cycle

As a more practical approach, the ideal vapor compression refrigeration cycle is used as a reference cycle for refrigeration systems. It differs from the Carnot cycle by having expansion without constant entropy, and superheated gas after compression. The subprocesses, illustrated in *Figure 2.3*, of the vapour compression cycle becomes:

- **1-2'** Isentropic compression. The lossless compressor work is given by:

$$\dot{W}_{is} = \dot{m}_R(h_{2'} - h_1) \quad 2.3$$

- **1-2** Real compression. Compressor work is governed by isentropic efficiency:

$$\dot{W} = \dot{W}_{is}/\eta_{is} \quad 2.4$$

- **2-3** Isobaric heat rejection at the condenser, given by:

$$\dot{Q}_C = \dot{Q}_E + \dot{W} = \dot{m}_R(h_2 - h_3) \quad 2.5$$

- **3-4** Isenthalpic expansion, constant enthalpy during expansion, $h_3 = h_4$.
- **4-1** Isobaric heat extraction at the evaporator, given by:

$$\dot{Q}_E = \dot{m}_R(h_1 - h_4) \quad 2.6$$

The logarithmic pressure enthalpy diagram (log P-h) is a useful tool for calculations and visualizing the vapour compression cycle. The diagram is unique for each refrigerant type and shows the saturation curve for the given working fluid. The temperature at the peak of the saturation curve is the critical temperature of the refrigerant. The pressure scale describes the absolute pressure logarithmically and the enthalpy scale shows the heat energy. *Figure 2.3* is a general P-h diagram, showing the vapour compression cycle of a heat pump, and its subprocesses.

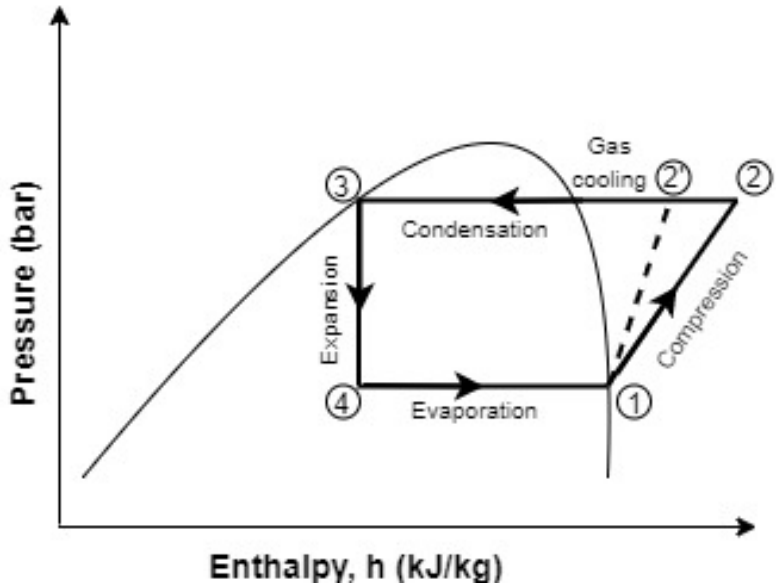

Figure 2.3: *Simple Log P-h diagram illustrating the ideal vapour compression cycle*

2.1.3 Realistic Vapour Compression Cycle

Even though the ideal vapour compression cycle is a good reference cycle for a heat pump, there are several other factors that will impact the cycle performance during realistic operating conditions [4]. *Figure 2.4* shows a principle Log P-h diagram of the realistic vapour compression system. From the diagram the deviations can be easily explained. From point 1-1’ there is superheating of the refrigerant, to make sure there is no liquid entering the compressor. Due to pressure loss through heat exchangers and piping, heat rejection (line 2-4) and heat extraction (line 5-1) is no longer isobar. Line 4’-4 is subcooling, to make sure there is no vapour bubbles entering the expansion valve. The degree of subcooling and superheating will vary from application to application, and is primarily determined by refrigeration charge [4].

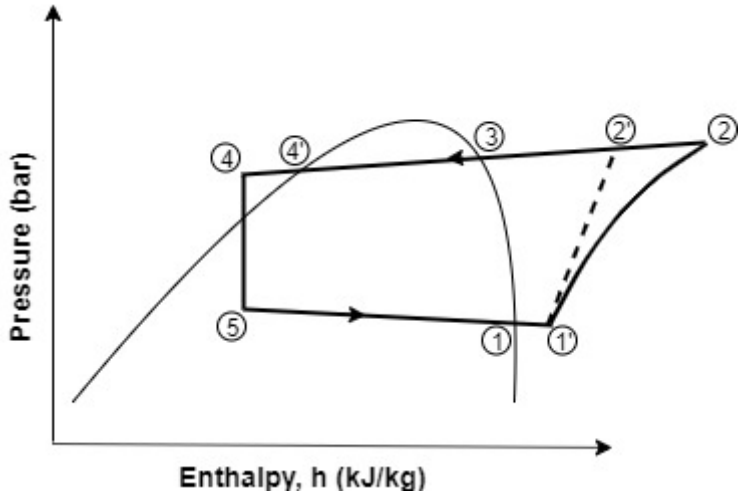

Figure 2.4: *Log P-h diagram illustrating the real vapour compression cycle with its sub-processes*

2.1.4 Compressor efficiency

The theoretical compressor work (1-2') is isentropic and does not account for mechanical and flow related losses. A real compressor will need to do more work to compensate for these losses, which is given by the isentropic efficiency $\boldsymbol{\eta_{is}}$. It is important to determine this efficiency to chart the real power consumption of the compressor during operation. The isentropic efficiency will vary depending on several factors such as compressor size, working fluid and pressure ratio [6]. It can be determined by the isentropic compression power $\boldsymbol{P_{is}}$ and the real compression power $\boldsymbol{P_{shaft}}$:

$$\boldsymbol{\eta_{is} = P_{is}/P_{shaft}} \qquad 2.7$$

The compressors displacement also differs between the theoretical size and the real size. The theoretical displacement $\boldsymbol{\dot{V}_{td}}$ is smaller than the real displacement $\boldsymbol{\dot{V}_{d}}$, and the volumetric efficiency $\boldsymbol{\lambda}$ needs to be determined.

$$\boldsymbol{\dot{V}_d = \dot{V}_{td}/\lambda} \qquad 2.8$$

2.2 Working Fluids

In this chapter, a brief introduction to working fluids will be given, as well as a presentation of commonly used refrigerants. Two natural working fluids will be compared to two synthetic refrigerants, with the aim of giving an impression of what separates refrigerants.

The working fluid, or refrigerant, is the "blood cells" of the heat pump. It's responsible for capturing and transporting the heat between source and sink. In the early 1900s natural refrigerants like CO_2 and ammonia dominated the marked, especially in industrial refrigeration processes [7]. In the 1930s synthetic refrigerants started to be developed, and gradually phased out the natural working fluids. The synthetic refrigerants were mainly Chlorofluorocarbons (CFC) or Hydrochlorofluorocarbons (HCFC), which was later banned in the Montreal protocol (1987) because of its high potential for ozone depletion (ODP) [8]. This led to the Hydrofluorocarbons (HFC) like R134a being developed - synthetic refrigerants without the ozone depleting chlorin. The HFCs, despite having zero ozone depletion potential, still has a high global warming potential (GWP). This has led to several regulations, through the Kyoto protocol (1997) [9] and the Kigali amendment (2016) [10]. Today the refrigeration industry is still highly dependent on synthetic working fluids, but with heavier regulations and restrictions, the marked for natural working fluids are likely to grow.

2.2.1 R134a (CH_2F-CF_3)

The R134a is a hydrofluorocarbon developed in the early 1990s. It was early on seen as a replacement for the much-used CFC R-12, due to its similarities in thermodynamic properties [3]. Because of its high molar weight (102,03), the R134a is best suited for high-performance turbo compressors. Its critical temperature is high, 101,1 ^oC, which make it suitable for high temperature applications. The critical pressure is 40,6 bar. The R134a also have horizontal isothermal curves, meaning there is no temperature glide [11]. This makes it suited for use in water-water heat pumps. During throttling, the losses with R134a is high, and it's recommended to use an external sub-cooler to minimize this [3].

Drawbacks to this refrigerant is high compressor volume, high throttling losses and the GWP. Another problem with R134a is operational problems due to acid formation caused by moisture at high temperatures.

2.2.2 R410A (HFC Mixture)

Refrigerant R410A is a HFC and is a common working fluid for heat pumps [11]. Like R134a it was developed in the early 1990s to replace the newly restricted HCFC R-22. R410A is 50%/50% mixture of HFK125/32, and the temperature glide is minimal (<0,2^oC) [3]. The critical temperature is 72,5 ^oC, at a pressure of 49,6 bar. Compared to the older R-22, the saturation pressure of the R410A is about 50% higher. This means the components needs to be specially designed for the increased pressure levels. It also reduces the compressor volume, which makes the R410A suited for more compact heat pump designs.

Drawbacks to this refrigerant is the high pressure levels requiring special designed components, which makes it more expensive. It has zero ODP but have even higher GWP than the R134a.

2.2.3 R717(NH_3)

Ammonia (NH_3) is a natural working fluid, first used in Carl Von Lindens refrigeration machine from 1876 [11]. Traditionally it has been used in bigger industrial refrigeration systems, like district heating plants. With increasing regulations and environmental focus, ammonia is increasingly used for larger heat pump installations [12]. R717 have a very high critical temperature and pressure level, at 132,3 ^oC and 113,3 bar respectively. The suitable area for an ammonia heat pump is both medium and high temperature application, in the range of 28-60 bar. The molar weight is very low (17,0), meaning the dimensions on pipes, valves, compressor and heat exchangers can be reduced. There is several risks and aspects to consider with ammonia as working fluid. It is highly corrosive on copper and copper alloys, meaning an ammonia refrigeration system needs to be completely copper free. It is also highly toxic, and deadly at concentrations of 1500-2000 PPM and above. At certain concentrations (15-28%) it is also explosive mixed with air. It's considered an environmentally friendly refrigerant, with zero ODP and GWP.

2.2.4 R744 (CO_2)

Carbon dioxide as a natural working fluid has a long history, but was "rediscovered" at NTNU-SINTEF in the 1980s, by Gustav Lorentzen et.al [7]. The R744 differs from other refrigerants in several areas. It has high critical pressure, but low critical temperature, 73,8 bar and 31,1 ^oC respectively. The high pressure gives high energy density, which means that the compressor volume is significantly decreased [3] (illustrated in *Figure 2.5*). Also dimensions on pipes, valves and other components is reduced. For that reason, R744 plants can be very compact.

The low critical temperature causes CO2 to have two types of heat rejection; Subcritical and transcritical. The subcritical happens within the saturation curve, as most refrigerants, through condensation. The transcritical heat rejection happens way above the critical temperature, and through temperature gliding as oppose to condensation [3]. The heat exchangers are for that reason referred to as gas coolers instead of condensers. R744 is non-flammable and non-toxic, which makes it preferable in many applications. It is also considered environmentally friendly, with zero ODP and GWP, when the CO2 is reused/captured from industrial processes.

2.2.5 Comparison

When choosing working fluid for a heat pump it's important to choose a refrigerant with suitable characteristics for the given application. The desired output temperature on the load side of the heat pump is often a dictating factor when choosing the refrigerant type. This makes the saturation temperature and saturation pressure important parameters for evaluation [3]. The safety/risks tied to the refrigerant is also important factors to consider. Ammonia, being both toxic and flammable, requires more safety measures and thoughtful planning. For that reason it's been avoided aboard ships and cars [7]. The R410a is commonly used for low- or moderate temperature applications, due to its relatively low critical temperature [11]. R134a and Ammonia is more suitable for higher temperature applications, especially with a two-stage operation. Despite its low critical temperature, CO_2 is optimal for high temperature application, like heating of domestic hot water. This happens in a transcritical operation. Of the four working fluids covered in this section, CO_2 has the highest volumetric heat performance [kJ/m^3] [3]. This gives the CO_2 an advantage, especially in high temperature applications, and the possibility high COP values, even at high temperature lifts. It also affects the compressor volume, shown in *Figure 2.5* [12]. An overview of important parameters for each of the four refrigerants is presented in *Table 2-1*.

A 2018 report presented by Novema Kulde of the European market for heat pumps and refrigeration systems [13] shows that natural working fluids is still rarely used. Both in Europe and Norway, natural refrigerants accounts for less than 1%. The R410a is dominating the market both in Norway and Europe with 83% and 88% respectively - while the R134a holds 7% of the Norwegian market and 8% of the European.

Table 2-1: *Overview of important parameters for the four working fluids*

Specifications	**R134a**	**R410A**	**R717**	**R744**
Molar weight	102,0	72,6	17,03	44,01
Boiling point, 1 bar [^oC]	-26,1	-51,4	-33,3	-78,03
Critical temperature, t_c [^oC]	101,1	72,5	132,3	31,1
Critical pressure, p_c [bar]	40,7	49	113,3	73,8
Sat.temp. at 25 bar, t_{25}	77	43	58	-12
ODP/GWP	0/1430	0/2090	0/0	0/0*
Toxic/Flammable	No/No	No/No	Yes/Yes	No/No

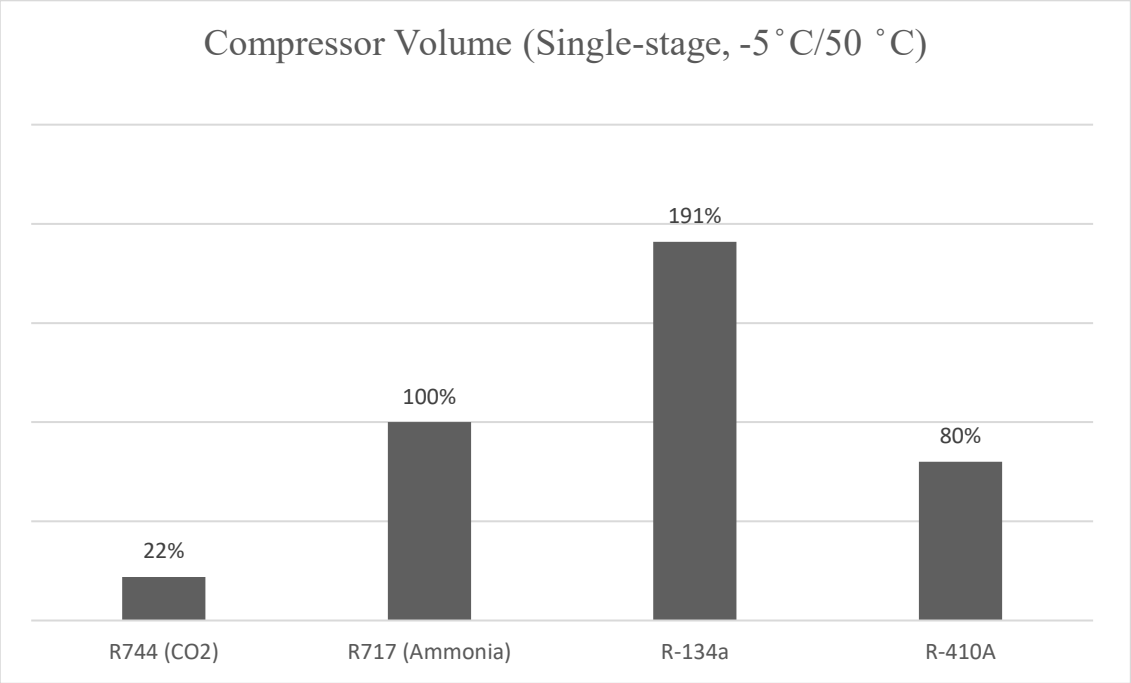

Figure 2.5: *Graphic illustration of compressor volume, with the R717 compressor size as a reference (100%) [12]*

2.3 CO_2 Refrigerant Cycle

Chapter 2.2 provided an overview of some of the characteristics that makes CO_2 quite unique and different from other working fluids. This chapter will explain the practical significance of these differences when planning and dimensioning a CO_2 heat pump system. For a subcritical CO_2 cycle, the theory is basically the same as for conventional working fluids. It is when going transcritical the principles changes, and the need for new theory emerges.

2.3.1 Modified Lorentz Cycle

For a transcritical CO_2 cycle the Carnot cycle is not a good reference cycle. In conventional vapour compression cycles heat is absorbed and rejected at approximately constant temperature and pressure. In a transcritical CO_2 cycle the heat is rejected through temperature gliding in a gas cooler [14]. For that reason, the modified Lorentz Cycle is the most generalised cycle for a transcritical CO_2 heat pump, shown in *Figure 2.6*.

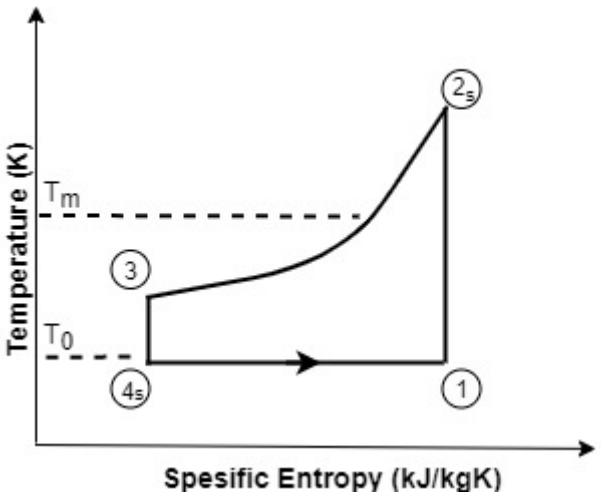

Figure 2.6: *T-s diagram illustrating the modified Lorentz cycle*

The coefficient of performance for the modified Lorentz cycle is given by the mean temperature during heat rejection T_m and the temperature at heat extraction T_0.

$$COP_{LZ} = \frac{T_m}{(T_m - T_0)} \qquad 2.9$$

Analogous to the Carnot efficiency, The Lorentz efficiency η_{LZ} is the relationship between the real COP and the Lorentz COP.

$$\eta_{LZ} = \frac{COP_{HP}}{COP_{LZ}} \qquad 2.10$$

2.3.2 The Ideal Lorentzen Cycle

A more practical reference cycle for the transcritical CO_2 cycle is the ideal Lorentzen cycle [14]. The cycle, visualised in a T-s diagram in *Figure 2.7*, can be divided into the following sub-processes:

- **1-2s** Isentropic compression
- **2s-3** Isobaric transcritical heat rejection through temperature gliding
- **3-4** Isenthalpic expansion
- **4-1** Isothermal heat extraction at constant pressure

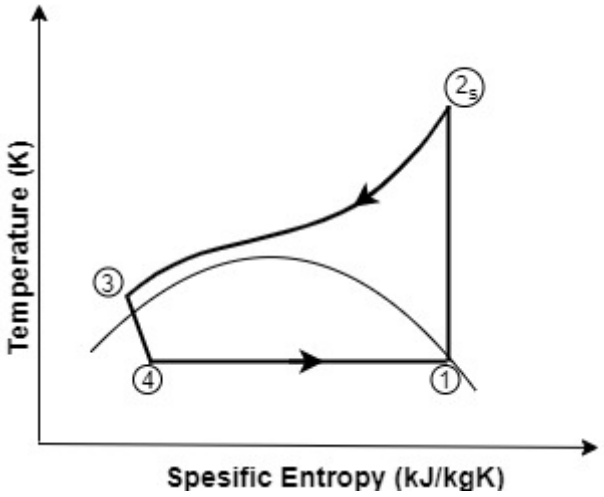

Figure 2.7: *T-s diagram illustrating the ideal Lorentzen cycle*

2.3.3 The Realistic Lorentzen Cycle

For the real Lorentzen cycle, the sub-processes deviate from the ideal cycle on several areas. The steps of the real Lorentzen cycle is illustrated in *Figure 2.8*.

- **1'-1** Non-isobaric superheating before entering the compressor
- **1-2** Irreversible non-adiabatic polytropic compression
- **2-3** Non-isobaric transcritical heat rejection through temperature gliding
- **3-4** Non-isenthalpic expansion
- **4-1'** Non-isobaric, non-isothermal heat extraction

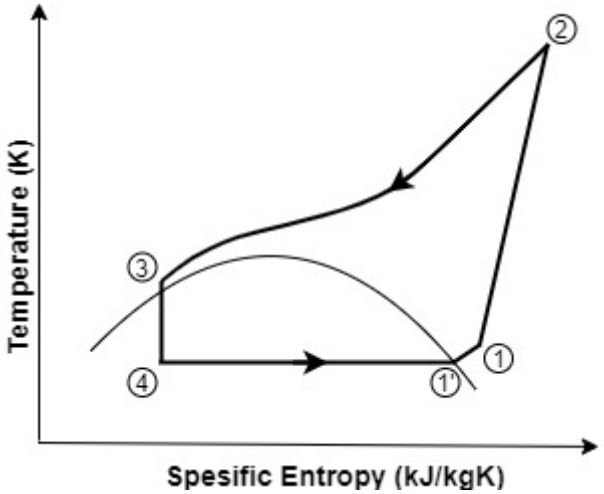

Figure 2.8: *T-s diagram illustrating the real Lorentzen cycle*

2.3.4 Temperature Characteristics

The low critical temperature is a dictating factor on how a CO_2 heat pump plant is designed and operated. For a subcritical operation, the maximum theoretical condensation temperature is the critical temperature at 31,1 °C. The practical upper limit is even lower, around 27-28 °C [7]. Most heating applications requires a higher temperature, which makes the transcritical operation preferable. In a transcritical process the refrigerant discharge temperature is potentially very high (>80 °C). Utilization areas is typically high temperature applications like heating of domestic hot water (DHW), high temperature radiators, or a combination. To achieve sufficient performance of a transcritical CO_2 heat pump, it's important that the heat rejection (temperature glide) happens over a large temperature range [14]. In other words, the gas needs to be sufficiently cooled down before expansion in order to achieve the highest possible COP.

In an optimal gas cooling heat exchange the temperature profile of the secondary fluid (typically water) and the CO_2 working fluid is virtually parallel (see *Figure 2.9*). In addition to being parallel, it's desired to have as low temperature difference as possible. The point where the two temperature profiles has the lowest temperature difference is called the "Pinch-point". The pinch-point is typically either inside the gas cooler or at the gas cooler exit, depending on the pressure level [7]. The temperature difference between the entering secondary fluid and the exiting CO_2 is called the temperature approach ΔT_A. To avoid big losses during expansion, it's desirable to have a low ΔT_A value. For well dimensioned plants the temperature approach can be as low as 2-4 K [7].

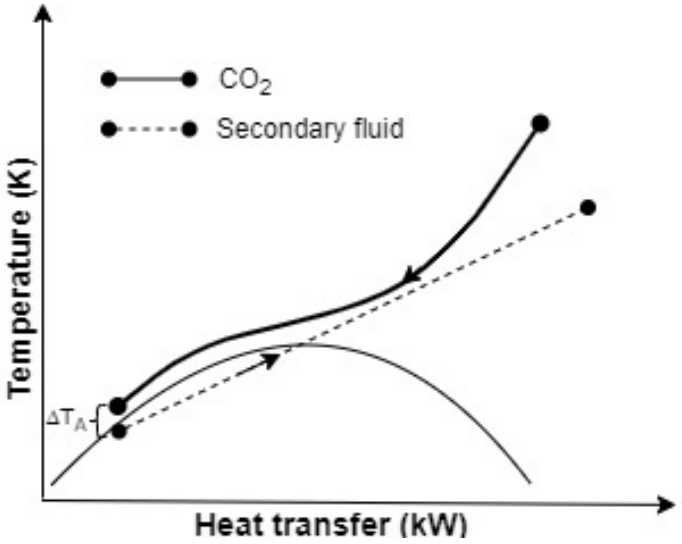

Figure 2.9: *Graph illustrating temperature behavior during a gas cooler heat exchange*

2.3.5 Pressure Characteristics

The critical pressure of CO_2 is 73,8 bar. The transcritical heat rejection is operating with pressures above this level. Controlling and maintaining the optimal pressure level in the gas cooler is very important for the performance of the CO_2 heat pump. This can be achieved with a pressure control valve mounted at the outlet of the gas cooler [7]. The optimal pressure level will vary from application to application, depending on several factors such as gas cooler outlet temperature and refrigerant charge. This will be further covered in chapter 2.3.6.

The specific heat capacity $\boldsymbol{c_p}$ of the CO_2 working fluid is affected by both pressure and temperature. The $\boldsymbol{c_p}$ value will vary along each isobar depending on the slope, as illustrated in *Figure 2.10* [15]. It's given as a relationship between change in enthalpy with respect to change in temperature, in equation 2.11:

$$\boldsymbol{c_p} = (\frac{\boldsymbol{\partial h}}{\boldsymbol{\partial T}})_p \quad [\frac{\boldsymbol{kJ}}{\boldsymbol{kg * K}}] \tag{2.11}$$

The heating capacity $\dot{\boldsymbol{Q}}_{\boldsymbol{GC}}$ [W] of the gas cooler is affected by the specific heat capacity, along with the mass flow rate $\dot{\boldsymbol{m}}$ [kg/s] and temperature difference $\Delta \boldsymbol{T}$ [K]:

$$\dot{\boldsymbol{Q}}_{\boldsymbol{GC}} = \dot{\boldsymbol{m}} * \boldsymbol{c_p} * \Delta \boldsymbol{T} \ [\boldsymbol{W}] \tag{2.12}$$

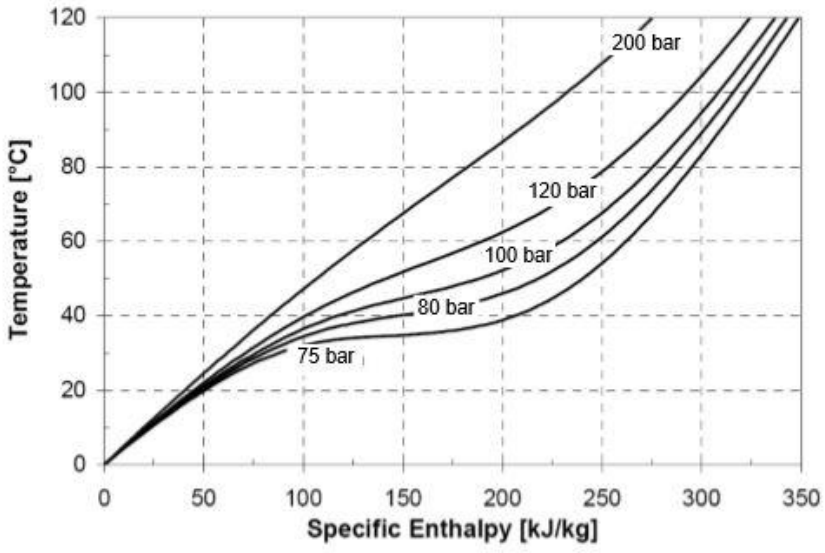

Figure 2.10: *T-h diagram with isobars for different pressure levels [15]*

2.3.6 Optimum Heat Rejection Pressure

Several studies have been done on pressure optimization in CO_2 refrigerant systems. A study conducted by T.S Zhao et.al [16] found that the maximum COP for a transcritical CO_2 process is achieved at an optimal heat rejection pressure. The study concluded that the most important factors affecting the optimum pressure level is the gas cooler outlet temperature, evaporation temperature and compressor performance. It was found that the for a given gas cooler outlet temperature $\boldsymbol{t_c}$ and evaporator temperature $\boldsymbol{t_e}$, the maximum COP can be expressed as equation 2.13. The gas cooler pressure $\boldsymbol{p_c}$ equals the optimal pressure $\boldsymbol{p_{opt}}$ when the partial derivate of the COP with respect to the gas cooler pressure equals zero:

$$\left[\frac{\partial COP}{\partial p_c}\right]_{p_c=p_{opt}} = 0 \qquad 2.13$$

The study further showed that with increasing gas cooler outlet temperature $\boldsymbol{t_c}$, the optimal pressure is increased. This is illustrated in *Figure 2.11*, for evaporator temperature at 10 ^{o}C and super heat temperature of 5 K. The findings suggest that the maximum COP is higher at lower gas cooler outlet temperatures. An approximate formula, equation 2.14, to determine the optimal heat rejection pressure at constant $\boldsymbol{\eta_{is}}$ was developed:

$$p_{opt} = (2,778 - 0,0157t_e)t_c + (0,381t_e - 9,34) \qquad 2.14$$

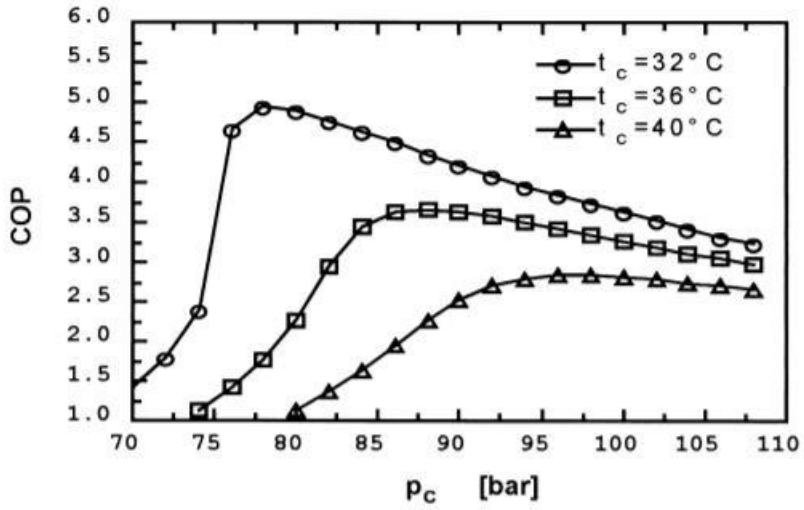

Figure 2.11: *Graph illustrating the relationship between COP and pressure for different t_c [16]*

The degree of superheat t_{sh} was found to have a smaller impact on COP, compared to the other parameters. At higher pressure levels the t_{sh} seemed to be more or less neglectable, but at lower pressures it had some impact on the COP. *Figure 2.12* illustrates the impact of degree of superheat at different pressure levels, at t_c=35 °C and t_e=10 °C.

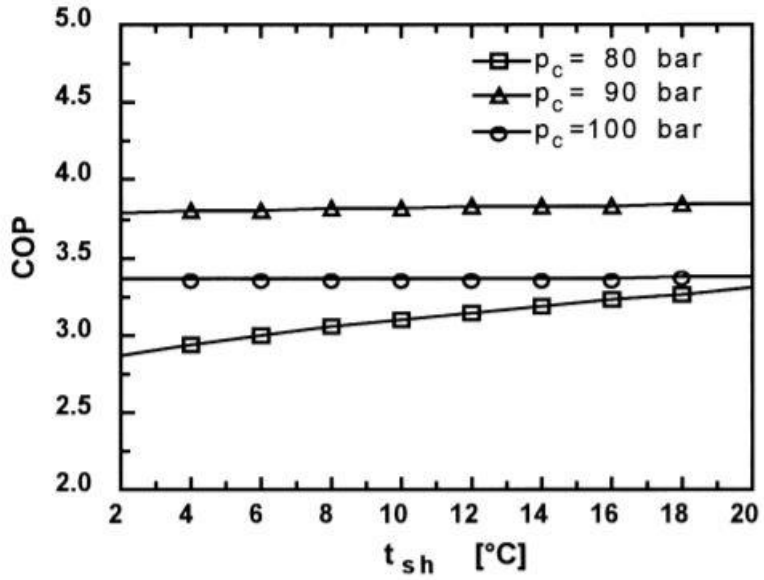

Figure 2.12: *Graph illustrating the relationship between COP and t_{sh} at different pressure levels [16]*

A study conducted by Peng-Cheng Qi et.al 2013 [17] supports the findings of T.S Zhao et.al. The study found a substantial decrease of COP at the optimal gas cooler pressure with an increasing t_c, at the range from 25 – 45 °C. The studies conclude that a CO_2 heat pump should be designed to have the lowest possible gas cooler outlet temperature to achieve highest possible COP. It was determined that the best way to assure optimal pressure is to control the compressor speed and expansion valve simultaneously.

2.3.7 Internal Heat Exchanger

An internal heat exchanger, often referred to as a suction gas heat exchanger (SGHX), is an important component in CO_2 heat pumps. It's placed between the suction gas line and gas cooler outlet line. The main purpose of a SGHX is to superheat the refrigerant before entering the compressor. A 2005 study by Ying Chen et.al [18] found that a well dimensioned SGHX can greatly contribute to high system performance for CO_2 heat pumps. They concluded that a system operating with relatively low pressures (<95 bar) and low evaporator temperatures (<5 °C) benefits the most from having a high efficiency SGHX, with η_{SGHX} in the range of 60-80%. At higher pressures (>11 bar), SGHX with high

efficiency could have a negative effect on COP, and the most beneficial η_{SGHX} for these systems was found to be between 40-60%.

2.4 Residential CO_2 Heat Pump Configurations

2.4.1 Single Gas Cooler DHW System

Figure 2.13 illustrates a single gas cooler CO_2 heat pump system for domestic hot water (DHW). This system has a low pressure receiver (LPR) between the evaporator and the suction gas heat exchanger (SGHX). The LPR is a CO_2 liquid reservoir which enables high-side pressure control with constant compressor capacity [19]. For pressure reduction, the expansion valve (back-pressure valve) opening is increased, leading to an overfed evaporator. The excess CO_2 liquid is captured in the LPR. For pressure increase, the expansion valve opening is decreased leading to an underfed evaporator. The excess liquid CO_2 in the LPR is evaporated and refed to the cycle. The DHW is heated through a single gas cooler. The city water entering the gas cooler is controlled by a variable speed drive (VSD) pump. This makes it possible to control the water outlet temperature through flow rate control. With a VSD pump at the secondary side, the compressor is usually on-off regulated. As previously discussed, the water temperature entering the gas cooler should be as low as possible to achieve maximum COP. For that reason, it's important to minimize the DHW and city water mixing at the bottom of the tank. This can be done by applying diffusers at the storage tank inlet and outlet, decreasing the water velocity [19]. The hot water is drawn from the top of the DHW tank and mixed with city water to give the desired supply tap water temperature (usually 50-55 °C).

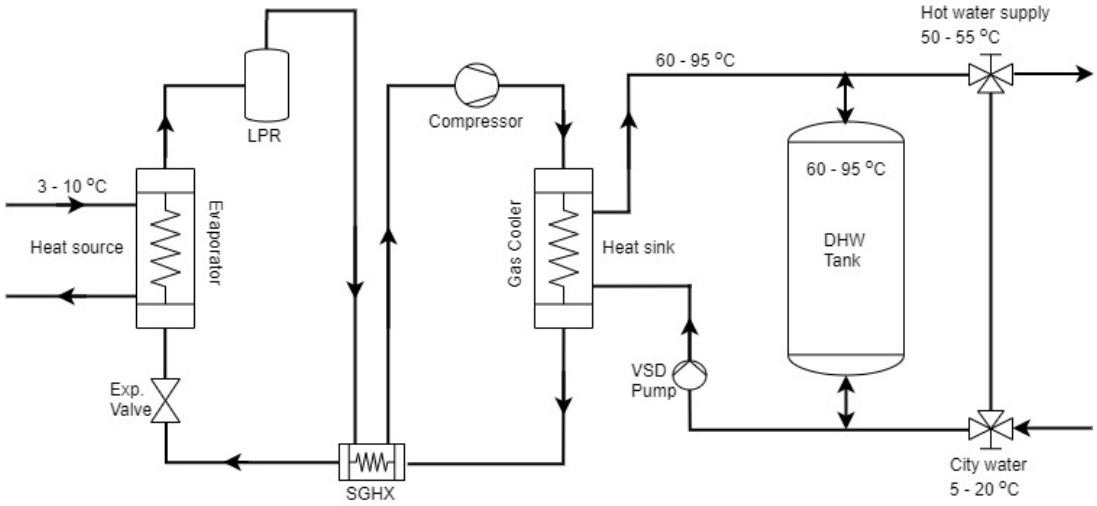

Figure 2.13: *Principle sketch of single gas cooler DHW system*

2.4.2 Tripartite Gas Cooler Combined Heating System

In a combined heating mode system, the hot side heat exchange happens in three separate gas coolers, each one serving a different purpose. *Figure 2.14* shows such a system, with a CO_2 heat pump covering both the DHW- and space heating demand. The tripartite gas cooler configuration is a good way to utilize the CO_2 at a large temperature range and assure sufficient refrigerant cooling.

The first gas cooler (GC) is the DHW reheater. At this stage the CO_2 is at its highest temperature, and this is utilized to reach the desired hot water temperature. Leaving the GC reheater the CO_2 is cooled down to a lower temperature (typically 40-50 °C) and is entering the space heating GC. At this temperature range it can provide supply water to low-temperature radiators or floor heating. The space heating GC can also be by-passed when there is no space heating demand, typically during the summer months. The last gas cooler is the DHW preheater. This is where the city water enters and is heated to about 20-30 °C. The goal of the preheater GC is to cool the CO_2 as much as possible, and to provide a lower water temperature difference over the reheat GC.

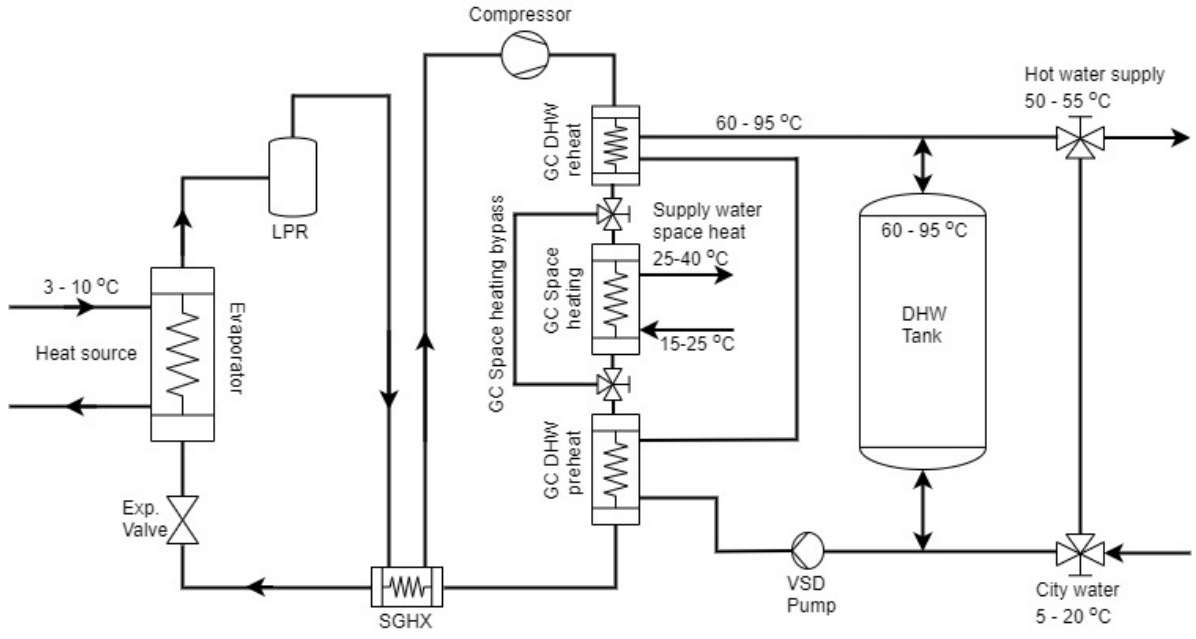

Figure 2.14: *Principle sketch of a combined mode system*

2.5 Hydronic Heating Systems

The purpose of domestic heating systems is to cover the heat losses due to transmission, infiltration and ventilation. In addition, the heating system should provide domestic hot water to the household. In Norway, according to the standard NS3031, the dimensioning

outdoor temperature used for calculating heating loads is the coldest average temperature over a three-day stretch in a 30 year period [20]. The type and design of such heating systems can be done in numerous ways. In hydronic heating systems, water is the medium distributing the heat around to the various zones. The water is heated up by a heating unit, typically a boiler or heat pump. This type of systems is usually found in larger buildings, such as schools and hospitals, but is not uncommon in residential buildings.

2.5.1 System Designing

Hydronic heating systems can be divided into two categories; High-temperature and low-temperature systems. High-temperature systems typically has supply/return temperatures of 90/70 ^{o}C or 80/60 ^{o}C and is usually found in older buildings. Low-temperature systems is better suited for heat pumps and solar collectors, with supply temperatures below 55 ^{o}C, and is the most common in modern hydronic systems [20]. These systems requires larger heating surfaces, but it's been found that low temperature heating provides a greater degree of thermal comfort for the residents [21]. In addition, most new buildings have significantly smaller transmission heat losses than older buildings, which makes the size of low-temperature radiators reasonable.

A hydronic heating system are usually designed as a one-pipe or two-pipe system. One-pipe systems are mostly used in smaller scale systems, due to the nature of the design. As all radiators are connected in series in a one-pipe system, the supply water temperature will decrease as it flows. This means that the heat surfaces of the radiators need to be larger downstream the system to achieve the same heat effect. In two-pipe systems, radiators are connected in parallel, meaning the supply water temperature is the same in all radiators (neglected heat loss in piping). *Figure 2.15* illustrates both system types.

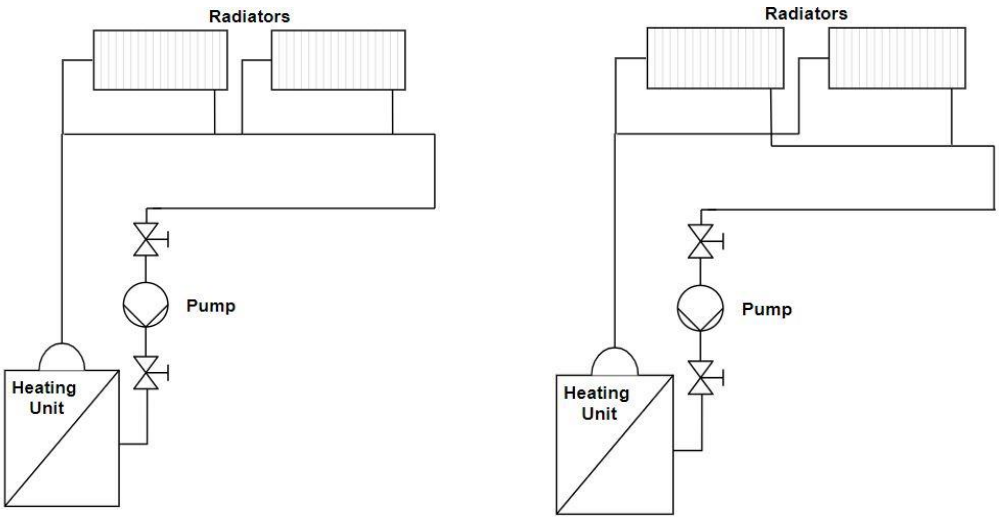

Figure 2.15: *Simple illustration of a one-pipe system (left) and two-pipe system (right)*

Floor heating is another option for space heating, which is well suited for low-temperature systems. Supply temperature for such systems is typically 30-45 °C, 50-80 W/m^2 [20]. The piping, usually plastic or steal, is imbedded in concrete or in the joists. For floor heating in joists, a challenge can be getting the heat evenly distributed all over the floor. This can be solved by using heat plates, typically aluminium, on top of the piping. It is also important with good insulation below the heat pipes, as it is desirable that as much heat as possible is going up into the floor.

2.5.2 Heat Power Regulation

With variating heating demand in a building, there is a need for heat power regulation. This is can achieved by either regulating the supply water temperature, or regulating the mass flow of the supply water [20]. Using temperature regulation, the mass flow is kept constant, while the desired supply temperature is regulated as a function of the outdoor temperature. The temperature can either be controlled by a three-way mixing valve or regulating the power of the heat production unit. The advantage with a temperature regulated system is the low pressure variations in the system due to the low variations in water mass flow. However, with a mixing valve controlled system, the heating unit typically overproduce during low demand periods. This makes the system less efficient from an energy-economic perspective. A proportional correlation between the heat power demand ($\boldsymbol{Q}$) and the outdoor ($\boldsymbol{T_0}$) and desired indoor temperature ($\boldsymbol{T_r}$) can be assumed. With the dimensioning outdoor temperature ($\boldsymbol{T_{0,min}}$) and max heat power ($\boldsymbol{Q_{max}}$), equation 2.15 is given as:

$$\boldsymbol{Q} = \frac{(\boldsymbol{T_R} - \boldsymbol{T_0})}{(\boldsymbol{T_R} - \boldsymbol{T_{0,min}})} * \boldsymbol{Q_{max}} \qquad 2.15$$

Using mass flow to regulate heating power, the supply water temperature is kept constant. Depending on the design of the system, this is typically achieved with a variable speed circulation pump or throttling valves at the different zones/radiators [20]. As previously mentioned, with mass flow regulation, the hydronic system is subject to a greater degree of pressure variations. The pressure drop ($\Delta \boldsymbol{P}$) in the piping can be expressed as the mass flow ($\dot{\boldsymbol{m}}$) squared, times the resistance number ($\boldsymbol{r}$), in equation 2.16:

$$\Delta \boldsymbol{P} = \boldsymbol{r} * \dot{\boldsymbol{m}}^{\boldsymbol{2}} \qquad 2.16$$

This equation expresses the system characteristics (pipe characteristics) and along with the pump characteristics can be used to identify the operating point. This is illustrated in *Figure 2.16*.

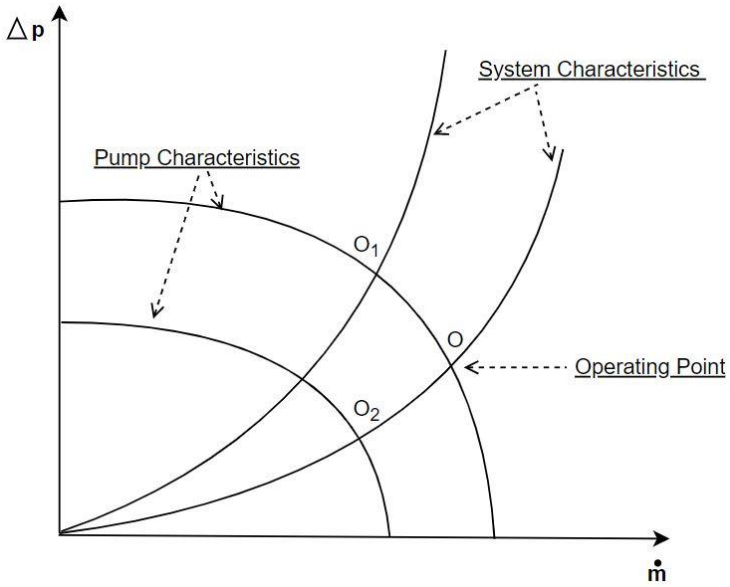

Figure 2.16: *Simplified characteristics chart*

The cross section point ($\boldsymbol{O}$) represents the operating point of a fully open system. With throttling certain sections of the system, the system characteristics curve becomes steeper, with a new operating point ($\boldsymbol{O_1}$). Operating point ($\boldsymbol{O_2}$) represents a fully open system with a pump with lower RPM. Measures to keep the driving pressure constant can be implemented to the system. This is typically done with a pressure differential regulator, with sensors on mounted on the supply- and return piping [20]. The regulator will then ensure a differential pressure equal to the pressure drop of a fully open system. Another option is using a bypass valve between the supply and return pipes, or a bypass at the circulation pump.

2.5.3 System Start-up Regulation

System start-up regulation is important to ensure that the dimensioned water mass flows is being distributed to the different zones of the system. A badly regulated system could cause some zones to be overheated while others may be underheated. One of the main issues that could cause problems in a hydronic system is air pockets in the pipes. An air pocket reduces the pipes cross sectional area and could cause noise and reduced water flow. Air venting is for that reason an important procedure in system regulation. When the flow is stopped, air will typically migrate to highest areas of the system [22]. With water flow, the stream needs a certain velocity to be able to carry the air. The velocity is dependent on several factors such as pipe diameter, flow direction and pipe curvature. It's common to have either manual or automatic air vents at high points of the system [22]. Automatic vents are usually float valves which closes when the water rises, and the air is let out. It's important to monitor the system pressure, as automatic vents can suck air into

the system under low-pressure conditions. This is not an issue with manual vents, but in return it requires management by maintenance staff.

Air venting is a prerequisite to get achieve a well-regulated system. After the system is vented, the regulation of valves can begin. The process is usually initiated with all valves fully open, while section for section is regulated (throttled) to match the dimensioned heat effect. One common strategy is to start with the secondary circuits furthest away from the heat production unit, and work back towards the primary circuit [20].

2.6 Geothermal Heat Source

In colder climate areas, the ground represents a stable heat source all year around. The heat pump is an ideal way to utilize the low temperature energy found at shallow depths. This energy is essentially solar energy stored in the ground. The heat can be extracted from soil, bedrock and groundwater. This chapter will provide an overview of some of the most common configurations for a ground source heat pump (GSHP). *Figure 2.17* is a flowchart of the different ways ground source heat is utilized by a heat pump.

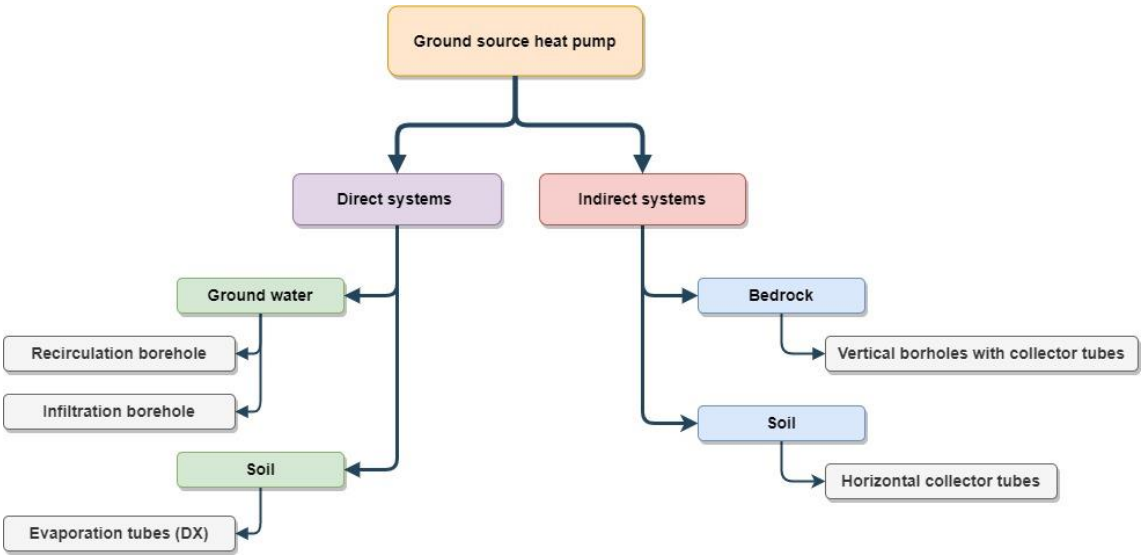

Figure 2.17: *Flowchart illustrating the different GSHP configurations*

2.6.1 Direct Systems

Direct systems are the oldest and cheapest GSHP systems. In water-water heat pumps, the ground water is pumped up, and directly used for heat exchanging in the evaporator. Ground water is an excellent heat source, with relatively stable temperatures. A thorough ground water analysis is important to map the water quality [11]. Iron and manganese can cause precipitation in valves, pumps and other components, and it's important that the ground water do not exceed the acceptable levels (Fe < 0,2mg/l, Mn 0,05mg/l) [11].

Usually an intake- and discharge well is bored, with a submerged circulation pump (illustrated in *Figure 2.18*). The discharge well must be dimensioned in such a way that it can absorb the quantities of return water.

2.6.2 Indirect Systems

Indirect systems have collector tubes, usually with circulating antifreeze brine, working as a borehole heat exchanger. The brine circulating in the closed loop collector tubes transports the heat from the boreholes to the evaporator of the heat pump. The loops can be laid both vertically and horizontally. The vertical configuration, illustrated in *Figure 2.18*, involves drilling wells at depths between 150-300 meters (depending on the soil/bedrock conditions), with a diameter of around 15 centimetres. The horizontal configuration is usually a cheaper alternative, as it only involves trenches down to a depth of 60-150 centimetres. On the other hand, its more area demanding, and the trench temperature is to a greater degree subject to seasonal variations.

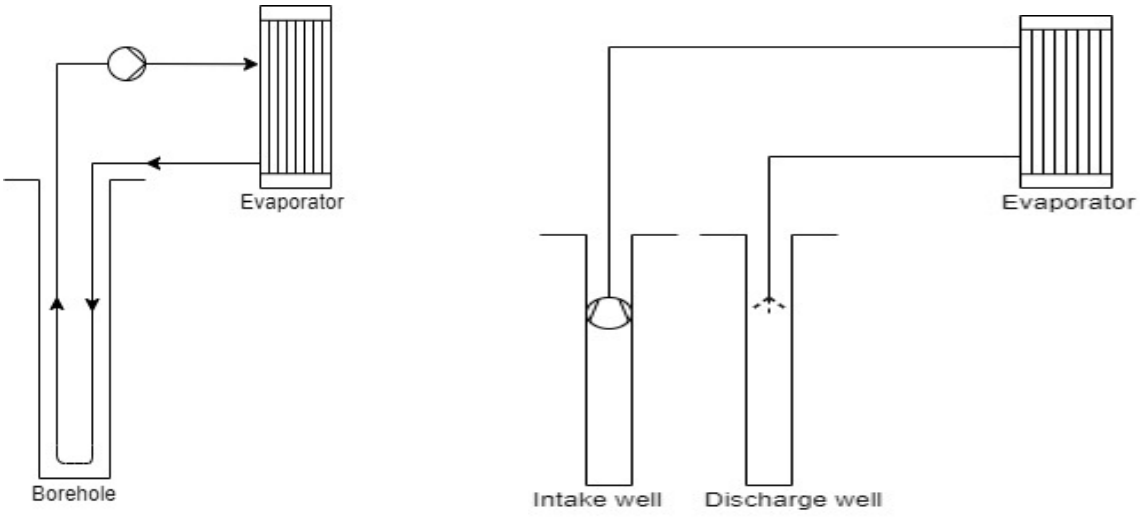

Figure 2.18: *Principle sketch of indirect system (left) and direct system (right)*

2.6.3 Thermal Response Test

A thermal response test (TRT) is a tool that is used to dimension geothermal borehole configurations as accurate as possible. The test makes it possible to specifically map the conditions and thermal properties in the ground at a given location. Especially for larger GSHP projects, a thermal response test is important. The TRT is performed by drilling a test borehole with collector tubes and a circulation pump. After being drilled, the test borehole is usually left at rest for 5-7 days for the temperature and groundwater to reach

normal levels [23]. After this period, the measurements begin. Important parameters extracted from a TRT is [24]:

- Ground water level
- Borehole resistance; the thermal resistance between the collector fluid and the borehole wall.
- Thermal conductivity
- Temperature gradient at different depths
- Temperature profile

The specific power output of the borehole is given by equation 2.17:

$$q = \frac{T_f - T_b}{R_b} \qquad 2.17$$

Where q [W/m] is specific power output, T_f [K] is the collector fluid temperature, T_b [k] is the borehole wall temperature, and R_b [mK/W] is the borehole resistance.

2.6.4 Ground Conditions in Trondheim

The amount of heat available for heat extraction will vary from location to location, depending on the ground and soil conditions. The level of groundwater, permeability, is also important as the active part of the borehole is dependent on the filling level of ground water [24]. In Trondheim, the bedrock is a part of the "Trondheimsfeltet", which is a geological province. There are several types of rock dominating in the larger Trondheim area, such as sandstone, limestone, slate variations and phyllite. The thermal properties of several bedrock types is presented in *Table 2-2* [25]. Due to the high variations of rock types in the Trondheim region, the permeability will vary as well.

Table 2-2: *Thermal properties of bedrock types*

Bedrock Type	Suitability	Thermal Conductivity [W/mK] (Mean)
Sandstone	Good	4,0
Slate	Average	2,7
Limestone	Average	2,7
Phyllite	Average	3,0
Porphyry	Less	2,4
Granite	Average	2,8

3 System Description

The CO_2 heat pump which is modelled and experimented on in this master project was designed by Jørn Stene in 2000-2004 as a part of his doctoral degree, at EPT NTNU. This chapter aims to describe the physical structure of the mechanical systems included in this master project. During the experimental phase of this project, the heat pump has been in a test rig at WINNS AS, before being moved to a residential location. The technical information for the heat pump has been retrieved from Jørn Stene's doctoral thesis [26].

3.1 CO_2 Heat Pump Structure

The CO_2 heat pump is a residential brine-water ground source heat pump. It is designed as a combined space heating and domestic hot water unit, originally with a capacity of about 6,5kW. The heat source is an indirect u-tube collector system, in a 150m deep bedrock borehole. The brine used in the boreholes is potassium format with freezing point of -20 °C. The gas coolers are in a tripartite configuration, with a DHW preheater, a hydronic floor heating gas cooler, and a DHW reheating gas cooler. The heat pump also consists of a suction gas heat exchanger, a sub cooler, two expansion valves, a low pressure receiver, an oil return system, and a CO_2 filling line. The general structure is illustrated in *Figure 3.1*.

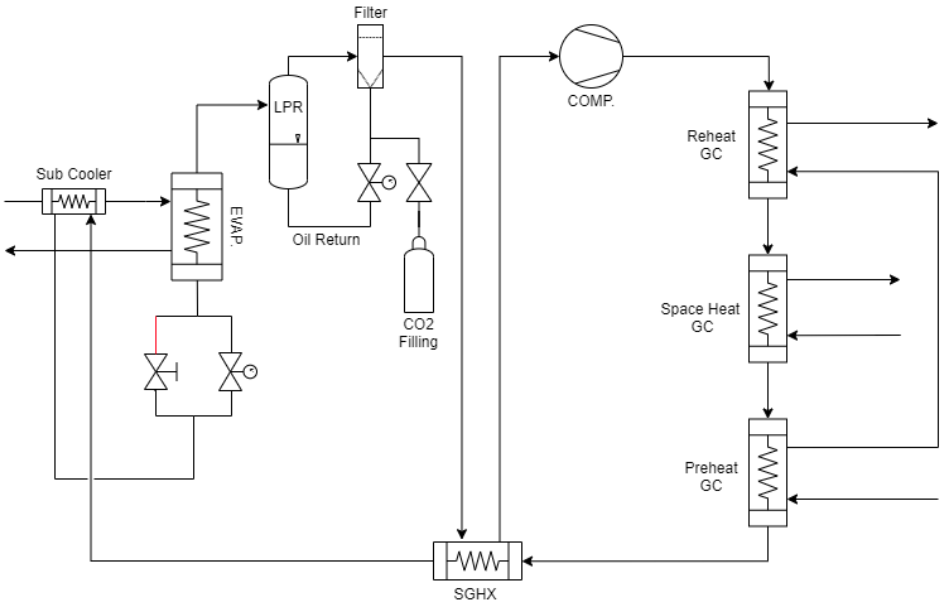

Figure 3.1: *Principle sketch of the CO2 heat pump*

3.1.1 Compressor

The compressor has been changed several times during the heat pumps lifespan. The current compressor is a semi-hermetic two-stage reciprocating compressor operated as a single-stage unit. It has a maximum capacity of 1450 RPMs (30 – 60 Hz), with a displacement volume of 1,12 m^3/h. The maximum pressure and discharge temperature are 150 bar and 160 °C, with a maximum power input of 1400 W. The compressor is showed in *Figure 3.2* [27].

3.1.2 Evaporator

The evaporator is a helical counter-flow tube-in-tube heat exchanger. Both brine and CO_2 tubes are stainless steel, with a tube length of 12 m. The CO_2 pipe, which is the inner tube, has an inside diameter of 8 mm. The surrounding brine tube has an inner diameter of 20 mm. The approximate weight of the evaporator is 17 kg.

3.1.3 Gas Coolers

3.1.3.1 DHW Preheating Gas Cooler

The domestic hot water preheater is a helical counter flow tube-in-tube heat exchanger. Both tubes are stainless steel, with an inner diameter of the CO_2 tube of 6 mm and 12 mm of water tube. The tube length is 14 m. The approximate weight of the preheater is 13 kg.

3.1.3.2 Space Heating Gas Cooler

The space heating gas cooler is a helical counter flow tube-in-tube heat exchanger. The tubing is stainless steel. The inner diameter of the CO_2 tube is 6 mm and the inner diameter of the water tube is 18 mm. The tube length is 15m. The approximate weight of the space heater is 18 kg.

3.1.3.3 DHW Reheating Gas Cooler

The domestic how water reheater is a helical counter flow tube-in-tube heat exchanger with stainless steel tubing. The inner diameter of the CO_2 tube is 6 mm and the inner diameter of the water tube is 12 mm. The tube length is 3,5 m, and total approximate weight of the gas cooler is 3 kg.

3.1.4 Suction Gas Heat Exchanger

The suction gas heat exchanger is a counter flow tube-in-tube unit, controlled by ball-vales at the inlet and outlet. The SGHX has stainless steel tubing, with the inner diameter of the

low-pressure tube of 8 mm, and 12 mm for the high-pressure tubing. The tube length is 2,3 m. The approximate weight of the SGHX is 2,5 kg.

3.1.5 Low Pressure Receiver

The low pressure receiver liquid reservoir is a 4 liter vessel. The oil return tubing from the bottom of the LPR is a stainless steel tube with inner diameter of 4 mm. The oil return tube is connected to the filter, as illustrated in *Figure 3.1*. The oil flow rate is controlled through a needle valve.

3.1.6 Sub Cooler

The sub cooler is simple designed counter flow heat exchanger, with a 6 m stainless steel tube twisted around the evaporator inlet pipe. The inner diameter of the tube is 8 mm. The sub cooler capacity is controlled through several ball valves.

3.1.7 Expansion Valves

The heat pump has two expansion valves, one back-pressure valve and one needle valve. One is manually operated, and one is electronic, connected in parallel (see *Figure 3.1*). The backpressure valve is controlling the high side pressure.

Figure 3.2: *The Semi-hermetic double stage compressor [27]*

3.2 WINNS Test Rig

The test rig at WINNS AS is an installation that makes it possible to perform operational testing of heat pumps in a controlled environment. The test rig is designed to simulate the

secondary side of a heat pump, circulating water through the condenser and evaporated when connected. The mass flow is controlled for each cycle individually through separate pumps. An internal heat exchanger is used to regulate the desired input temperature on both the evaporator and gas cooler. At the cold side there is a buffer tank, and at the hot side there is a cooling coil, in order to control the temperature through mixing valves. *Figure 3.3* is a principle sketch of the test rig.

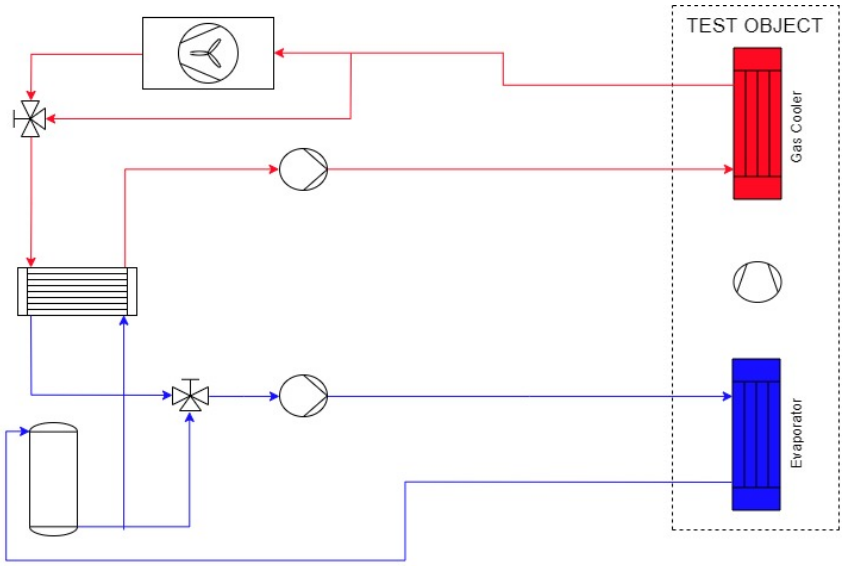

Figure 3.3: *Principle sketch of the test rig*

3.3 Hydronic System at Residential Location

The hydronic system at the residential location consists of a domestic hot water system and a floor heating system. In this section, the configuration of these systems will be described individually. The control strategies will be further explained in chapter 4.3.5.2.

3.3.1 Floor Heating System

The floor heating system provides heating to about 280 m^2 of occupied space. The system consists of three circuits in parallel, supplying floor heating to each story. A buffer tank of 100 litres feeds the system with heated water through a variable speed circulation pump. Throttling valves at each circuit regulates heating through the mass flow at the different stories. An electrical heat element in the buffer tank is used as the peak load/back up system. The space heating gas cooler is connected to the buffer tank. The supply water temperature is regulated schematically through a linear relationship with the outdoor temperature. A controller communicates with the variable speed pump after the buffer

tank, and the peak load element, to regulate the desired supply temperature. The hydronic floor heating system is illustrated in *Figure 3.4*.

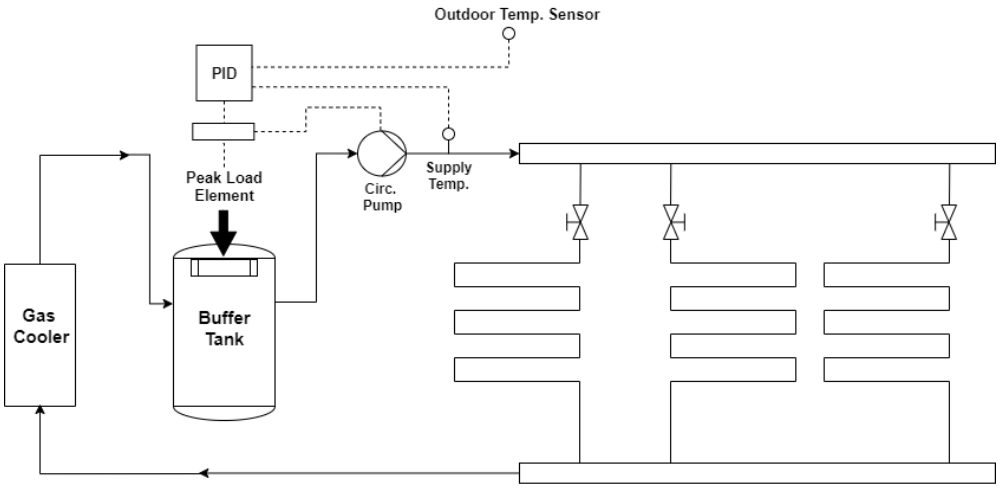

Figure 3.4: *Principle sketch of the hydronic floor heating system*

3.3.2 DHW System

The domestic hot water system provides hot water to the whole house, with a total of 9 occupants. The accumulator tank consists of four tanks connected in series, with a total volume of 400 litres, and a set point temperature of 70 °C. The tank has a diffusor to minimize mixing of hot and cold water. A peak load/back up electrical heating element is located in the last tank. The pre- and reheating gas coolers are connected to the accumulator tank through a constant speed circulation pump. The water mass flow through the gas coolers are controlled through a throttling valve. A controller communicates with both the throttling valve and the peak load heating element to ensure desired hot water temperature is maintained. There is also a valve for bypassing the preheating GC.

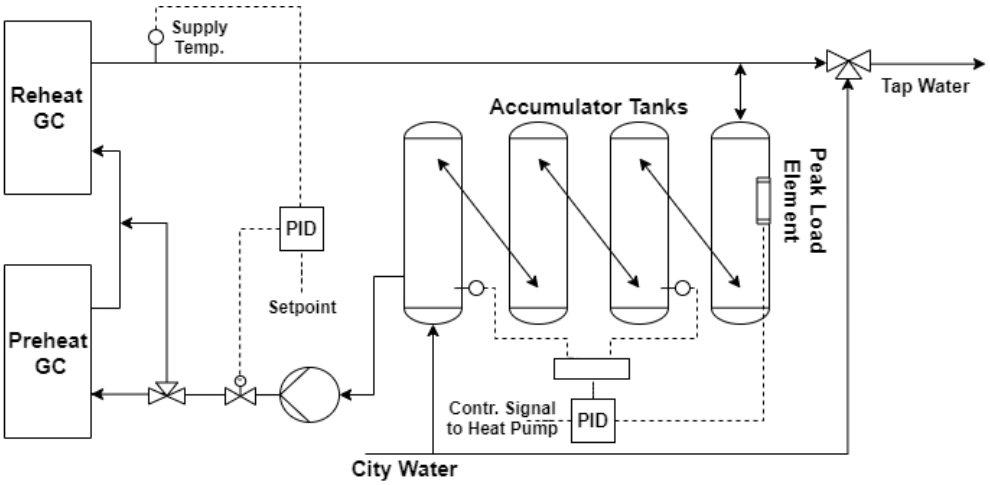

Figure 3.5: *Principle sketch of the DHW system*

4 Methodology

In this chapter, the methodology of the master project will be presented, with a brief introduction to the working tools utilized. The development of the dynamic CO_2 heat pump model will be thoroughly covered step by step, along with reasoning of the decisions made during the process. Lastly, the methods and strategies during the operational testing at Winns, and implementation of the heat pump at the residential location will be covered.

4.1 Working Tools

4.1.1 Draw.io

Draw.io is a free online drawing and diagramming program by JGraph Ltd. It was founded by Gaudenz Alder in 2000 as a diploma thesis at the Swiss Institute of Technology. In this thesis, most of the charts, diagrams and sketches has been drawn in the process engineering mode of draw.io.

4.1.2 CoolPack

CoolPack is a program with a collection of technical calculation programs for use in dimensioning, optimization and energy analysis of refrigeration systems. The software was developed by the Technical University of Denmark (DTU) and was financed by the Danish Ministry of Energy up until version 1.33 [28]. CoolPack has been greatly used for developing simple base models to use as a reference for more complex modelling.

4.1.3 Simple One Stage CO_2 Cycle (SOSCC)

This software is a continuation of CoolPack, developed at DTU, with focus on the CO_2 transcritical cycle. The program can perform simple CO_2 cycle simulations in a log-Ph diagram, for both one- and two-stage cycles. It has been utilized for extracting thermophysical properties and for validation of more complex models.

4.1.4 Modelica Language

Modelica is an object-oriented programming language, developed by Hilding Elmqvist in 1997. It is widely used for component-oriented modelling of a broad spectre of complex engineering systems.

4.1.5 Dymola

Dymola is a simulation and modelling software based on the Modelica programming language. It was established in 1978, as Hilding Elmqvist's PhD. It has been developed and improved over the years and is today a strong modelling tool for complex engineering systems. In this project, Dymola 2020 has been used for developing the CO_2 heat pump model. In addition to the Standard Modelica Library, the TIL Library has been used, along with the visualisation tool TLK DaVE. The TIL library offers a large selection of refrigeration systems specific components. TLK DaVE has been used to plot diagrams specifically for the developed model.

4.1.6 IDA ICE

IDA ICE (Indoor Climate and Energy) is simulation software developed by EQUA. It is used to simulate the performance of buildings, or zones of a building. The software can calculate important HVAC parameters such as cooling demand, heating demand, indoor air quality and energy budgets. Modelica is the underlying language. The building or structure can also be visualized in a 3D model. In this master project, IDA ICE has been used to make a model of the residential location in which the heat pump will be operated.

4.2 Model Development

One of the main objectives of this master project was to develop a strong dynamic model of the residential CO_2 heat pump system. The goal was to build a model that will give realistic values when simulated during different conditions and operating modes. The model was developed in Dymola 2020, based on a combination of the following:

- Calculated values using well established equations.
- Values and information specifically tied to components from Jørn Stene's PhD [26].
- Reference models developed in "CoolPack" and "Simple One Stage CO_2 Cycle".
- Qualified assumptions.

4.2.1 Reference models

The reference models were developed to give an overall view of the CO_2 heat pump cycle, and as a tool to compare and validate the values of the Dymola model as it was developed. *Figure 4.1* shows such a reference model, developed for 90 bar high side pressure simulations. Several CoolPack and SOSCC models were developed, with different pressure levels and evaporator temperatures. The CoolPack models requires certain fixed input values to perform the simulations. The input values for *Figure 4.1* is:

- 6,5kW heating capacity ($\dot{Q}_{GC}$)
- Gas cooler outlet temperature 18 °C (T_4)
- Isentropic efficiency 75% (η_{is})
- Thermal efficiency of internal heat exchanger 40% (η_{SGHX})
- Heat loss factor compressor 10% (f_Q)
- High pressure 90 bar (P_{GC})
- Evaporator temperature 0 °C (T_E)

All the input values are stationary in CoolPack, but this is not necessarily the case in a realistic operation. The heating capacity of 6,5kW is the dimensioned capacity, but previous tests done showed that the capacity can get as high as 7kW [26]. The current capacity is uncertain, but the dimensioned capacity is a good base value for a reference model. The gas cooler outlet temperature is dependent on several factors such as pressure levels, inlet water temperature, gas temperature and mass flow rates. These are factors that needs dynamic modelling to characterize. For this reference model, 18 degrees was used for the gas cooler outlet temperature. A suction gas heat exchanger was also implemented in this reference model. The 2005 study by Ying Chen et.al [18] showed the importance of a well dimensioned SGHX for high COP in a CO_2 heat pump. In this particular model, the SGHX efficiency was set to 40%, but several levels of efficiencies were tested in different models. The evaporator temperature at 0 °C equals a low side pressure of 35 bar. This value is based off a secondary side brine temperature of 5-10 °C. For the compressor, the heat loss factor and isentropic efficiency was set to 10% and 75% respectively. These values were based on findings in Jørn Stene's PhD [26].

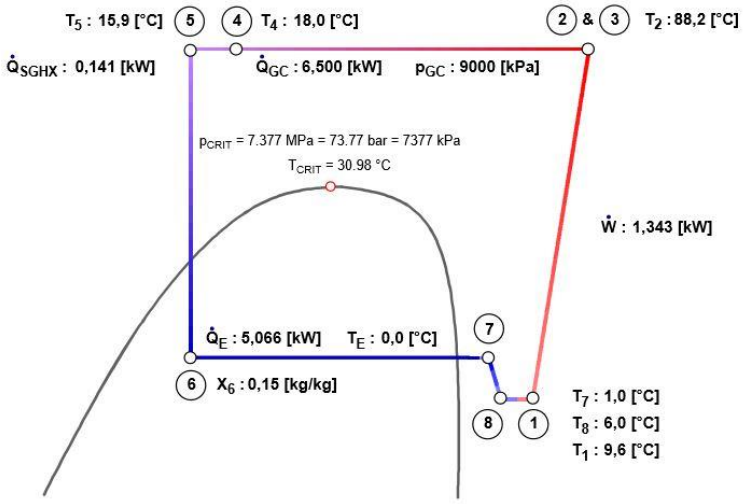

Figure 4.1: *90 bar reference model developed in CoolPack*

4.2.2 Dynamic Dymola Modelling

The dynamic model of the CO_2 heat pump system was developed in Dymola, using the Modelica language. The solver used in the simulations is the Dassl-algorithm, which is a numerical algebraic differential equation solver. With an integration tolerance of 1E-4, it has been able to provide stable simulations at a variety of time intervals and input values. Several simplifications have been made in the model structure. Pressure drop through the heat exchangers and piping is not accounted for, in addition to heat losses in piping between components. Constant heat transfer models (Constant Alpha [W/m^2K]) for R744, brine and water has been used throughout the model. The heat transfer model for R744 was based on a 2010 study by R. Mastrullo Et.al [29]. The heat transfer values for brine and water were based on established heat transfer charts [30].

Developing a dynamic model in Dymola is a step by step process. The challenge with complex dynamic modelling is to get every component in the system working together and operating as one unit. It has been important to validate each component individually before proceeding. In this section the process of building the model will be covered, explaining the structure of the model in steps.

4.2.2.1 Evaporator

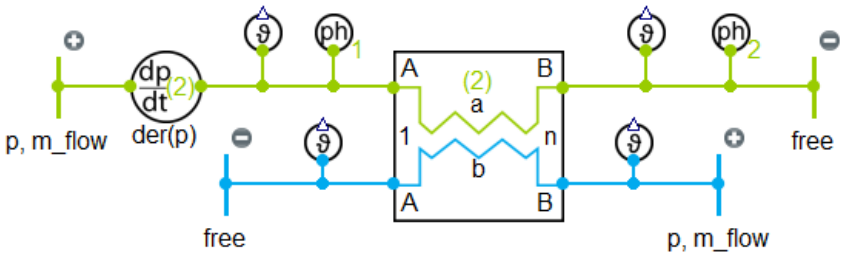

Figure 4.2: *Model of the evaporator in Dymola*

The first component of the system to be modelled was the evaporator, illustrated in *Figure 4.2*. The blue line (Tube b) represents the brine side, while the green line (Tube a) is the CO_2 refrigerant side. The evaporator is tube-and-tube counter-flow brine/refrigerant heat exchanger selected from the TIL-library. As potassium formate is not available as a liquid in Dymola, the brine selected for the secondary side was 30% propylene glycol, which have relatively matching properties. To be able to run simulations on individual components or parts of a system, fixed boundary conditions needs to be implemented. The boundaries at the entering side was set to be pressure and mass flow determined, to ensure constant mass flow of brine and CO_2 refrigerant over the evaporator. The CO_2 and brine mass flow were set to 0,025 kg/s and 0,30 kg/s respectively. In addition, a pressure state element (dp/dt) was placed on the refrigerant side to provide the evaporator pressure during the

whole simulation. To easily monitor the simulation, temperature and pressure-enthalpy sensors were placed on each side of the evaporator. All materials in the evaporator is stainless steel. *Table 4-1* provides an overview of the most important parameters of the modelled evaporator.

Table 4-1: *Evaporator specifications (*LinearEnthalpyDistribution) (**LinearTemperatureDistribution)*

Parameter	Tube a	Tube b
Constant Alpha [W/m^{2}K]	3000	1200
Constant pressure drop [Pa]	0	0
Length of coil [m]	12	12
Inner tube diameter [mm]	8	12
nCells	10	10
Thermal Resistance [K/W]	1/4000	1/4000
Initialization	LED*	LTD**

4.2.2.2 LPR and Compressor

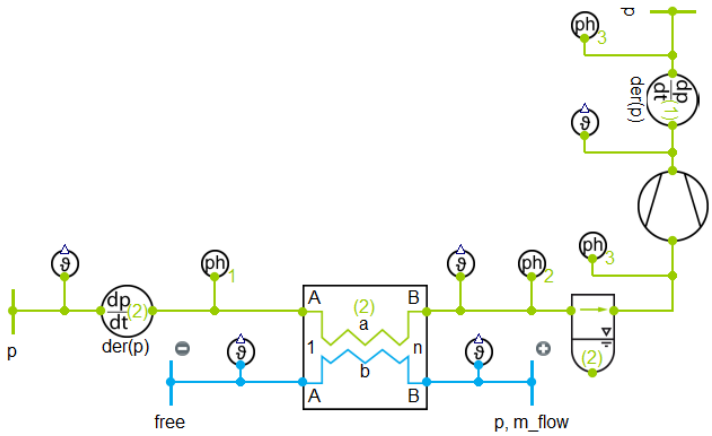

Figure 4.3: *Dymola model with evaporator, LPR and compressor*

The low pressure receiver was implemented after the model of the evaporator was tested and verified. The liquid reservoir was placed on the refrigerant line between the evaporator and the compressor, at the same pressure state as the evaporator. The volume of the vessel was set to 4 litres. The characteristic line of the outlet conditions was set to ideal, with an initial filling level of 60% refrigerant.

The compressor was selected from the TIL-library, the efficiency based model with fixed speed. For simulation purposes, the speed of the compressor was set at an average speed of its operating range, at 45 Hz. At this point, no active control unit were added to the compressor. Volumetric and isentropic efficiency was both set to 75%, with a displacement

volume of 4,125e-6 m^3. In addition to the compressor, a second pressure state element was added, to initiate the high side pressure. At this point the boundaries was set to pressure determined on the refrigerant side, and several ph- and temperature sensors were added. *Figure 4.3* illustrates how the model looked at this point.

4.2.2.3 Tripartite Gas Cooler Configuration

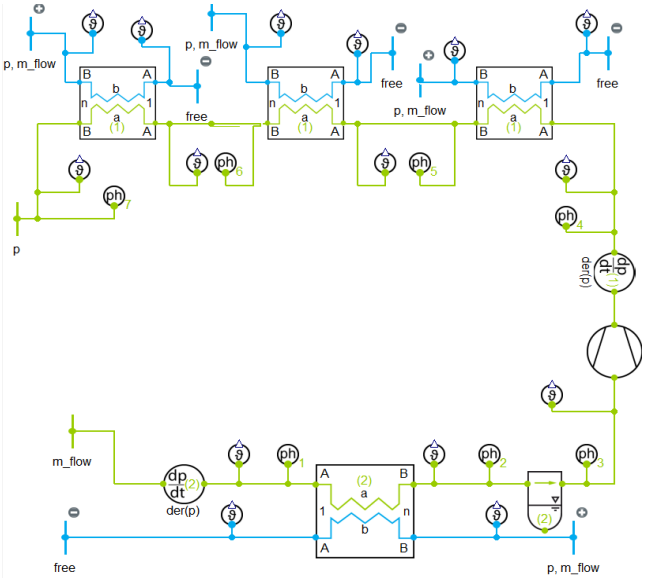

Figure 4.4: *Dymola model with the tripartite gas cooler configuration*

The next step of the modelling was to implement the gas coolers. The first gas cooler to be modelled was the DHW reheater. This gas coolers role is to heat the water to desired hot water temperature of 60-70 °C. Boundaries at the water side of the gas cooler was set to provide constant water mass flow over the reheater. The mass flow rate of water was calculated based on an inlet/outlet temperature of 30/65 °C, with a heat effect of 2,2 kW, at 0,016 kg/s. At the refrigerant side, a constant mass flow boundary was established, providing a CO_2 mass flow rate of 0,025 kg/s. This value was directly extracted from the 90 bar CoolPack reference model. During the gas cooler modelling, the high side pressure was kept constant at a pressure of 90 bar. The space heating gas cooler was modelled with the same refrigerant mass flow and pressure conditions as the reheater. At the secondary side, constant pressure- mass flow boundaries were established, based on an inlet/outlet temperature of 25/35 °C and 2,7 kW heat effect. The third gas cooler, the preheater, was modelled to provide water temperatures at 7/30 °C. The water mass flow rate at the secondary side of the reheater was used for the mass flow at the preheater. This gave a heat effect of 1,5 kW. *Table 4-2* provides an overview of the important modelling parameters of each gas cooler.

Table 4-2: *Overview of the gas cooler parameters*

	Reheat GC		Space heat GC		Preheat GC	
Parameter	**Tube a**	**Tube b**	**Tube a**	**Tube b**	**Tube a**	**Tube b**
Constant Alpha [W/m^{2}K]	3000	1200	3000	1200	3000	1200
Constant Pressure drop [Pa]	0	0	0	0	0	0
Length of coil [m]	3,5	3,5	15	15	14	14
Inner tube diameter [mm]	6	12	6	18	6	12
nCells	10	10	10	10	10	10
Thermal resistance [K/W]	1/4000	1/4000	1/4000	1/4000	1/4000	1/4000
Initialization	LED	LTD	LED	LTD	LED	LTD

4.2.2.4 Closed DHW Circuit, Expansion Valve and Heat Ports

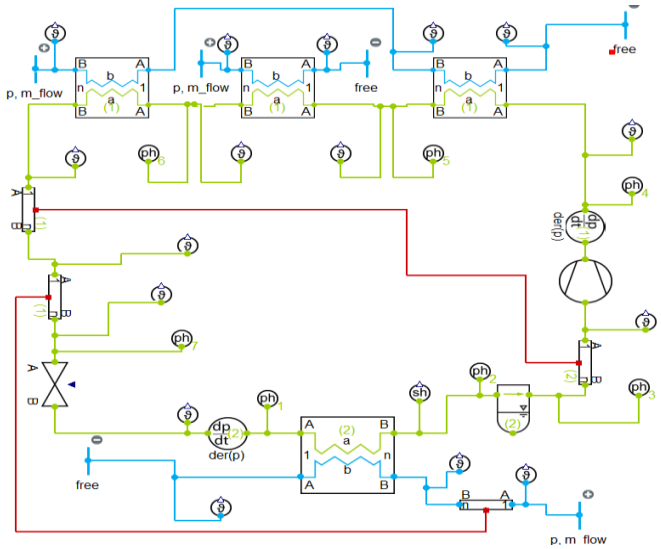

Figure 4.5: *Dymola model with expansion valve and heat ports*

After all the gas coolers was modelled, the preheat- and reheat gas cooler was connected into one circuit. The refrigerant circuit was then closed, with the implementation of the expansion valve. At this point, no control unit was connected to the valve, instead a fixed effective flow area of 0,4e-6 m^2 was used. To prepare for the suction gas heat exchanger and the sub cooler, heat ports were established. The heat ports were initially given the heat transfer model constant AlphaA of 100 W/K, for both the SGHX and the sub cooler. The purpose of the temporarily implementation of heat ports was to observe how the system would react to these heat exchangers before implementing them as components.

4.2.2.5 SGHX and Sub Cooler

The SGHX heat port was replaced by a tube-and-tube refrigerant/refrigerant counter flow heat exchanger, and the sub cooler heat port was replaced by a tube-and-tube.

Brine/refrigerant counter flow heat exchanger (illustrated in *Figure 4.6*). The specifics of these heat exchangers are listed in *Table 4-3*.

Table 4-3: *SGHX and sub cooler specifications*

	SGHX		Sub Cooler	
Parameter	**Tube a**	**Tube b**	**Tube a**	**Tube b**
Constant AlphaA [W/K]	80	80	200	200
Constant pressure drop [Pa]	0	0	0	0
Length of coil [m]	2,3	2,3	6	1
Inner tube diameter [mm]	8	12	4	25
nCells	5	5	5	5
Thermal Resistance [K/W]	1/4000	1/4000	1/6500	1/6500
Initialization	LED	LED	LED	LTD

4.2.2.6 System Completion with Control System

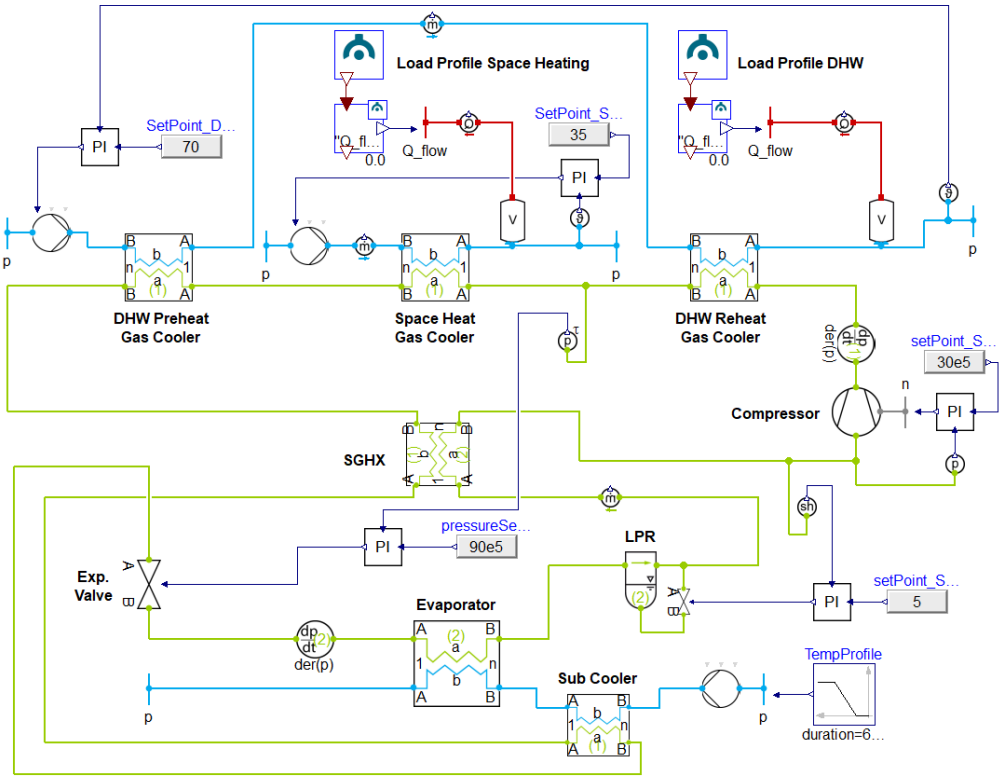

Figure 4.6: *The complete Dymola model with component labelling*

Figure 4.6 shows the finished structure of the model, with illustrative text and hypothetical input values. With the modelling of the refrigerant cycle completed, the control system was implemented. The system consists of a total of five PI-controllers, three on the refrigerant

side and two on the hydronic side (see specifications in *Table 4-4*). The expansion valve was changed from fixed effective flow area, to input defined. A PI-controller (PI-Valve) was connected to the input port of the valve. The control strategy was now to get the expansion valve to operate as a back-pressure valve, regulating the high side pressure through throttling. The PI-controller uses a reference pressure sensor between the reheat GC and space heat GC, along with a set point element. The set point element feeds the regulator with the desired pressure level, which then regulates the back-pressure valve accordingly. The control strategy for the compressor was to actively regulate the low side pressure with within the limits of the operating frequency. A mechanical boundary which enables speed input was implemented to the compressor. The PI-controller (PI-Comp) was set to operate with a frequency range of 35-60 Hz.

An oil return circuit were added to the low pressure receiver. The task of the oil return is to regulate the refrigerant quality to ensure a desired level of superheat. A PI-controller (PI-OR) regulates the valve opening, with a reference superheat sensor placed at the compressor suction line.

A total of three circulation pumps were implemented on the secondary sides of the system. At the hydronic side of the space heater, a variable speed pump was implemented to enable mass flow regulation. A PI-controller (PI-SH) regulates the pump through a reference temperature sensor and an input temperature value. A volume element of 100 litres were implemented to the hydronic line to represent the buffer tank, in which the load profiles were added (Will be further explained in chapter 4.2.3). The same control strategy was implemented for the DHW system. The PI-controller (PI-DHW) regulates the pump to achieve the desired set point DHW temperature. A volume element of 400 litres where added to represent the accumulator tank. The DHW load profile were added to the volume element. Both PI-controllers are set with an activation time of 15 min, in order for the refrigerant cycle to reach system stability before the secondary sides are actively controlled.

At the brine side of the evaporator, a constant speed circulation pump was implemented to ensure mass flow regulation. No control unit were added to this pump, instead input block with scheduled mass flow strategies were utilized. In addition, a bore hole temperature profile element was added in order to simulate changes in brine temperature. This makes it possible to implement a seasonal temperature schedule. The PI-controllers were tuned through testing, inspired by the "Good Gain Method" [31]. The setpoints (input values) to the controllers will vary depending on the type of control strategy or scenario simulated. What input values used during what simulation will be informed in the presentation of the results in chapter 5. A summary of the input equations/algorithms can be found in Appendix C.

Table 4-4: *PI-Controller specifications*

	Controller				
Parameter	**PI-DHW**	**PI-SH**	**PI-Valve**	**PI-Comp**	**PI-OR**
Prop. Gain (k)	1E-4	1E-4	1E-11	1E-7	1E-3
Integrator time (Ti) [s]	10	10	10	15	20
Limits (Operating range)	(0,01-0,1)	(0,01-0,2)	(1E-7–3E-6)	(35-60)	(0-1)
Initial output	0,016	0,06	0,5E-6	55	0,7E-7
Activation Time [min]	15	15	0	0	0

4.2.3 Residential Model

In order to get realistic load profiles for space heating and domestic hot water production, a model of the residential location was created using the IDA ICE software. The following information were used as a basis to develop the house model:

- 3 floors (zones), 288 m^2 total heated area
- Unheated basement
- 70 mm massive wood structure with 200 mm isolation
- 3 layer, well insulated windows
- A total of 9 occupants
- Climate data for Trondheim
- Set point room temperature of 21 ^oC

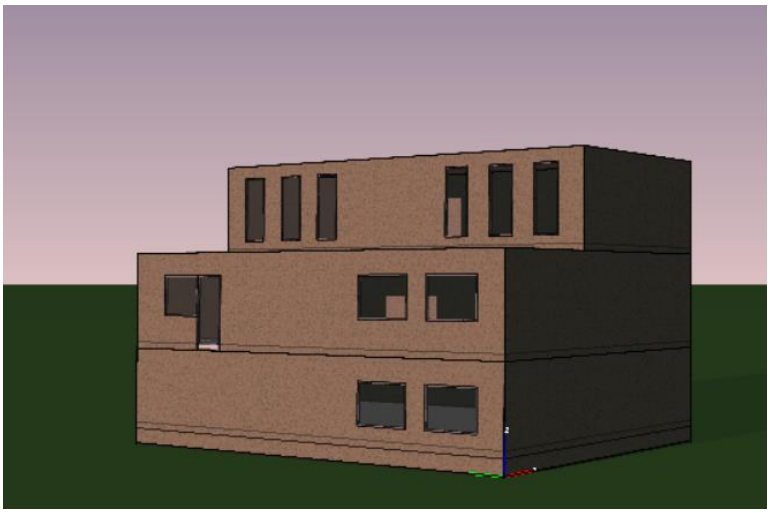

Figure 4.7: *3D visualization of the residential model developed in IDA ICE*

Figure 4.7 is the model of the residential location in 3D view. Window placement, building shape and orientation is made to represent the actual building and location as accurately possible. Structures such as balconies and appendages are neglected. U-values of walls

and windows are 0,21 and 1,1 W/m^{2}K respectively. In order to simulate the heat demand for the given building, the mode "ideal heater" has been used. This gives the necessary heat energy required to maintain the set point temperature of 21 ^{o}C in all zones. An occupancy schedule for all floors has also been implemented to account for internal heat gains, along with lightning and technical equipment. In addition, a schedule for domestic hot water consumption was made. The DHW schedule was partly made by talking to the occupants, and partly by use of statistics for average consumption per person. There is no mechanical ventilation in the building, so a schedule for window opening and window shading had to be made to avoid overheating during the warmest months.

The load profiles developed from the IDA ICE model were extracted into excel CSV-files in order to be useable for Dymola. It was then implemented in the "TILfilereader"-blocks, an import block and a translator block, for both the DHW and space heating hydronic system. The load profile was then connected to a heat port as input values, extracting heat (Q-flow) in Watts from the buffer tanks (volume element). *Figure 4.8* illustrates this model set-up.

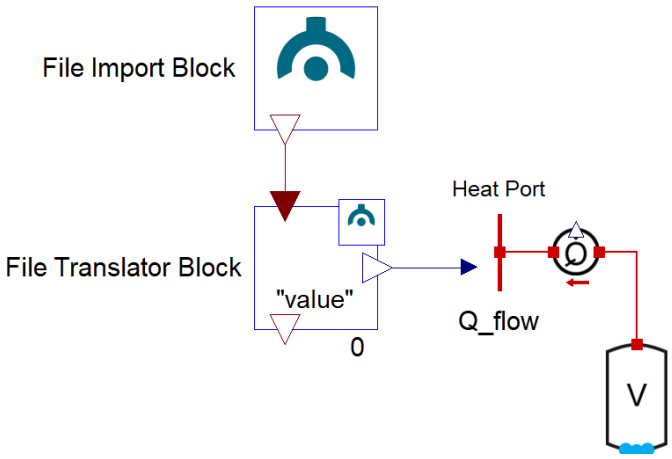

Figure 4.8: *Load/User profile import in Dymola*

4.3 Experimental Phase

The other main objective of this master project was to test, optimize and prepare the CO_2 heat pump for moving to a residential location in order to get operational data from a real-life operation situation. During the experimental phase, the heat pump was located at WINNS AS locations at Strindheim in Trondheim. The heat pump was set up in their test rig, which enabled testing in a controlled environment with every part of the system monitored. Initial test sessions were conducted, to get an overview of the current state of the heat pump and plan what needed to be done.

4.3.1 Initial Testing

Before the initial testing, 3,8 kg CO_2 refrigerant were filled into the system. The test rig was providing a water temperature of 15,5 °C with a mass flow of 0,2 kg/s to the evaporator. The space heating gas cooler were provided 0,035 kg/s water with a temperature of 15 °C. The water temperature at the secondary side of the preheating gas cooler were 9 °C at a mass flow of 0,015 kg/s. *Figure 4.9* shows the heat pump in the test rig during the initial testing.

The following discoveries were made:

- Several temperature sensors were appearing off.
- Trouble with pressure build-up, even with valve almost closed.
- Compressor shutting off due to lack of superheat of refrigerant.
- The preheater provided little to no heating of DHW before entering the reheating gas cooler.
- Sub-optimal configuration on the manual bypass valves at the SGHX and sub-cooler.

Figure 4.9: *The heat pump in the test rig during initial testing*

4.3.2 Troubleshooting

The temperature sensors were the first priority in the troubleshooting process, as several are directly involved in the system control. There is a total of 16 sensors in the system, tagged from RT001 to RT016 (see *Figure 4.10*), 8 on the secondary sides and 8 on the refrigerant side. After the initial testing there were 7 sensors in particular that raised suspicions:

- Sensor RT002 – Located between SGHX and compressor (CO_2)
- Sensor RT003 – Located between LPR and SGHX (CO_2)
- Sensor RT004 – Located between reheating GC and space heating GC (CO_2)
- Sensor RT008 – Located between sub-cooler and expansion valve (CO_2)

- Sensor RT011 – Located at the preheating GC secondary side inlet (Water)
- Sensor RT012 – Located at the preheating GC secondary side outlet (Water)
- Sensor RT013 – Located at the reheating GC secondary side inlet (Water)

To investigate and verify all sensors, a physical inspection was done, utilizing freeze spray. Sensor RT002 is involved in the control of the compressor as the reference temperature for saturation pressure to ensure sufficient superheat before entering the compressor. As a safety measure, the compressor shuts off at too low superheat values. This happened several times during the initial testing. It was noted that RT002 and RT003 always displayed the same temperature, and after inspection it was determined that a double tagging in the automation software had occurred. The same issue was discovered with sensor RT004 and RT008. These errors were corrected in the PLC-software.

At the secondary side, sensor RT011, RT012 and RT013, the issue did not seem to be a tagging issue as all sensors reacted to the freezing spray. After a physical inspection of the piping, a fault in the positioning of the preheater bypass valve was discovered, causing the cold city water to mix with preheated water before entering the reheater.

The pressure build-up issue was after a while identified as an expansion valve issue. As illustrated in *Figure 3.1* (Chapter 3.1), the heat pump has two expansion valves connected in parallel. It was discovered that some refrigerant was leaking through the manual expansion valve, causing the automatic expansion valve to struggle with keeping the set point pressure. This issue was fixed manually.

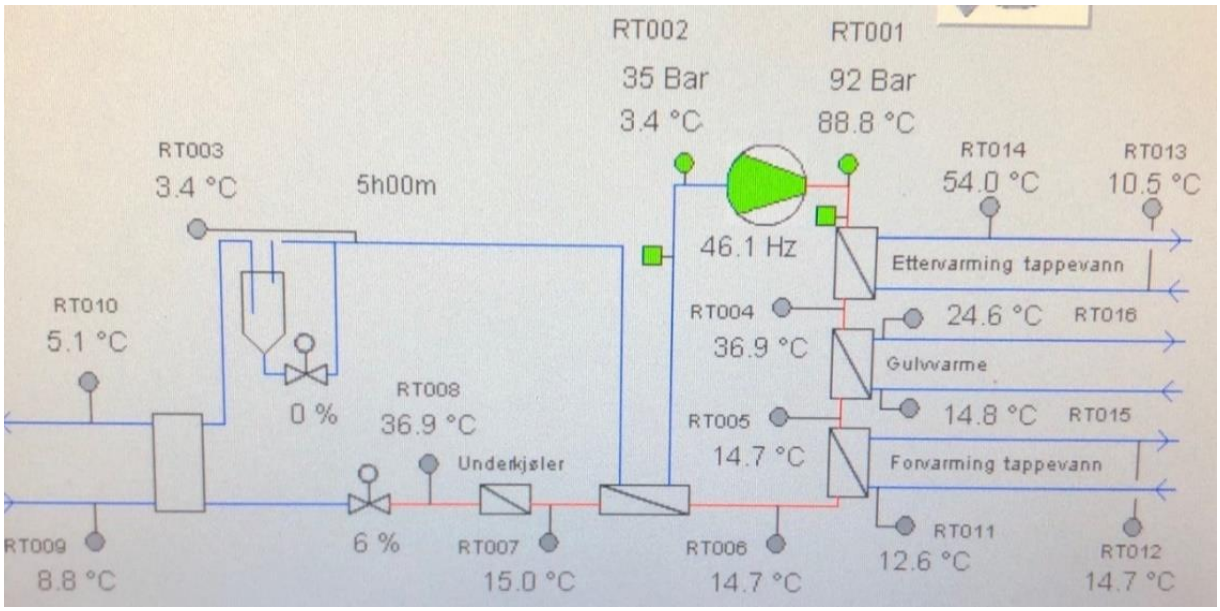

Figure 4.10: *Picture of the PLC monitor screen, with temperature sensors from RT001-RT016, during a test session.*

4.3.3 Instrumentation and Equipment

As a part of enabling optimized operation of the CO_2 heat pump, several instrumentation strategies were implemented. The control of the CO_2 happens through a programmable logic controller (PLC). The PLC has built in relays for both digital and analog signals. All sensors, transmitters, switches, valves etc. are physically connected to the relays of the PLC. This makes it possible to easily program, monitor and alter the control of the heat pump. During the test phase, there was installed three energy meters and a CO_2 mass flowmeter. The energy meters were added to the PLC in order to monitor important parameters such as energy- and power use, and for calculation of COP. This section will contain a description of the equipment implemented.

4.3.3.1 RHEONIK Coriolis Flowmeter

The RHOENIK Coriolis RHE08 flowmeter (RHM) were implemented to monitor the CO_2 mass and mass flow. The RHM consists of one flow sensor and on transmitter. The remote unit is connected to the sensor via a single multi-conductor cable. It is beneficial to install the flow sensor at the lowest practical level of the system, to avoid gas bubbles to cluster on the sensor. In the CO_2 heat pump, the sensor is placed between the sub cooler and the expansion valve. The RHM uses analog signals, in a range of 4 – 20 mA, whereas a given signal represents a flow rate. During calibration, the Dymola model was in part used for reference mass flow rates in order to get accurate values. *Figure 4.11* shows the remote unit of the RHM during calibration. The RHM were also added to the PLC.

Figure 4.11: *The Rhoenik RHE08 remote unit during calibration*

4.3.3.2 Kamstrup MULTICAL 603

The Kamstrup MULTICAL 603 is an energy meter that can handle mixed fluids. It has a temperature range of -40 °C to 140 °C, with an accuracy of ±(0,15 + 2/ΔT)%. For that reason, it was chosen as the preferred energy meter for the borehole (brine) side. It can handle flows from 0,6 to 15 000 m^3/h. The communication module for the MULTICAL 603 is M-Bus. The MULTICAL were connected to the inlet and outlet of the borehole, with a mass flow and two temperature sensors, after the heat pump were moved to the residential location.

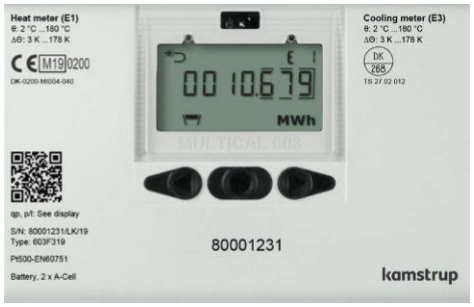

Figure 4.12: *Display of the Kamstrup MULTICAL 603*

4.3.3.3 Kamstrup MULTICAL 403

The MULTICAL 403 is an energy meter that can be implemented in most hydronic systems. It consists of a flow sensor, two temperature sensors and an integrated calculation software. The temperature range of the MULTICAL 403 is 2 °C to 180 °C, with an accuracy of ±(0,4 + 4/ΔT)%. The MULTICAL 403 also communicates with the PLC via M-bus. There were implemented two M403's, one for the space heating and one for the total DHW heating (preheater and reheater combined). These were mounted during the test phase.

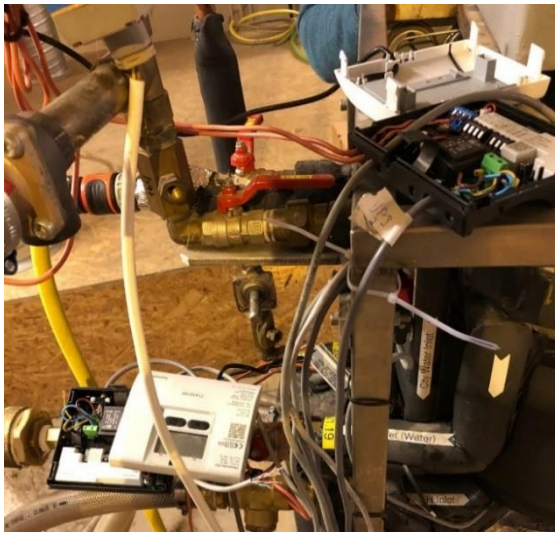

Figure 4.13: *The two MULTICAL 403 energy meters during mounting*

4.3.4 Final Testing

Before the heat pump was moved to residential location, a final test session was done to ensure proper operation. The heat pump was once more connected to the test rig. The goal of the final testing was to get answers to the following questions:

- Are the problems discovered at the initial testing fixed?
- What are realistic set-point temperatures for the DHW and space heating water?
- How high does the CO_2 compressor outlet temperature get? (Risk of boiling when there is no DHW production?)
- How is the overall performance and is it ready to operate at the residential location?

The heat pump was operating for about 2,5 hours in the test rig under constant supervision. None of the previous troubles occurred during this test session. *Figure 4.14* shows the PLC screen during testing after the system had reach approximate steady state conditions. The DHW outlet temperature reached just above 70 °C, while simultaneously heating the space heating water from about 27 to 39 °C. During the 2,5 hours of operation, the maximum CO_2 temperature observed was 91,2 °C at 93 bar. The test session gave satisfactory answers and the heat pump were operating properly. It was therefore decided that it was ready to be moved and operated at the residential location.

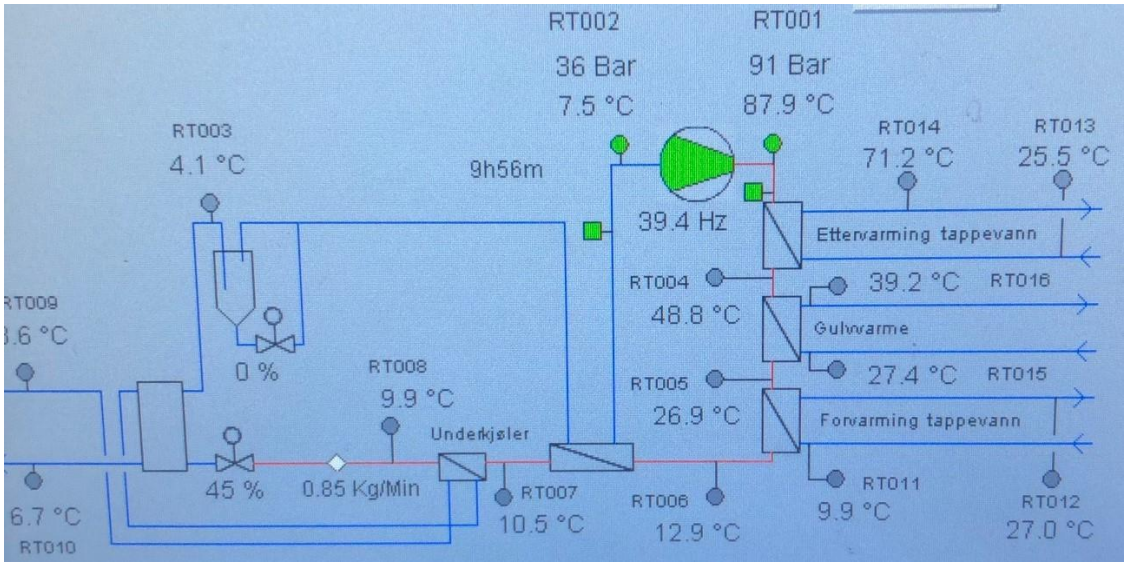

Figure 4.14: *The PLC screen during the final test session*

4.3.5 Setup at Residential Location

After the final testing and preparations, the heat pump was moved to the residential location. It was set up in the basement and connected to hydronic- and borehole systems. *Figure 4.15* shows the heat pump implemented in the basement.

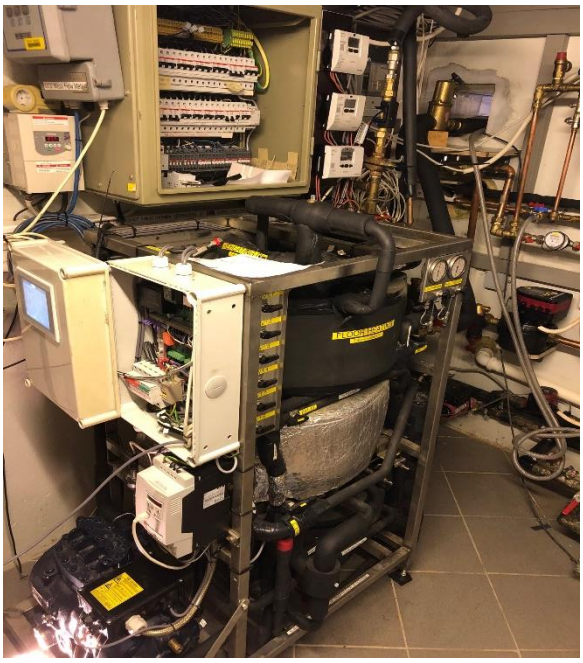

Figure 4.15: *The heat pump implemented at the residential location*

4.3.5.1 Data Logging

The data logging was carried out via an extern computer, connected to the same modem as the PLC of the heat pump. The IP-addressee of the PLC were implemented in order to establish communication. Nortend, a software developed at Winns AS, were utilized for the data logging. The software contains a database of all communicating sensors and equipment of the PLC. The sensors of interest were extracted into the logging setup, where scaling, units and time steps were defined. The software offers both live graphing as well as CSV-file exportation option. The following sensors were imported for logging:

- All temperature sensors (RT001 – RT016) + (RT301-RT315)
- Backpressure valve and oil return valve position (0 – 100%)
- High- and low side pressure sensors
- Energy meters
- Compressor speed (frequency) and power
- Degree of superheat
- Suction gas saturation temperature
- CO_2 mass flow meter

A guide of the logging setup can be found in Appendix E.

4.3.5.2 Control Strategy

Several control strategies were planned with the goal of getting a well-functioning heat pump system without needing much interaction from the occupants. For control of the supply temperature of the floor heating system, a linear function generating the desired temperature should be implemented in the PLC. The bandwidth of the supply water temperature was set 25 °C to 35 °C, where an outdoor temperature (RT307) of 5 °C generates a setpoint of 28 °C and below -5 °C generates maximum supply temperature of 35 °C. If set-point temperature is not reached withing 2 hours, a 240V signal activates the peak load element in the buffer tank.

The temperature regulation of the DHW from the reheating gas cooler will be controlled through a 0-10V signal to the motor valve (SC001) regulating the mass flow, with a 70 °C setpoint. With fully loaded accumulator tanks, a 0V signal closes the valve. The circulation pump (JP003) is controlled through a 240V on/off signal. The pump starts when the temperature sensor (RT306) at the bottom of the second last tank is at 30 °C. The shut off signal is given when the temperature sensor (RT314) at the bottom of the first tank (where city water is fed) reaches 25 °C. The peak load element is activated with a 240V signal when the temperature sensor (RT302) in the middle of the last tank gets below 45 °C. Should the DHW temperature (RT300) entering the gas coolers get higher than CO_2 temperature at the space heating GC outlet (RT005), the three-way valve (SC002) will bypass the preheating GC. This is important to avoid heating of CO_2 in the last gas cooler.

To avoid boiling in piping during periods of no DHW production, different pressure operation setpoints will be implemented. The operating bandwidth during combined mode heating or just DHW heating is 90-95 bar. With fully loaded accumulator tanks, and only space heating demand, the operating pressure is 78-82 bar. The frequency range is set to 35-60 Hz.

The speed of the borehole pump (JP004) is regulated with a 0-10V signal. When the temperature between the borehole inlet (RT009) and the evaporator (RT003) is 8 K, the pump runs on minimum RPM. At higher temperature difference, the pump will speed up.

To ensure system safety, several operating limits is implemented to the PLC. If these limits is reached, the compressor will automatically be shut off. The high side pressure limit is 105 bar, while the low side pressure limit is reached when the saturation temperature of the CO_2 gets -25 °C or below. The shutoff criteria for superheat is set to 1K for the lower limit, and 35K for the upper limit.

A full piping and instrumentation diagram (P&ID) with sensors and equipment of the whole system is showed in *Figure 4.16*, on the next page.

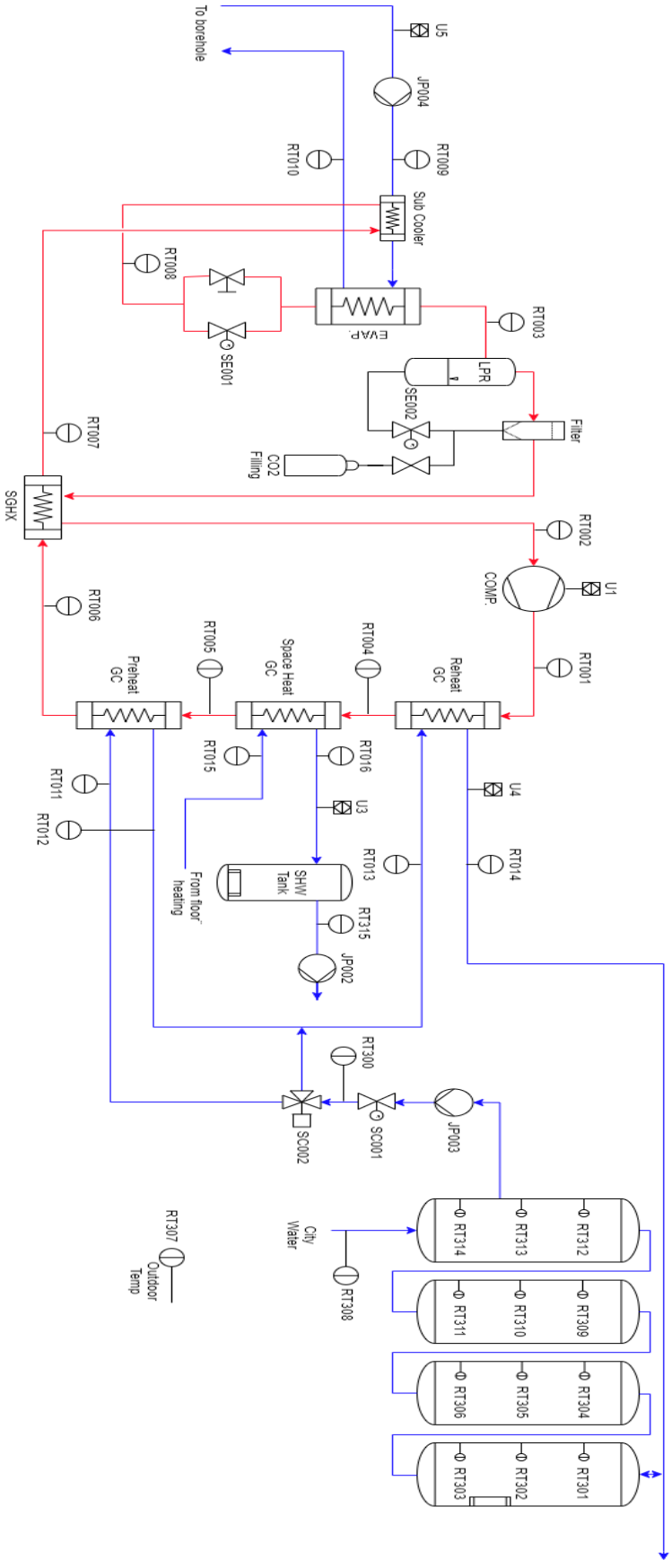

Figure 4.16: *P&ID of the residential heat pump system*

5 Results

In this chapter, the results from the Dymola simulations and the operational data will be presented. The chapter starts off with a sensitivity analysis, where the model and logged data from the real heat pump is compared. The model will then be further used as a tool to analyse the system solutions and performance. A presentation of logged data from a week of operation at the residential location then follows. Important factors such as system performance, COP, delivered heat, compressor performance and optimum pressure will be analysed.

5.1 Model Validation and Simulation Analysis

As a tool to determine the validity of the Dymola model, a sensitivity analysis of both the model and the operational heat pump has been performed. The operational testing and measuring were done at the residential location, with the purpose of recreating the operating conditions in the model to have a solid foundation for direct comparison. The model validation is focused around the CO_2 refrigerant cycle performance, and for that reason load profiles from IDA ICE has not been implemented. Instead the inlet boundary conditions at the secondary sides has been implemented in such a way that it corresponds with the conditions during the operation of the heat pump. The raw data from both the logged data and the model has been extracted as CSV files for direct comparison. The Nortend logger has 60 logging points per hour, while the Dymola model has 720.

The following secondary side conditions formed the base for the operational- and model sensitivity analysis:

- **DHW inlet**: Flow rate of 45 l/h and quasi-permanent temperature of 9,5 ^{o}C (± 0,6 ^{o}C)
- **Space heating water inlet**: Flow rate of 405 l/h and quasi-permanent temperature of 22,5 ^{o}C (± 0,5 ^{o}C)
- **Evaporator brine inlet**: Flow rate of 665 l/h and an initial temperature of 6,4 ^{o}C with an approximate linear temperature drop of 0,4 ^{o}C over the timespan of the measurements.

Following the model validation, system characteristics during different operating modes simulated in Dymola and simulations with IDA ICE load profiles will be presented.

5.1.1 Comparison of Sensitivity Analysis

The sensitivity analysis was performed during a time span of 60 minutes. The essence of the analysis was to observe and compare the system changes, as the evaporator pressure was lowered until a level in which the compressor reached its maximum frequency (60 Hz), with a super heat setpoint of 5 K. The high side pressure setpoint was set to 92 bar.

Figure 5.1 and *Figure 5.2* shows the compressor speed and the corresponding evaporator pressure level of the model and the real heat pump compared. The modelled compressor starts at the bottom of the operating frequency bandwidth at 35 Hz. The real compressor starts at a slightly higher frequency, at 38,5 Hz. The model can be observed reacting quicker to the input signals, while the real compressor has a delayed reaction. Both compressors reach the maximum speed of 60 Hz after about 38 minutes. The evaporator pressures in *Figure 5.2* shows slightly higher oscillations for the logged data. During full speed in both compressors, the pressure level of the model can be observed being consistently between 0,2 to 0,6 bar lower than the real heat pump.

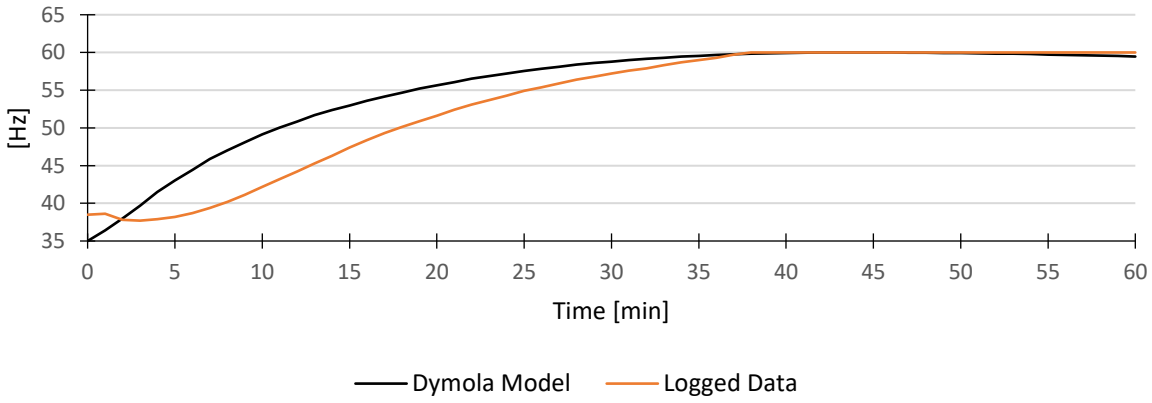

Figure 5.1: *Comparison of the compressor speed (Frequency)*

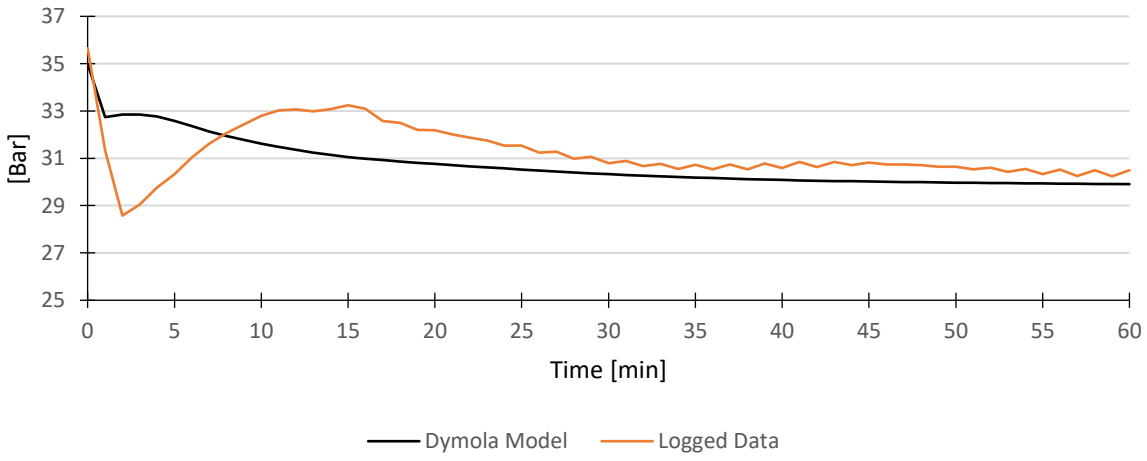

Figure 5.2: *Evaporator pressure level comparison*

The degree of refrigerant superheat at the suction line during the sensitivity analysis is showed in *Figure 5.3*. The model quickly rises to a super heat level just below the setpoint of 5 K, before it drops about 1 K. The super heat level stabilizes after about 35 minutes, just above the setpoint. The logged data for the real heat pump shows a slower rise than the model, and oscillates between 3 K to 5 K, with a trendline of about 4 K.

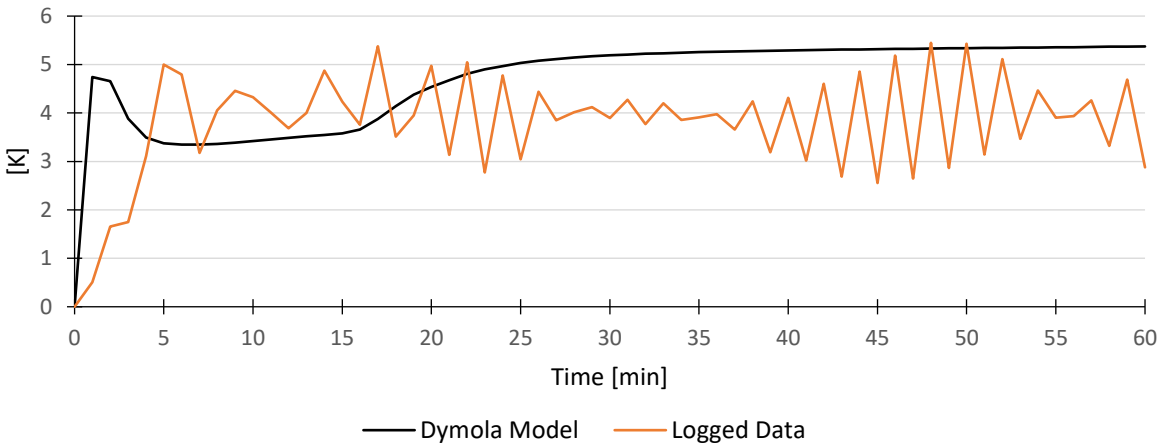

Figure 5.3: *Level of suction gas superheat*

Figure 5.4 shows the mass flow of CO_2 refrigerant. The initial mass flow rate can be observed being substantially larger for the Dymola model. From about minute 15 to 30, the mass flow of both the model and the real heat pump is nearly identical. The last 20 minutes of the analysis, a deviation of about 0,0009 kg/s between the model and the logged data can be observed.

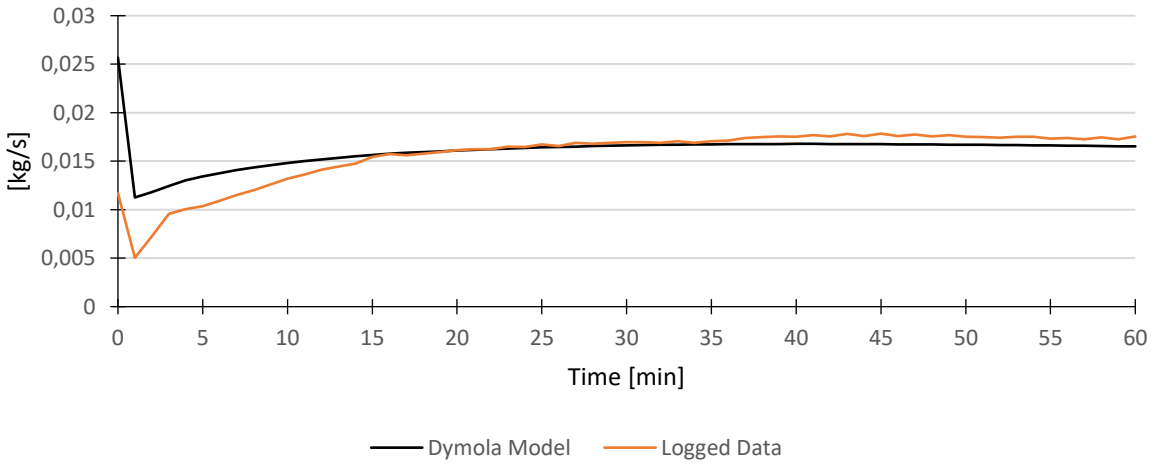

Figure 5.4: *Comparison of CO_2 refrigerant mass flow rate*

Figure 5.5 and *Figure 5.6* shows the high side pressure level and the discharge CO_2 temperature respectively. The Dymola model reaches the setpoint of 92 bar in about 1 minute, from an initial pressure level of 80 bar. The setpoint is kept constant the rest of the analyse period. The logged data shows a quick pressure rise, from an initial pressure level of 57 bar. A small overshoot can be observed from about minute 5 to 17. The pressure is then kept at 92 bar, with only minor oscillations. I good correlation between model and measured discharge CO_2 temperature can also be seen in *Figure 5.6*. The temperature of the model expectedly rises quicker, corresponding with the quick pressure rise. The last 30 minutes, the measured temperature stabilizes about 0,5 to 1 °C above the model temperature.

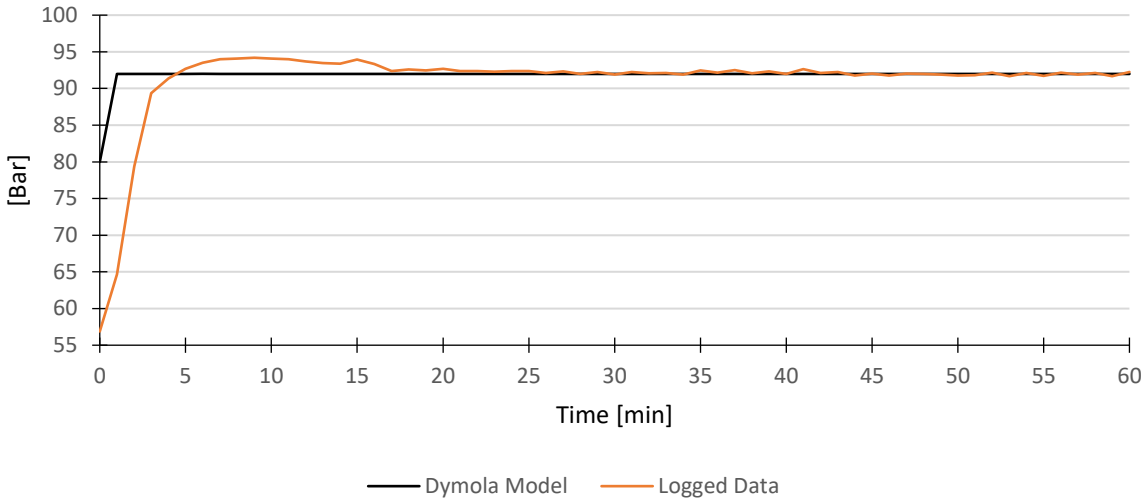

Figure 5.5: *High side pressure level compared*

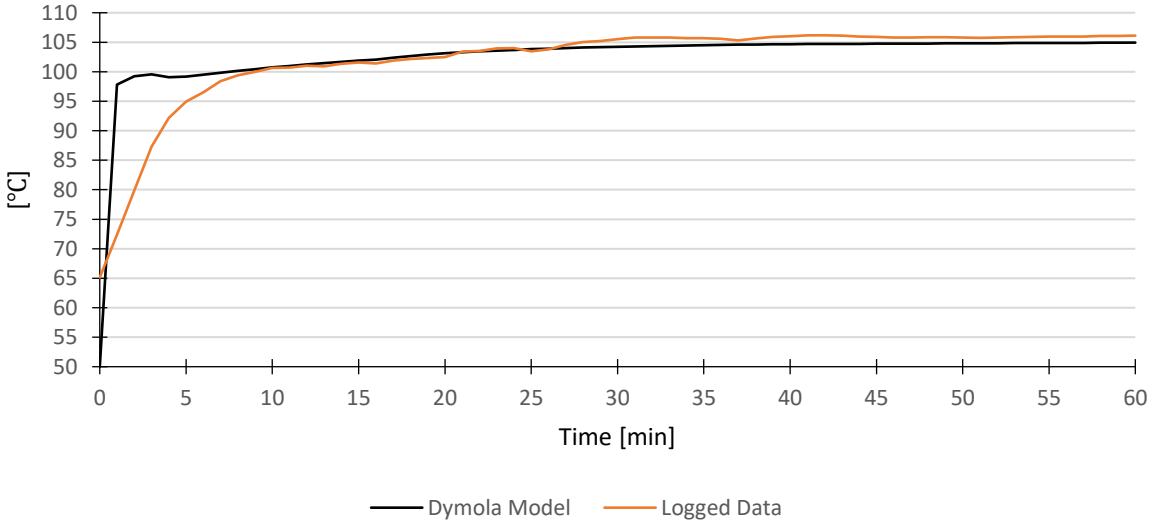

Figure 5.6: *Compressor discharge CO_2 temperature*

The temperature profile of the CO_2 at the tripartite gas cooler outlet (preheater outlet) is shown in *Figure 5.7*. The logged values peaks at about 19 °C at ca. 1 minute. The peak of the model is at initiation, at just above 16 °C. The deviation between model and logged values is about 1 – 1,5 °C up until minute 40, after which the correlation increases.

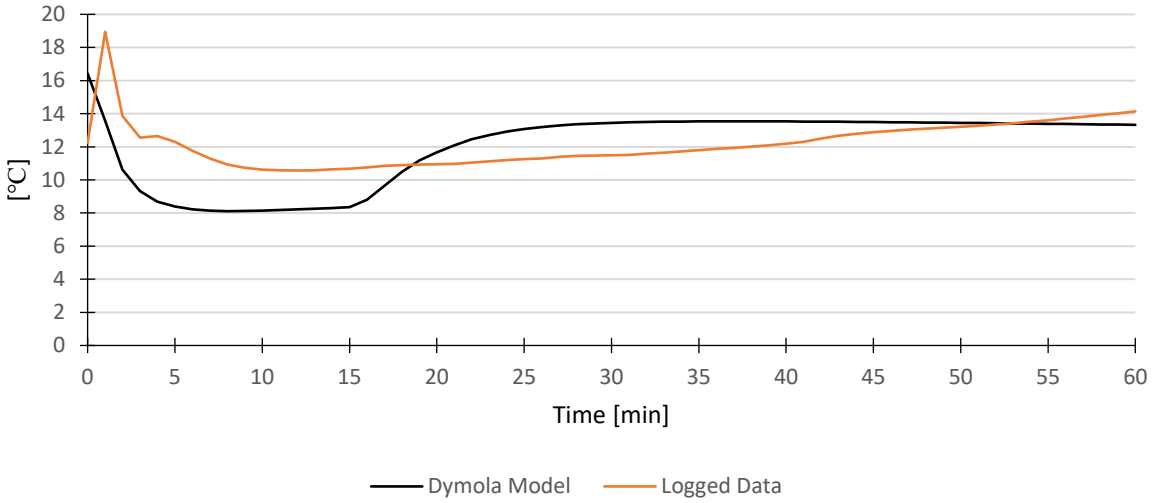

Figure 5.7: *Gas cooler outlet temperature of CO_2 refrigerant*

5.1.2 System Characterists and Performance

The Dymola model has been used to investigate system characteristics and performance during different operating setpoints and conditions. The following secondary side conditions were utilized during all simulations in chapter 5.1.2:

- **DHW inlet**: Constant temperature of 7 °C, with active mass flow regulation to achieve setpoint of 70 °C.
- **Space heating water inlet**: Constant temperature of 25 °C, with active mass flow regulation to achieve setpoint of 35 °C.
- **Evaporator brine inlet**: Constant temperature of 6 °C and constant brine flow rate of 665 l/h.

5.1.2.1 Optimum High-side Pressure Analysis

To observe how the system characteristics behaves during variable high-side pressure control, a ramp input was implemented to the back-pressure valve. The ramp is activate after 10 minutes gradually increasing the pressure from 80 to 100 bar in a time span of 30 minutes. With this control strategy, the compressor was set to operate at maximum frequency of 60 Hz.

Figure 5.8 shows the heat rejection (presented with negative values) of the three gas coolers, with the pressure level as a reference graph above. At about 5 minutes, a change can be observed for all three gas coolers, especially the space- and reheater. This can be tied to the activation of the PI controllers for the secondary side circulation pumps. Another interesting observation is the behaviour of the gas coolers during pressure increase. With increasing pressure and discharge temperature, the reheating gas cooler gradually "takes over" the heating capacity. It should be noted that the total heating capacity of the gas coolers increases with increasing pressure, but not significantly. The total capacity at 80 bar is about 4,25 kW, while at 100 bar it's about 4,77 kW. At about 27 minutes, there is a cross section point between the space- and reheating gas cooler in which the capacity is equal. The pressure at this point is about 91,5 bar, which could indicate a pressure optimum for combined mode operation with equal demand for both space heating and DHW.

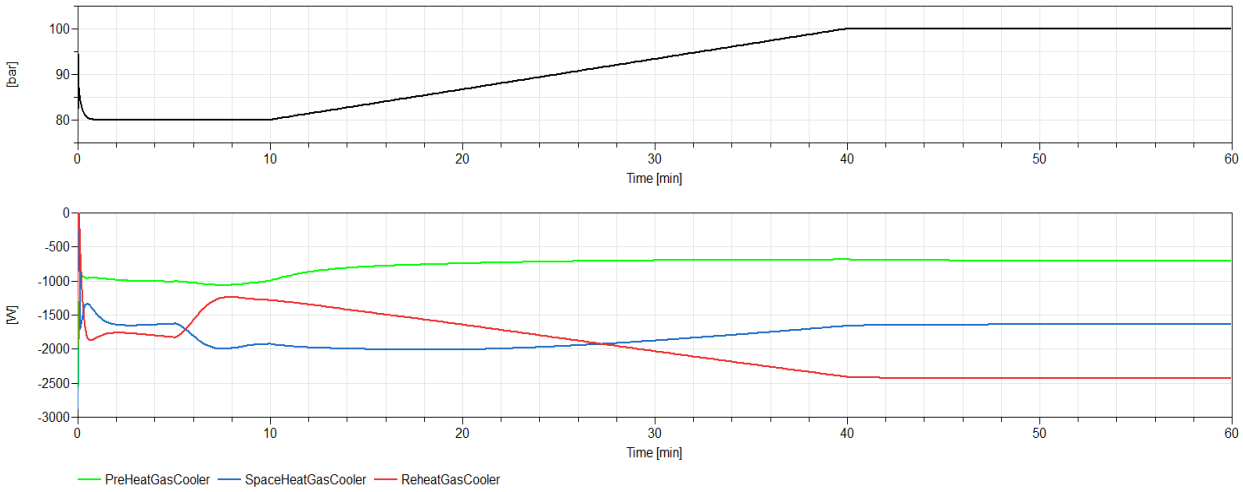

Figure 5.8: *Gas cooler heat rejection [W] during variable high-side pressure*

The COP of the modelled heat pump during pressure increase is shown in *Figure 5.9*. The highest COP value observed is 4, at 80 bar. This value however appears before the circulation pump PI-controllers is activated, meaning the heat pump system is not fully operational at the time of the peak COP. A gradual decrease in COP can be observed as the pressure is increased. It settles at 3,4 at 100 bar pressure. It is not a linear relationship between pressure increase and COP decrease, but the graph illustrates that the increase in heating capacity is to a larger degree coming from compressor work rather than from the evaporator. This is logical, as the compressor is working it maximum frequency (60 Hz) and is not able to lower the evaporator pressure significantly. At the interesting pressure level of 91,5 bar, the COP is 3,56.

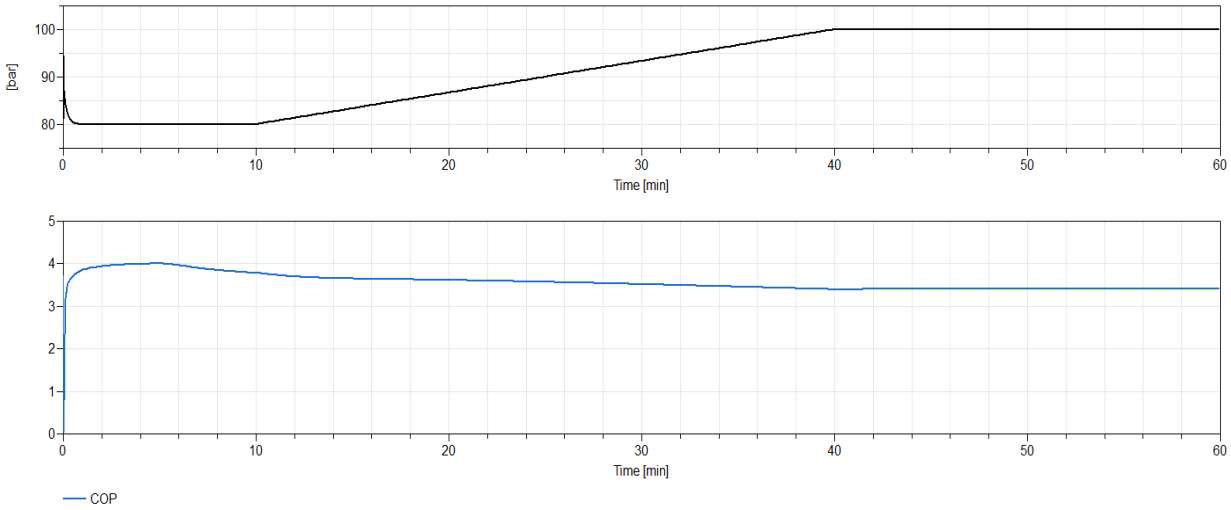

Figure 5.9: *Graph showing the COP behavior during pressure increase*

Figure 5.10 shows the heat exchange of the suction gas heat exchanger and the sub cooler during high-side pressure increase (The sign difference (+/-) is due to the predetermined flow direction in Dymola). Some oscillations the first 5 minutes of the simulation can be observed, as the system stabilizes. The peak heat exchange occurs at about 82 bar for both the SGHX and sub cooler. The graph also indicates a proportional relationship, with similar reaction pattern, but the sub cooler being more sensitive to pressure changes. This could be explained by the sub-cooler being downstream from the SGHX, experiencing an amplified effect. As the pressure increases, and the pinch-point is moving closer to the tripartite gas cooler outlet, the heat exchange is decreased in both heat exchangers. This is reasonable, as the temperature of the CO_2 is lower at the gas cooler outlet giving a lower LMTD in both the SGHX and the sub cooler.

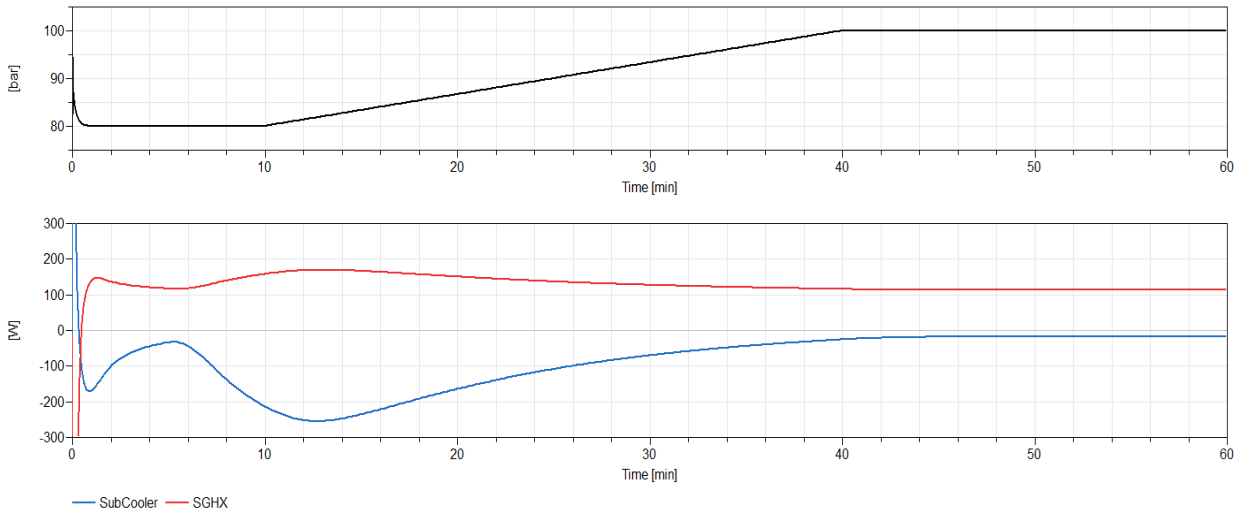

Figure 5.10: *SGHX and Sub Cooler heat exchange [W] during pressure increase*

Table 5-1 is an overview of instantaneous values of the most important parameters at three main pressure levels during the simulation. The complete set of continuous graphs for all the parameters presented in this table can be found in Appendix D.

Table 5-1: *Parameter comparison at three main pressure levels*

Parameter	**@ 85 bar**	**@ 90 bar**	**@ 95 bar**
Evaporator pressure [bar]	29,71	29,55	29,49
Evaporator effect [W]	3451,2	3484,3	3498,8
Compressor shaft power [W]	1191,5	1254,4	1335,8
Preheating GC effect [W]	834,5	758,5	727,3
Space heating GC effect [W]	2008,2	1960,3	1823,5
Reheating GC effect [W]	1548,4	1849,8	2140,7
Total heating capacity [W]	4391,1	4568,3	4691,5
SGHX effect [W]	147,4	128,5	118,5
Sub cooler effect [W]	163,5	80,4	38,1
Discharge gas temperature [°C]	98,7	103,3	108,7
Temperature approach [K]	7,9	5,07	3,6
System COP	**3,69**	3,61	3,51

5.1.2.2 Hot Water Production

The amount of hot water produced, in combined mode heating, at different setpoint pressure levels has been investigated. Three simulations with high-side pressure of 85 bar, 91,5 bar and 100 bar during a 24 hour period has been performed. In all simulations, the compressor has been running on 60 Hz. *Figure 5.11* shows the amount of 70 °C domestic how water (DHW) produced at the three different setpoints. The highest amount DHW produced were at 100 bars, with 1027,6 litres, at an average COP of 3,4. The 91,5 bar high-side setpoint produced 881,12 litres, with an average COP of 3,57. At 85 bar high-side pressure, least DHW were produced, with 728,23 litres. In return this setpoint achieve the highest average COP of 3,65.

The amount of 35 °C space heating water (SHW) produced is shown in *Figure 5.12*. The 100 bar setpoint produced the least amount of SHW, with 3388,9 litres. This is significantly less than the 91,5 bar setpoint which produced the most, at 3945,3 litres. The 85 bar produced 3695 litres, also well above the amount produced at 100 bar. These results correspond well with the GC heat rejection findings presented in *Figure 5.8* in chapter 5.1.2.1.

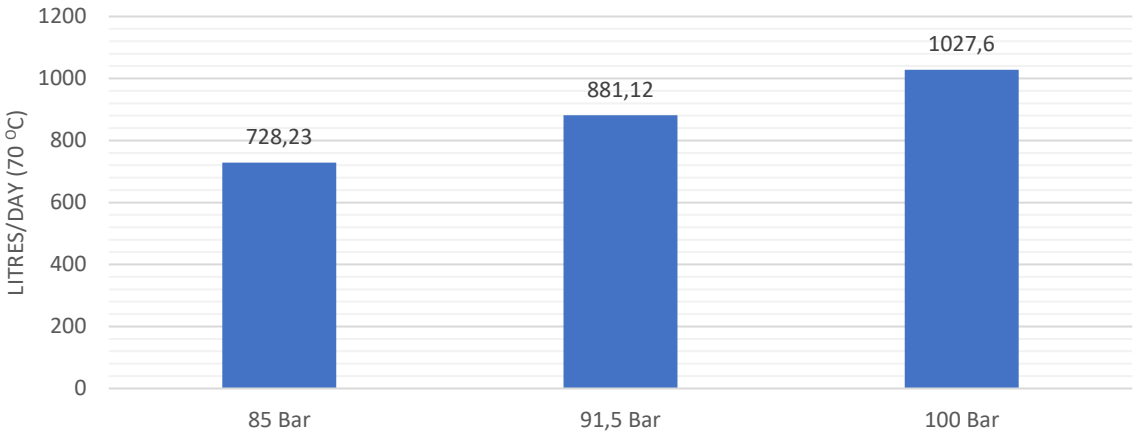

Figure 5.11: *Amount of DHW produced in a 24-hour period at different pressure setpoints*

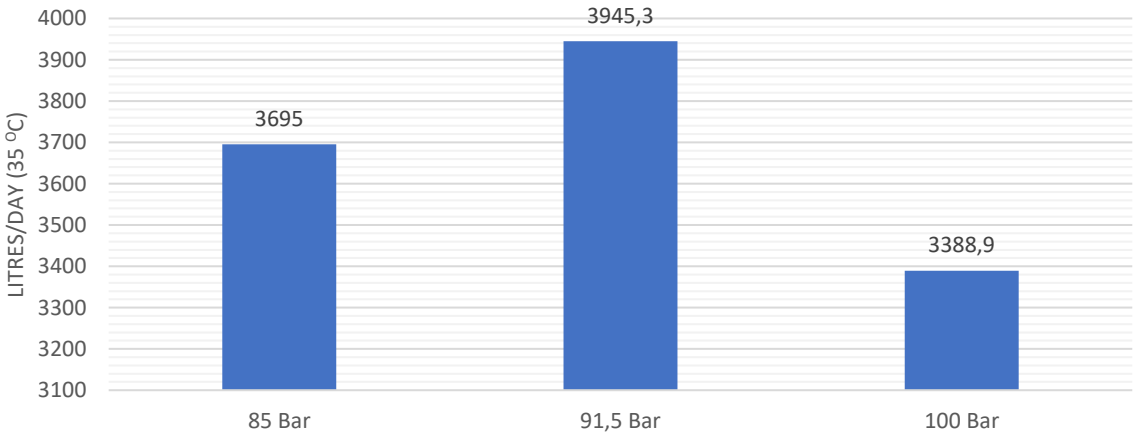

Figure 5.12: *Amount of SHW produced during a 24-hour period at different pressure setpoints*

5.1.3 Simulations with IDA ICE Load Profiles

Load profiles from the residential model created in IDA ICE has been implemented to the model to simulate realistic operating conditions. Three different operating scenarios has been recreated. One is a winter simulation, with continuous space heating demand as well as DHW demand. The other is a summer scenario, with no space heating demand, but normal demand of DHW. The last scenario is a fall vacation scenario where the occupants are not present in a week, causing no DHW demand. A moderate demand of space heating is however present. These cases will cover the three plausible operation modes of the heat pump; combined mode heating, space heating mode and DHW heating mode.

5.1.3.1 Combined Mode

A week in late February has been simulated in IDA ICE, along with a DHW scheduled demand. The control strategy during this simulation, is high-side pressure regulation dependent the demand. The heat pump is to operate at 92 bar as long as the DHW tank temperature is below 65 °C. If the temperature is 60 and above, the pressure setpoint is 82 bar. The compressor is working on maximum frequency as long as the setpoints in both buffer tanks are not reached.

Figure 5.13 shows the IDA ICE space heating profile compared to the delivered heat from the space heating gas cooler. The space heating gas cooler is working on full capacity, around 2 kW, but is not able to cover the heating load alone. The small oscillations in heat capacity which can be observed for the space heating GC is due to the pressure setpoint changes, between 82 and 92 bar.

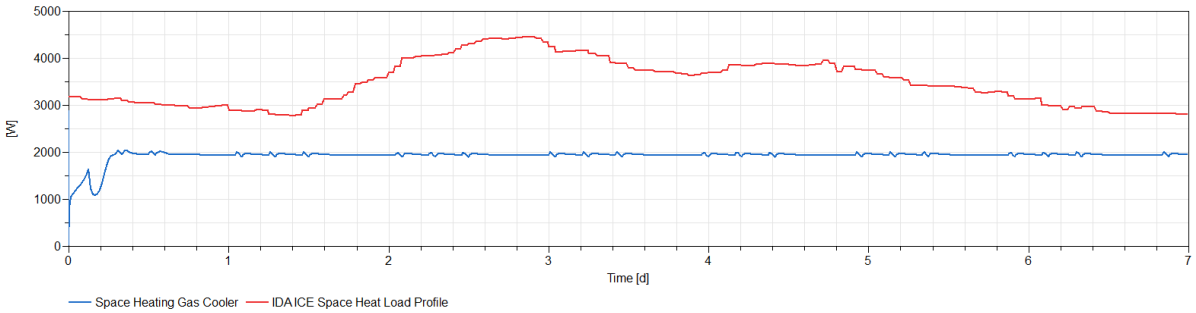

Figure 5.13: *The space heating demand vs gas cooler heat rejection*

The total heat delivery from the pre- and reheating gas coolers vs the scheduled DHW load profile is shown in *Figure 5.14*. In this graph, the oscillations due to changing in pressure setpoint can be easily observed. The heat pump is able to cover the scheduled DHW demand during this period. The two gas cooler is delivering between 2,35 kW to 2,64 kW in total, depending on pressure level.

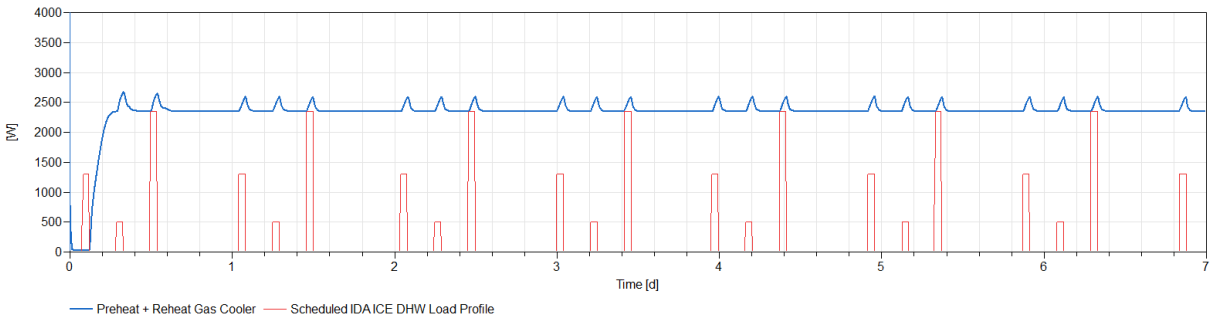

Figure 5.14: *DHW demand vs gas cooler heat rejection*

Figure 5.15 shows the achieved temperatures of both the DHW and SHW tanks and their respective setpoints. As illustrated in the graph, the heat pump is able to maintain the temperature of the DHW around the setpoint of 65 °C throughout the week. As the temperature drops below 65 °C, the pressure increases in order to maintain the setpoint temperature. The quick reloading of the DHW indicates that this control strategy is working as intended. The temperature of the SHW however falls well below the setpoint, and the heat pump is not able to cover the load without the peak load element. The average COP during this simulation was 3,58, peaking at 3,62.

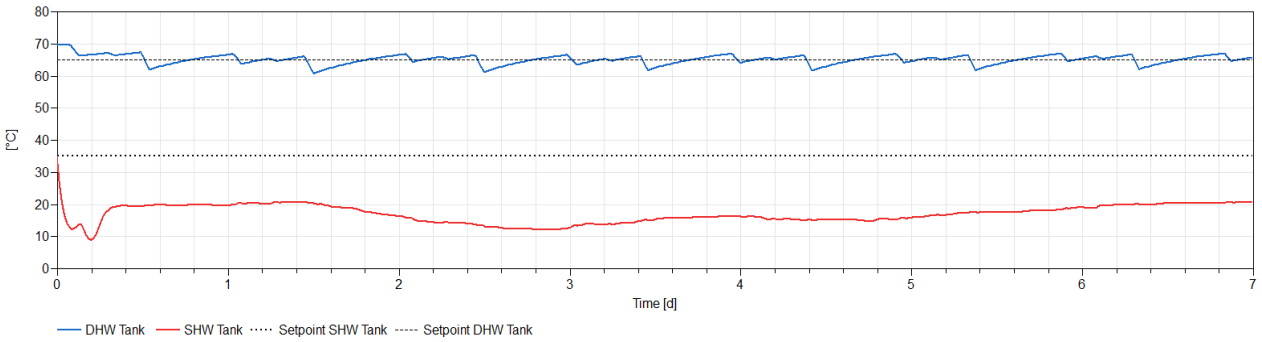

Figure 5.15: *Achieved temperature vs setpoints of DHW and SHW*

5.1.3.2 DHW Heating Mode

For the DHW heating mode simulation, a different DHW demand schedule from IDA ICE was used. The demand is less frequent, but with higher simultaneous loads. This is to give a chance to observe how the system reacts to big consummations of DHW, and how quick the heat pump is able to reload the tanks. The control strategy implemented in this scenario is fixed high-side pressure of 92 bar, with variable compressor speed control. The compressor speed is regulated between 60- and 35 Hz depending on if the setpoint of 65 °C in the tank is reached. The supply water temperature to the tank has a setpoint of 70 °C, controller through the mass flow rate. During this simulation the SHW circulation pump were turned off. The simulation time is 168 hours (1 week).

Figure 5.16 shows the IDA ICE DHW load profile compared to the heat rejection from the pre- and reheating gas coolers. The DHW demand gets as high 5,6 kW. From the graph it can be observed how the heat rejection from the gas coolers increases quickly when DHW consumption occurs. This is a result of the compressor speeding up as the temperature of the tank gets below the setpoint temperature. As the setpoint is reached, the compressor speed gradually decreases. At about hour 80, it can be observed how the heat pump is already working on reloading the tank at full compressor speed, as a new block of DHW

consumption occurs. This elongates the period in which the heat pump is working on maximum capacity of just above 4,2 kW.

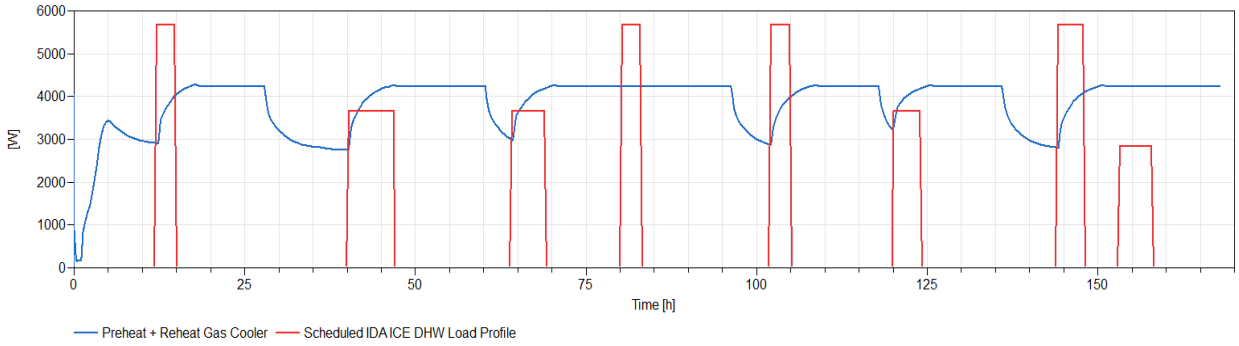

Figure 5.16: *Total heat rejection of gas coolers vs DHW demand*

Figure 5.17 illustrates the temperature profile of the DHW tank and can be seen in relation with the results presented in *Figure 5.16*. As the DHW demand occurs, the temperature in the 400 litre tank drops fairly rapidly. Depending on how low the temperature gets, the heat pump uses about 10 to 15 hours to reload the tank to the setpoint temperature.

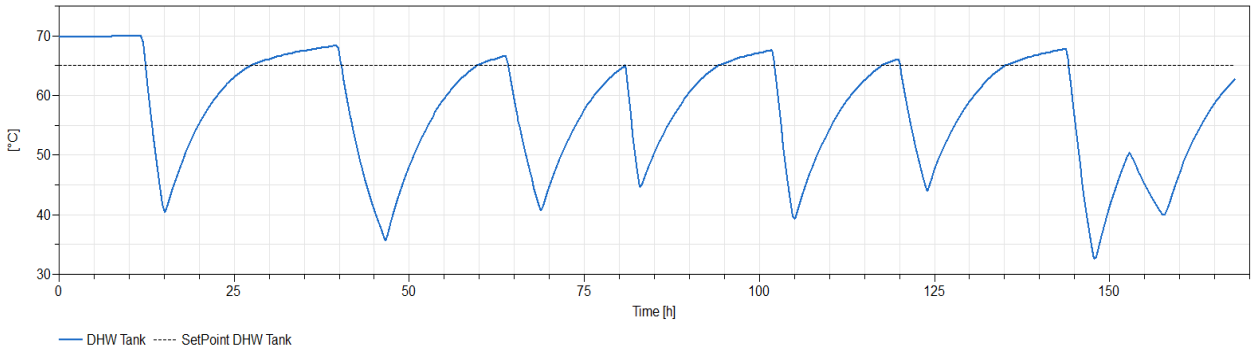

Figure 5.17: *Temperature profile of the DHW tank*

The relationship between the COP and the compressor frequency is shown in *Figure 5.18*. The graph shows how the compressor works within its frequency range (35-60 Hz), increasing and decreasing dependent on the of the DHW tank temperature. With decreasing compressor speed, the COP increases, peaking at around 3,49. At 60 Hz, the COP is relatively stable at 3,17. This indicates that the control strategy is working to its purpose. There could however be a trade-off point between how low the compressor should be allowed to step down, and how quickly the DHW tank needs to be reloaded. In this simulation the tank temperature setpoint is reached before every new block of DHW consumption, except at hour 150. An increased lower Hz limit will give a quicker response time, but also higher energy use.

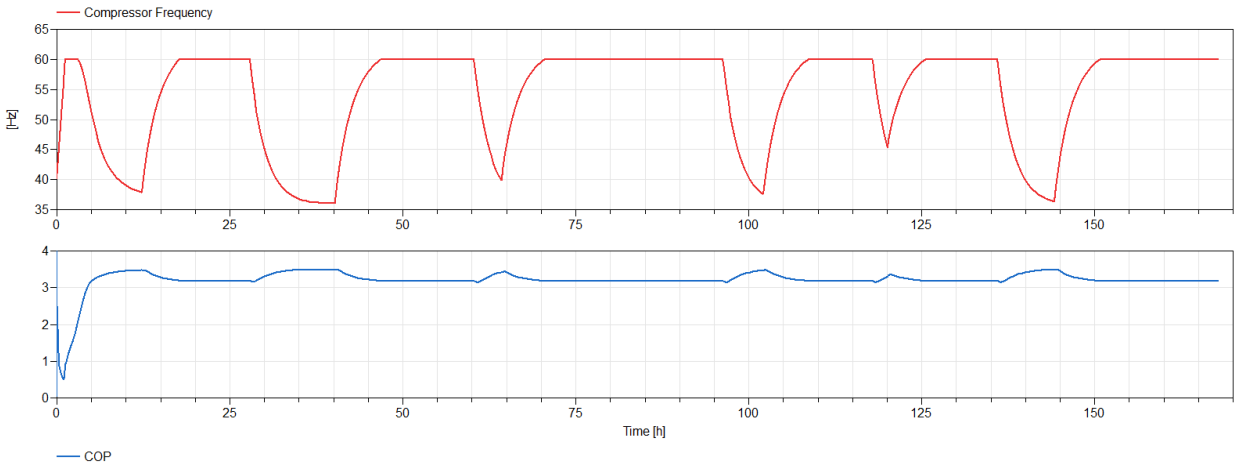

Figure 5.18: *COP seen in relationship with compressor frequency*

5.1.3.3 Space Heating Mode

During the space heating mode simulation, the DHW circulation pump was switched off. As for DHW heat mode simulation, the control strategy is compressor frequency regulation, with fixed high-side pressure at 80 bar. This is to avoid to high CO_2 discharge temperature, with the risk of boiling in stagnant DHW water. The setpoint of the SHW tank in this simulation is 32 °C, which is used to regulate the compressor. This simulation has a timespan of 168 hours as well.

Figure 5.19 shows the IDA ICE load profile compared to the heat delivery from the space heating gas cooler. The heat pump is able to cover the moderate heating demand during the whole week. The control strategy, with decrease in compressor frequency according to the SHW tank temperature can be observed as drops in the heat from the gas cooler.

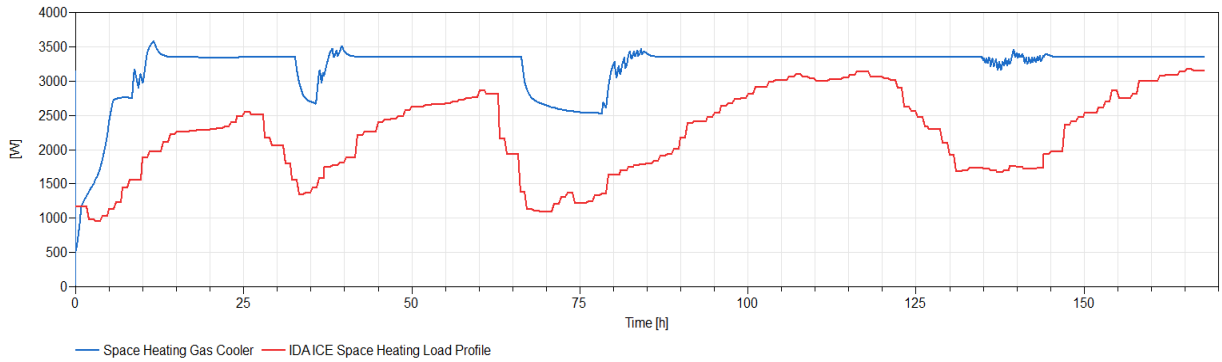

Figure 5.19: *IDA ICE load profile compared to the space heating GC*

The temperature profile of the SHW tank during the simulation period is shown in *Figure 5.20*. The setpoint of 32 °C is marked with a black dotted line. As the space heat demand increases, the temperature in the tank drops. Some overshoots after reloading the tank can be observed as peeks in the temperature. The biggest temperature drop can be seen between hour 100 and 125, correlating with the highest demand during the simulation period. The first two temperature drops, the heat pump manages to reload the tank relatively quickly.

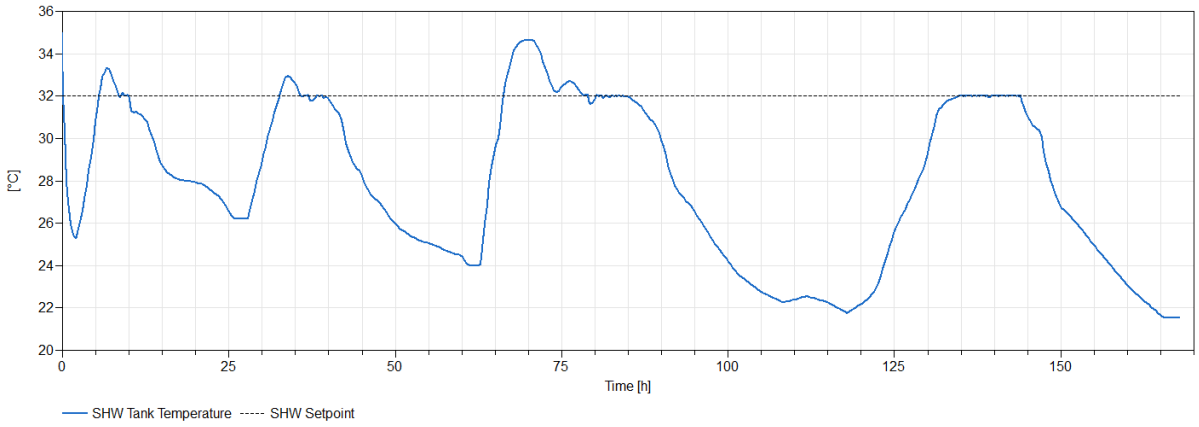

Figure 5.20: *Temperature of the SHW tank*

Figure 5.21 shows the COP in relation the compressor frequency. As the SHW tank setpoint temperature is reached, the compressor frequency is lowered. The COP can be observed increasing during these periods, peaking as high as 3,25. During 60 Hz, the COP is stable at 2,84.

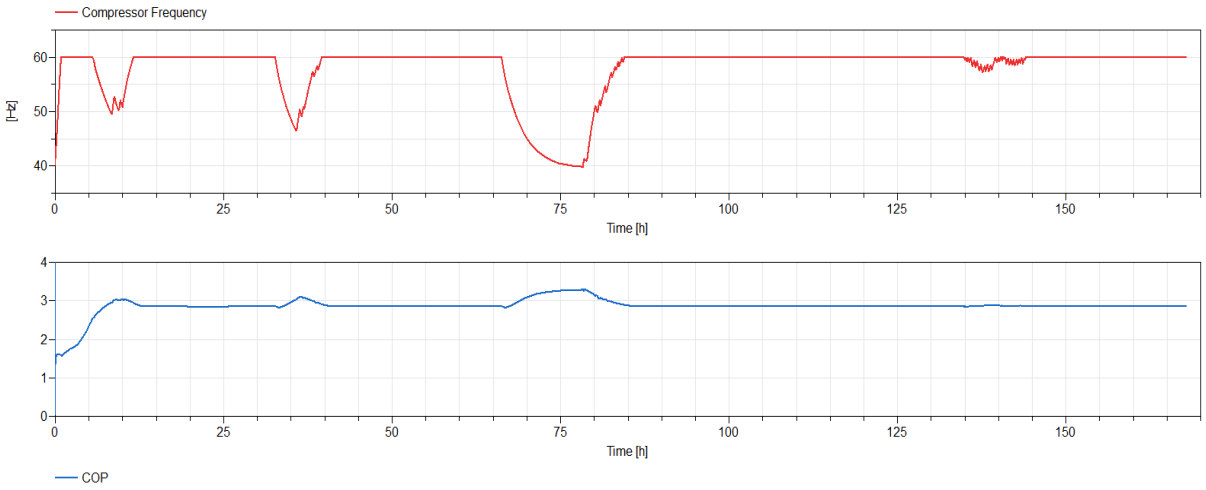

Figure 5.21: *Compressor frequency vs COP*

5.2 Operational Results

In this section, the logging results from the heat pump at the residential location will be presented. During the operation period, both combined mode heating and space heating mode was utilized. The logging was done during a week of operation in the month of May, during an unusually cold period. *Figure 5.22* shows the outdoor temperature during the seven days of logging. As seen in the graph, the week starts off cold, with temperatures just above 0 °C. At the end of the week the temperature rises, but never reaches above 8 °C. The cold weather caused a constant space heating demand.

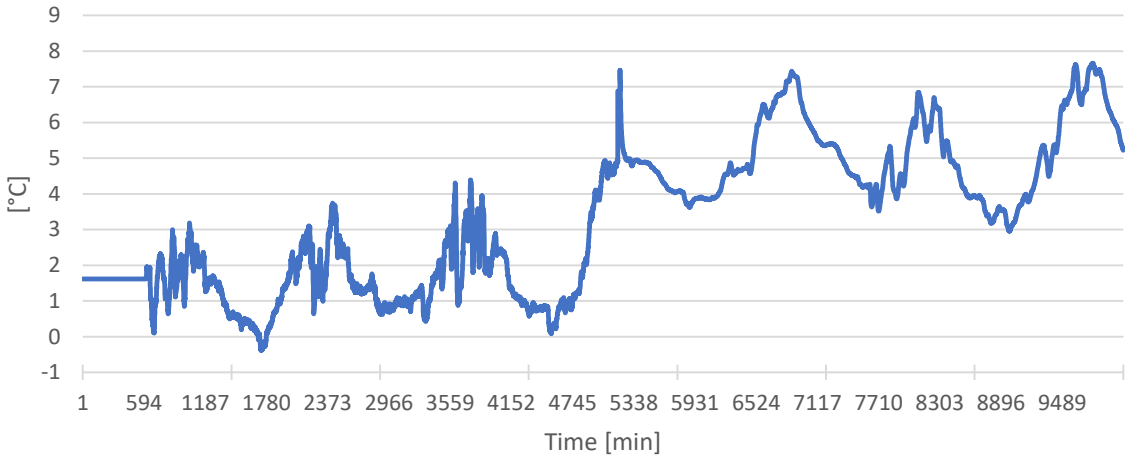

Figure 5.22: *Outdoor temperature profile*

5.2.1 Refrigerant Side

The logged compressor frequency during operation is presented in *Figure 5.23*. Due to the fairly high space heating demand, the compressor is working on 60 Hz for most of the space heating only period. 11 times during the logging period, the compressor shut off due to unknown reasons and had to be manually turned back on. This can be observed as sudden drops in frequency. Smaller drops in frequency can be seen after the compressor is turned back on. *Figure 5.24* shows the values from the energy meters U3 and U4, for space heating and DHW heating respectively. During the majority of the week, the heat pump operates in space heating mode, with a relatively constant heat rejection of 4,3 kW. During combined mode the capacity reaches as high as 4,8 kW, but on average around 4,4-4,5 kW. The average COP during space heating only and combined mode was calculated to be 3,07 and 3,18 respectively.

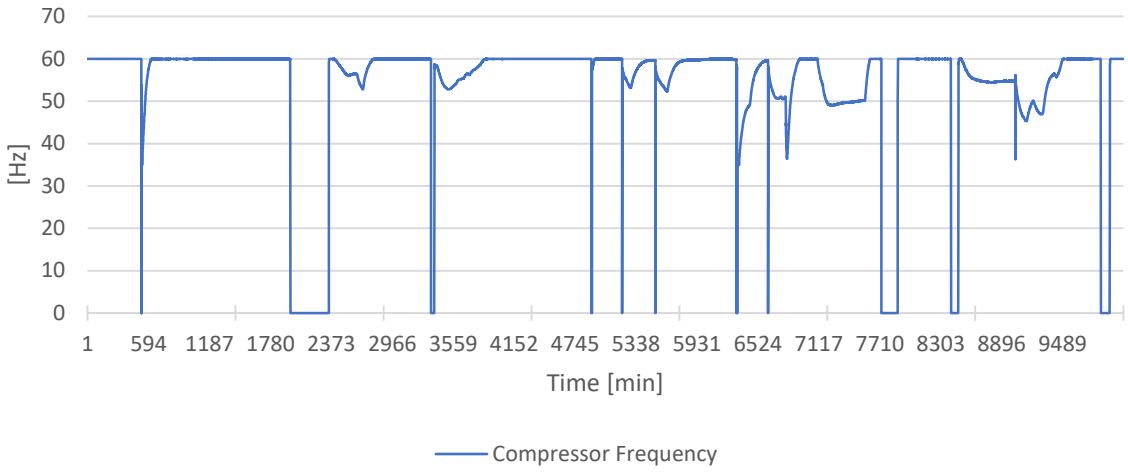

Figure 5.23: *Compressor frequency during the week of operation*

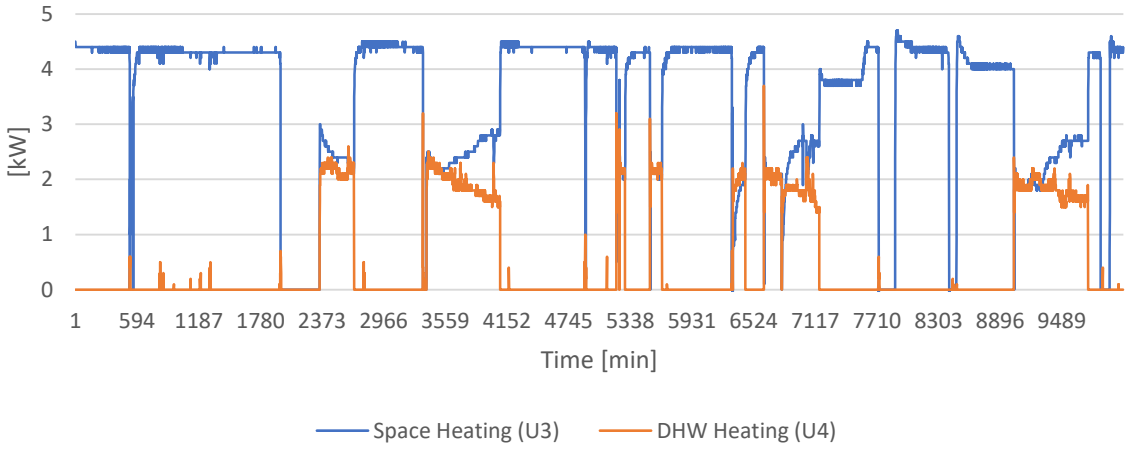

Figure 5.24: *Logged values for energy meters U3 and U4*

The temperature of the CO_2 at the different stages of the tripartite gas cooler configuration is showed in *Figure 5.25*. The compressor stops can also be observed in this figure as sharp drops in temperature. As expected, the discharge temperature and reheat GC outlet temperature is approximately identical during space heating only mode, as there is little to no heat exchange through the reheater. The same analogy goes for the space heating outlet temperature and the preheating outlet temperature. The temperature of the CO_2 entering the space heater is stable below 100 °C, at about 95-99 °C. This means the risk of boiling in the stagnant DHW to a large degree is avoided, considering that the 2-3 bar pressure in the piping causing a boiling point higher than 100 °C. During combined mode heating, the reheating GC outlet temperature drops to about 40-45 °C. A drop in preheating GC outlet temperature can also be observed, but not significantly. The reason is a fairly high water temperature entering the preheater, about 15-20 °C.

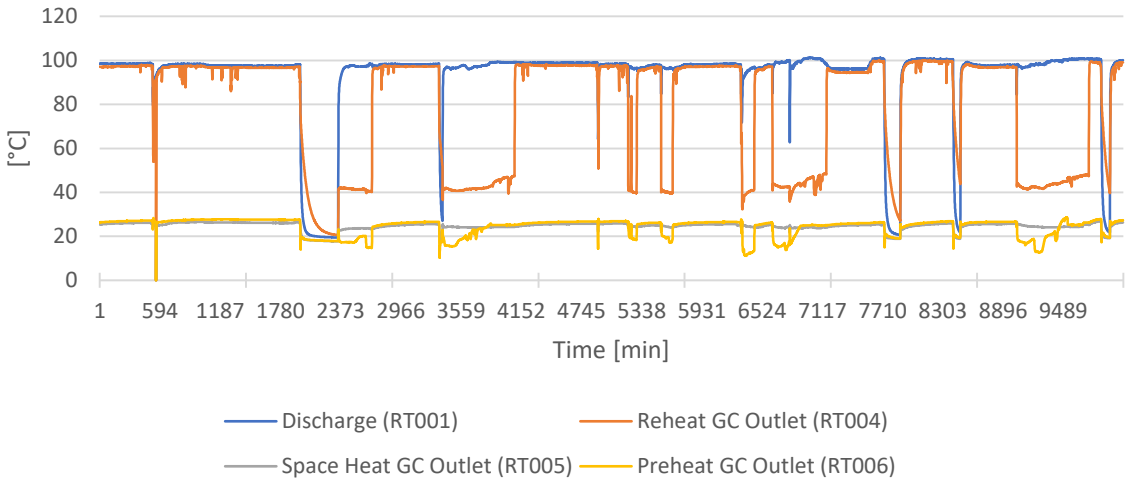

Figure 5.25: *CO_2 temperature through the gas coolers*

During the sensitivity analysis, high oscillations were observed for the superheat. The same trend can be seen in *Figure 5.26*, during this logging period. The mean degree of superheat is approximately 8 K during the whole week, except during the compressor shut offs, which causes big spikes. The bandwidth of the oscillations varies from below 1 K to above 6 K.

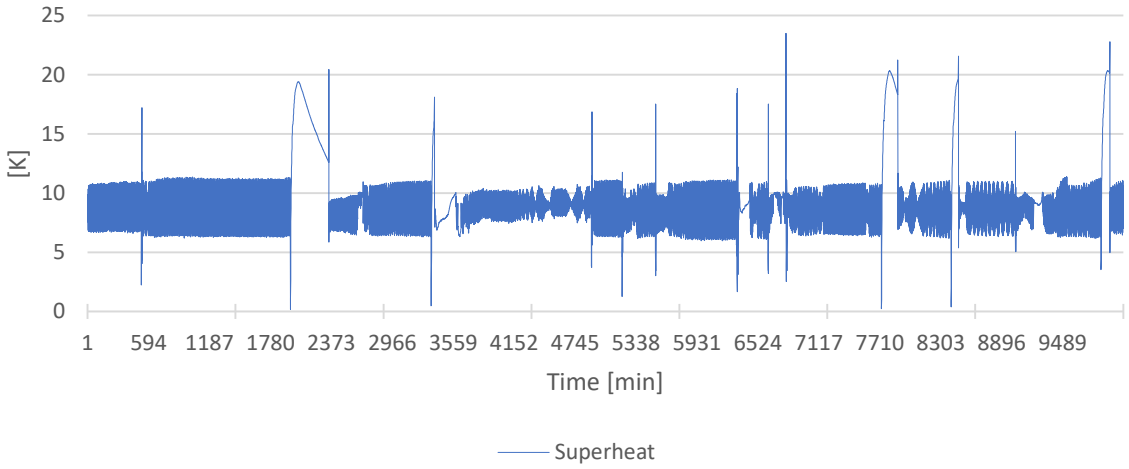

Figure 5.26: *Degree of superheat in the suction gas line*

The high- and low-side pressure during the operation is showed in *Figure 5.27*. The pressure at the high-side is stable between 78-82 bar the whole week, except during compressor shut off. The low side pressure is stable between 28-30 bar. During this operation, the high-side pressure was not increased during combined mode heating.

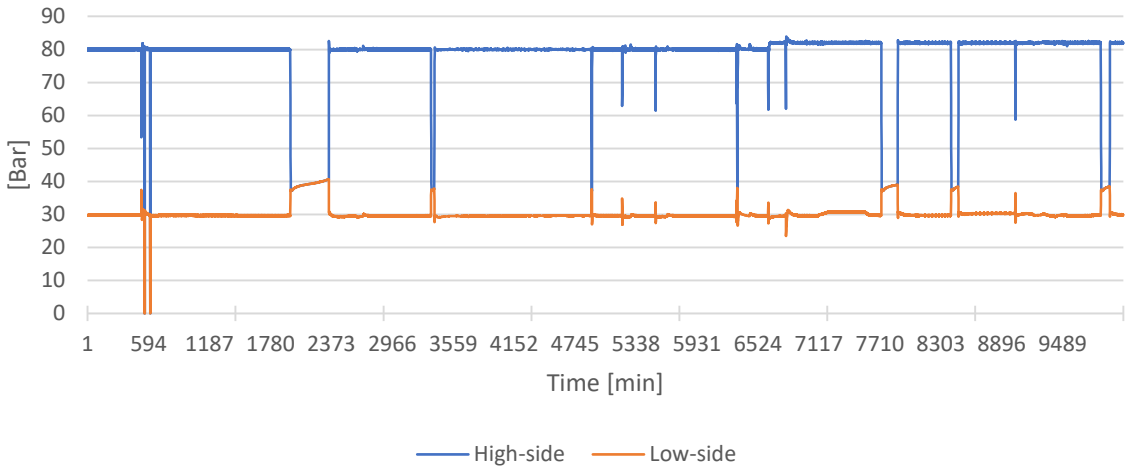

Figure 5.27: *High- and low-side pressure*

5.2.2 Accumulator Tanks

Figure 5.28 illustrates the accumulator tanks with their respective temperature sensors, which will be presented in this section. Tank 1 is where the city water is fed, and tank 4 is where hot water is fed and distributed.

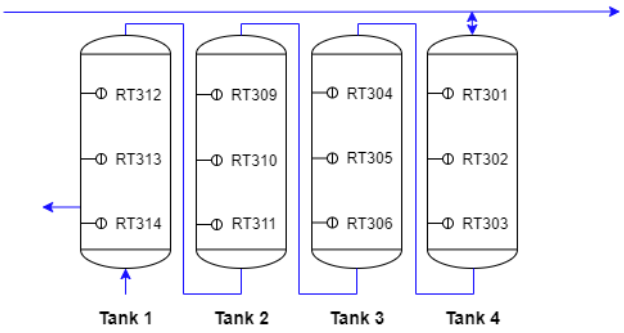

Figure 5.28: *Overview of the accumulator tanks with sensors*

5.2.2.1 Tank 1

The temperature profile of the first accumulator tank is showed in *Figure 5.29*. During the start of the first day the temperature in the tank is stable, with no production or consumption. At about minute 594, halfway through the first day, the temperature of the tank drops, meaning there was DHW consumption. The first tank is more subject to big temperature differences as it is the tank in which the city water is fed. On three occasions the temperature at the bottom of the tank (sensor RT314) gets above 30 °C.

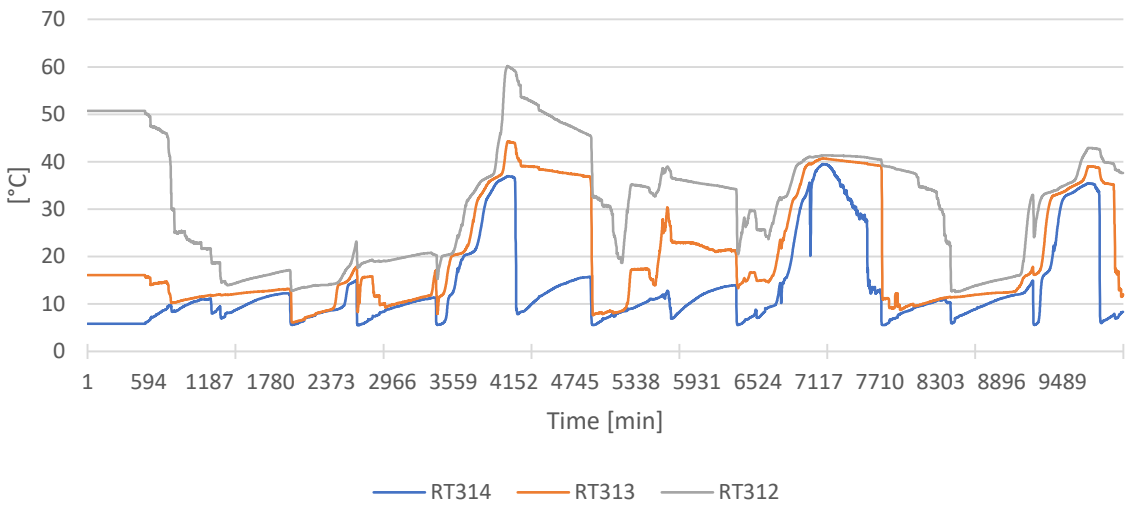

Figure 5.29: *Temperature profile for Tank 1*

5.2.2.2 Tank 2

Compared to the temperature profile of the first tank, tank 2 has a more uniform temperature throughout the tank, and less temperature difference between the "layers". It is however, like tank 1, subject to fairly big temperature drops during high DHW consumption. The uniform temperature of the tank drops to about 17 °C at its lowest, after the first big DHW consumption. The tank is also more quickly reloaded than tank 1. *Figure 5.30* shows the temperature profile of tank 2.

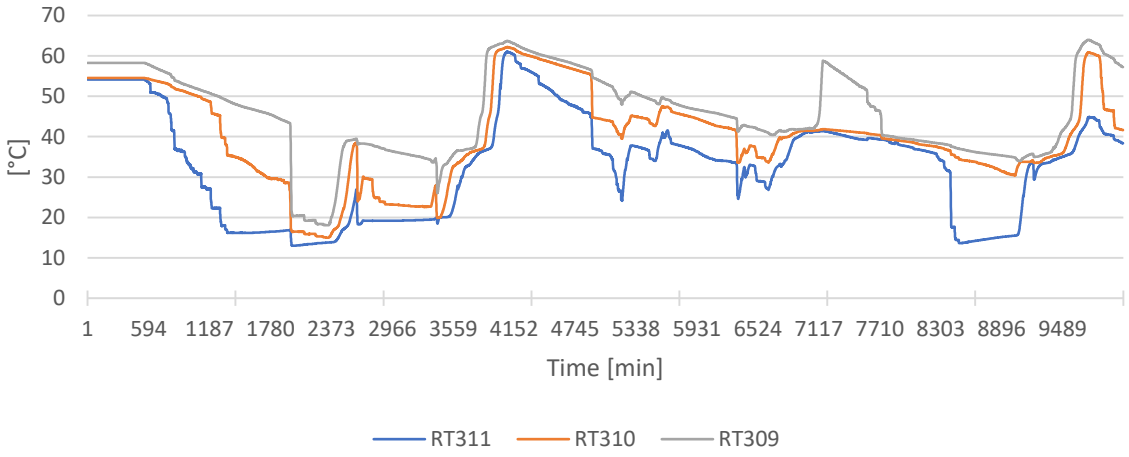

Figure 5.30: *Temperature profile for Tank 2*

5.2.2.3 Tank 3

The temperature profile of tank 3 is presented in *Figure 5.31*.. The tank is fully reloaded three times during the logging period. The first reload was done in 9,3 hours, the second

in 6,1 hours and the last took 11,3 hours from when the combined mode heating was activated. At about minute 2620 the second day, the top layer (RT304) can be observed being heated to 63 °C. This corresponds with the short period combine mode was activated, but not long enough to reload the entire tank. In tank 1 and 2, had some reload related to this period, but not significantly.

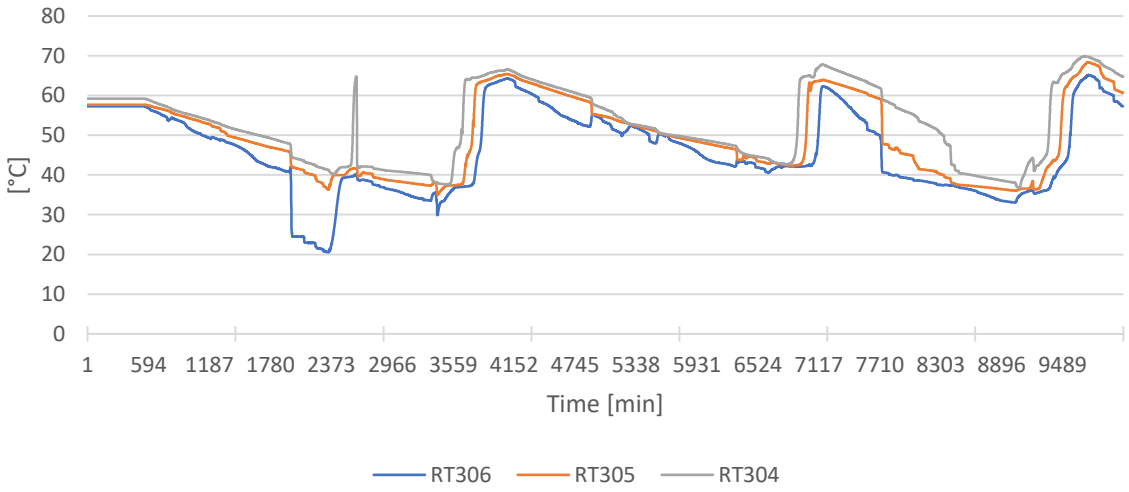

Figure 5.31: *Temperature profile for Tank 3*

5.2.2.4 Tank 4

Tank 4 is the last accumulator tank in the series and is naturally the least subject to temperature changes and a fairly uniform tank temperature during the whole operation week. The first short period of combined mode heating can be observed being sufficient enough to reload the entire tank, in about 4 hours. The lowest temperature observed in tank is 35,6 °C in the bottom layer (RT303), and 43,4 °C at the top layer (RT301).

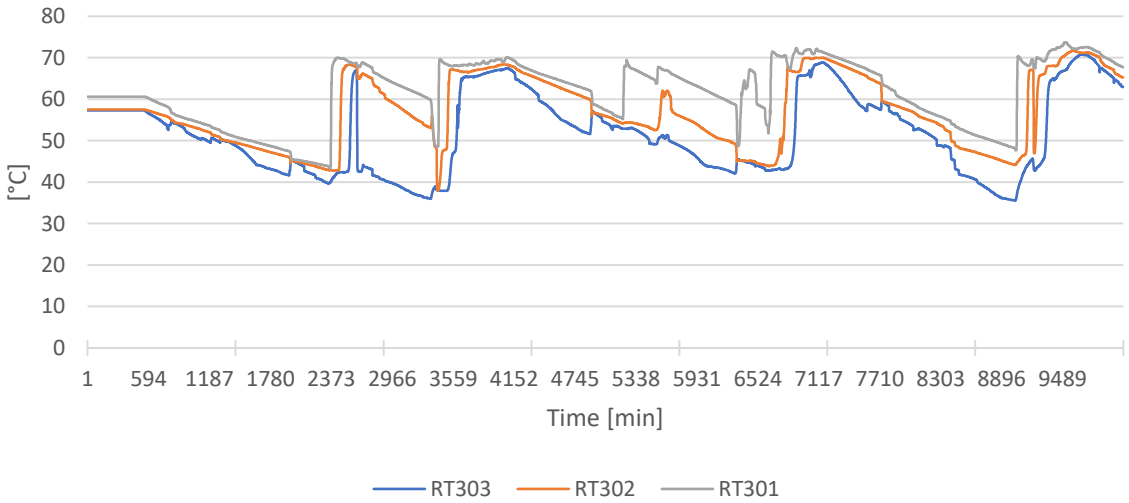

Figure 5.32: *Temperature profile for Tank 4*

6 Discussion

This chapter contains an overall analysis and reflection of the results and findings presented in the chapter 5. The validity of the Dymola model, as well as the results from the different simulations will be discussed and compared with established theory. In addition, the experimental testing and operational data will be evaluated.

6.1 Validity of the Dymola Model

The dynamic Dymola model were developed to be an accurate and realistic representation of the real residential CO_2 heat pump system. A valid model could then be used as a tool to optimize and analyse the system characteristics and components. As a mean to validate the model, a sensitivity analysis was performed at the residential location. The secondary side conditions and input values were then recreated in the model, with the purpose of giving a basis for direct comparison of system characteristics.

On an overall level, the correlation of the logged data from the actual heat pump, and the results from the Dymola model were very good. There was however a bigger deviation on some areas more than others. The evaporator pressure of the model reached 0,5 to 1 bar lower than what was logged for the real heat pump during maximum frequency (60 Hz). This could indicate that the model compressor was designed a bit too large compared to the real compressor. It should also be taken into consideration that the model has an ideal pressure model, with 0 Pa drop through components. However, it could be argued that the CO_2-cycle is relatively insensitive to pressure loss due to very high absolute pressure [19].

A fairly big deviation was also observed in the level superheat in the suction gas line. The logged values showed relatively big oscillations for the real heat pump, and the setpoint of 5 K were only sporadically reached. The superheat in the model actually exceeded the 5 K setpoint with 0,25-0,35 K. This could also to some degree be tied to the model compressor being slightly too big. However, the degree of oscillations in the real heat pump might indicate sub-optimal tuning of the oil return valve controller (too high gain, and too low integral). It could also be due to the tracking interval of the superheat sensor, causing the controller to receive "delayed" signals.

An aspect that were reoccurring in the majority of the compared data were the difference in reaction time during the initial minutes of the analysis. In all cases, the model had a quicker reaction time to the input values than what was measured for the real heat pump.

This was an expected finding, as the model does not account for mechanical inertia and signal delays, which is present in the actual heat pump system. Another aspect is the difference in logging points between the Nortend logging software and the Dymola software, with 60 and 720 logging points per hour respectively. This could make the graphs for the real heat pump to appear more ragged and inconsistent than the smoother Dymola graphs.

6.2 System Performance Analysis in Dymola

The Dymola model was utilized as a tool to investigate optimum high-side pressure, production and different operating modes. Different input values and control strategies were used in each simulation, to cover a broad spectre of possible real life scenarios. Much of the purpose with such a model is to be able to do testing which would otherwise require much time and effort should they have been performed in the real life system.

6.2.1 Optimum Pressure

The optimum pressure analysis was done with a ramp input, providing a pressure increase from 80 to 100 bar during a 30 minute timespan. The results showed that the highest COP was achieved at the lower pressure levels. At 80 bar, the COP was around 3,8 to 4, while at 100 bar the COP dropped down to 3,4. It should be noted that these COP values occurred under ideal conditions. At 100 bar the heat pump had a maximum capacity of about 4,77 kW, while about 4,25 kW at 80 bar. These findings indicate that the pressure level should be operated as low as possible, while still providing sufficient heat capacity. The decrease in COP with increasing pressure can be seen in relation to the compressor power and evaporator heat. The results showed that the increase in heat capacity is to a larger degree due to increase in compressor power rather than evaporator increase in evaporator heat extraction. As expected, the highest discharge CO_2 temperature was observed at 100 bar pressure, at 114 ^{o}C. There seemed to be a proportional relationship between CO_2 discharge temperature and high side pressure.

It was also observed how the heat capacity were distributed between the three gas coolers at the different pressure levels. At lower pressure levels (<90 bar), the space heating gas cooler had the highest capacity. With increasing pressure, the capacity of the reheating gas cooler increased, while the space- and preheating gas cooler capacity decreased. At about 91-92 bar, an equilibrium between the capacity of the space heating GC and the reheating GC was observed. The total capacity of the heat pump at this pressure was about 4,6 kW, and this could be an optimum pressure setpoint for combined mode operation.

This was also showed in the hot water production. The pressure range 91-92 bar provided the most even distribution between DHW and SHW production.

The results showed a smaller temperature approach as the pressure level increased. This is well documented in established theory, as the pinch point is moving towards the gas cooler outlet with increasing pressure. It was also observed that the suction gas heat exchanger and the sub cooler had smaller impact during higher pressure. This could be seen in relation with the temperature approach. The lower gas cooler outlet temperature is giving a smaller LMTD over the heat exchangers, causing a smaller heat transfer. These findings supports the findings in the 2005 study [18] presented in chapter 2.3.7, which showed that internal heat exchangers are most important at lower pressure levels.

6.2.2 Operating Modes

Dymola model simulations were done to test the heat pump model during combined mode, DHW heating mode and space heating mode operation. These are the three plausible scenarios the heat pump will operate under, and for that reason it was chosen as interesting cases to investigate. For this purpose, the load profiles from the IDA ICE residential building model for both space heating and DHW consumption was used. As an indoor climate analysis of the residential building was not one of the main objectives in this project, the IDA ICE model is not necessarily as accurate as it could be. The effort put into making the model reflects the extent in which it was to be used, and for that reason several simplifications were made. The main purpose of the IDA ICE residential model was to give the Dymola model something to "work with", which could be a hypothetical real life operating scenario. The DHW consumption was scheduled in blocks throughout the day, with some periods with relatively high demand, and some with moderate demand. Replicating a DHW consumption can be challenging, as there are several factors playing in, and can vary a lot from household to household. The load profiles presented in the results should give an idea of what the demand could look like, without necessarily being 100 % accurate.

The combined mode simulation had a moderate DHW consumption and a fairly high space heating demand implemented. The results showed an average COP of 3,58 during, peaking at 3,62. The control strategy, regulating the high-side pressure according to the DHW demand, gave small peaks in the COP when operating on 82 bar. However, the DHW demand were fairly frequent, and the 82 bar setpoint were only kept for short periods of time. This indicates the operating strategy could be beneficial, especially during periods with less frequent DHW consumption. As the space heating demand were never met, the compressor worked at maximum frequency during the whole simulation. This shows the need for a peak load system during winter operation.

The DHW heating mode simulation had a fairly high DHW consumption. The main reason was to test the heat pumps abilities to provide domestic hot water. The simulation showed that the heat pump was able to cover the demand and reload the tank in about a 10 hour period. In a real life scenario, this would typically be done during the night, meaning the heat pump would be able to provide DHW for the next morning. The temperature of the tank (volume element) drops as low as 32 °C during the highest consumption. It should be noted that the volume element in Dymola is not the most realistic representation of an accumulator tank, as it does not account for the temperature layering which occurs in a real tank. Ideally the volume element would have several temperature, like the real tanks, and not just represented by one uniform temperature. However, it does give an indication of how fast the tank is able to be completely reloaded and can therefore be a useful tool for analysis. During this simulation, the DHW heating mode had a capacity of about 4,2-4,3 kW.

During the space heating mode simulation, a moderate load profile from IDA ICE were used. The heat pump was able to cover the load with gas cooler heat delivery of around 3,4 kW. The control strategy of regulating the low-side pressure through compressor frequency proved to be efficient in terms of increasing the COP during low demand periods. During low demand periods, the COP increased with 0,4.

The simulations of the different operating modes indicate that the heat pump works most efficiently during combined mode operation. This is logical, considering the nature of its design, which is to utilize the large temperature glide of the CO_2 refrigerant through three gas coolers. When one or two of the gas coolers is taken out (not utilized), the CO_2 is not sufficiently cooled down, causing higher expansion losses and lower COP. This corresponds well with the established theory presented in chapter 2. It is however able to provide both DHW and space heating separately, with relatively high COP. The lowest COP were observed during space heating only mode. It would be beneficial for the COP with lower return temperature of the space heating water, which would cause further cooling of the CO_2.

6.3 Experimental Testing and Operation

During the first phase of the practical part of this master project, experimental testing of the CO_2 heat pump in the test rig at Winns was conducted. The goal was to prepare the heat pump in a controlled environment before moving it to the residential location. A weakness with the testing was the relatively short timespans the heat pump was operated. Due to working hours and setup time in the rig, the heat pump was never ran longer than 2-3 hours contiguously. The sudden compressor stops were therefore not discovered

during the experimental testing phase. In addition, the discharge CO_2 temperature was underestimated during the final testing in the rig. As described in chapter 4.3.4, the highest discharge temperature observed was just above 91 °C at with a high-side pressure above 90 bar. This can be tied to the fact that the compressor was not ran on full frequency. In hindsight, the heat pump should have been operated for a longer contiguous period, and at greater range of the compressor capacity. Due to delays in the project, a lot of the control strategies described in chapter 4.3.5.2 where not implemented in time for the operation at the residential location. Instead, most of the control were done manually.

The compressor stops were first observed at the residential location, after several hours of operation. The logged data didn't not give any conclusive answers, as there were no particular trend or instability in the parameters that would indicate overload or otherwise explain the shutoff. A possibility could be an electrical issue with the frequency converter on the compressor, as it seemed to black out during the stops.

During the week of operation at the residential location, both combined mode and space heating only were utilized. Due to the cold weather causing a constant space heating demand, DHW only mode was not activated during this period. The results showed a lower average COP during the combined mode operation than what was observed in the Dymola model simulation for combined mode. This can be tied to the big variation in inlet water temperature (RT011) to the preheating gas cooler. Whereas the inlet water temperature in the model was constant at 7 °C, the temperature of the inlet water of the real system fluctuated between below 10 °C to above 30 °C, with an average inlet temperature of about 19 °C. As previously discussed, the level of CO_2 refrigerant cooldown is crucial for achieving the highest possible COP. This also emphasizes the importance of having a bypass at the preheating gas cooler when the water inlet temperature gets too high. Without a bypass, scenarios where the inlet water will actually heat up the CO_2 in the last gas cooler will occur. This is obviously not a wanted scenario and will greatly impact the system efficiency negatively. The capacity of the system during combined mode heating was on average 4,4-4,5 kW, peaking at around 4,8 kW. Comparing with the Dymola model, which had a total capacity between 4,34 - 4,65 kW during combined mode. It should be noted that the high-side pressure level had a constant setpoint between 80 - 82 bar during in the real system, whereas the model had a variable high-side pressure regulation, between 82 and 92 bar.

The analyse of the accumulator tanks showed that the setup worked well to its intent. The design, with several buffer tanks connected in series, is common in larger plants and heating systems, but usually not found in residential applications. The fourth tank, in which the hot water is distributed from, experienced the smallest variations in temperature. It was also quickly reloaded after periods of high consumption.

7 Conclusion

The goal of this master project was to investigate a prototype residential CO_2 heat pump through testing and dynamic computer modelling. The Dymola model of the heat pump system was designed to handle a variety of load profiles and input values. To validate the model, a sensitivity analysis comparison between the real heat pump and the model was done. The comparison showed a good correlation, and its therefore reasonable to conclude that the model is valid representation of the real system. Logging of the heat pump at the residential location was done during a week of operation. The following discoveries and conclusions can be drawn from the simulation results and the operational testing:

- The heat pump originally had a dimensioned capacity of 6,5 - 7 kW. Since then several altercations, such as new compressor and expansion valve, has been done. The simulations and operational testing indicate that the current maximum capacity of the heat pump realistically is at 4,5 – 5 kW.

- Sufficient cooling of the CO_2 refrigerant is crucial for the highest possible COP, i.e. the water inlet temperature to the preheating gas cooler should ideally be as low as possible. During space heating mode, the return temperature from the hydronic heating system should also be as low as possible.

- Being able to bypass the preheating gas cooler is of great importance for ensuring high system performance over time. This is to avoid the water to heat up the CO_2 in the gas cooler during periods with high inlet water temperatures.

- Of the three plausible operation modes simulated, the combined mode operation achieved the highest COP, both on average and maximum. The DHW mode came second, and the space heating mode last.
  - $COP_{comb,max} = 3,62$ $COP_{comb,avg} = 3,58$
  - $COP_{DHW,max} = 3,49$ $COP_{DHW,avg} = 3,17$
  - $COP_{SH,max} = 3,25$ $COP_{SH,avg} = 2,84$

- The results indicate that the optimum pressure for maximum COP is in the lower range (80 – 85 bar). During ideal conditions in the model, a COP of 4 was observed at 80 bar. This pressure range also seemed to be optimum for maximum space

heating water production. The optimum pressure for maximum DHW production is in the higher range (95-100 bar). For combined mode heating, a moderate pressure range seemed to maximize production of both SHW and DHW (90-92 bar).

- Fixed high-side pressure, controlling the low-side pressure through compressor frequency, can highly increase the system COP during low demand periods. Control through variable high-side pressure with fixed low-side pressure seemed to have a smaller effect on increasing the COP.

- The SGHX and sub cooler is most beneficial at lower pressure levels (<90 bar). However, during periods with high water inlet temperatures and less cooling of the CO_2, they can have a high effect even at higher pressures.

- The design of the accumulator tank, consisting of four smaller tanks in series, worked well as a buffer during high DHW consumption. The distribution tank (tank 4) experienced the smallest temperature variations and was quickly reloaded.

An overall conclusion based on the findings in this master project is that CO_2 refrigerant in a transcritical operation is well suited for DHW heating due to its unique abilities. In combined mode, it is able to provide both space heating and DHW heating with a COP above 3,5, meaning it uses under a third of the energy conventional electrical heating systems would have used. Residential CO_2 heat pumps have the potential to be a large energy saver for the building sector.

8 Further Work

There is several areas that can be further developed in the Dymola model. Especially on the secondary sides of the model, improvements can be done. The main improvement would be to implement a bypass circuit between the pre- and reheating gas coolers, with active control. This would give an opportunity to further investigate the benefits and importance of a bypass route. An electrical peak load system could also be implemented to the model. In addition, a pressure drop model through the components on the refrigerant side could be developed. These suggestions would further increase the realism of the model.

For the real heat pump, the issues with sudden compressor shutoffs should be identified with certainty, and fixed. Except for this problem, the heat pump proved to run smoothly and performed well. Also, the automation for the control strategies described in chapter 4.3.5.2 should be implemented and tested. For the benefit of the occupants, heating systems should be operated as automatic as possible, without the need to interact other than adjusting thermostats.

An overall goal, looking from a long-term perspective, undoubtably should be to standardize the control and production of residential CO_2 heat pump units. The market and potential is definitely there, but the effort needs to be put in making it easy to buy, high on reliability and easy to operate and maintain.

References

[1] "Lov om klimamål (klimaloven). 2017." [Online]. Available: https://lovdata.no/dokument/NL/lov/2017-06-16-60.

[2] "Bygningsenergi." [Online]. Available: https://www.standard.no/fagomrader/bygg-anlegg-og-eiendom/bygningsenergi/.

[3] J. Stene, *VARMEPUMPER - Grunnleggende varmepumpeteknikk*. SINTEF, 1997.

[4] R. Radermacher and Y. Hwang, *Vapor Compression Heat Pumps - with Refrigerant Mixtures*. Taylor & Francis Group, 2005.

[5] K. Ochsner, *Geothermal Heat Pumps A guide for Planning & installing*. Earthscan, 2008.

[6] ASHRAE, *Handbook of Fundementals, I-P edition*. 2017.

[7] H. Haukås, J. Stene, A. Hafner, H. Rekstad, and T. Eikevik, "KOMPENDIUM - CO2 (R744) som kuldemedium," *Nor. Kjøleteknisk Foren.*, 2016.

[8] "The Montreal Protocol on Substances that Deplete the Ozone Layer," *Ozone Secretariat*. [Online]. Available: http://ozone.unep.org/en/treaties-and-decisions/montreal-protocol-substances-deplete-ozone-layer.

[9] T. Gerden, "The adoption of the kyoto protocol of the united nations framework convention on climate change," *Prisp. za Novejso Zgodovino*, vol. 58, no. 2, 2018.

[10] UNEP, "The Kigali Amendment to the Montreal Protocol: HFC Phase-down," *28th Meet. Parties to Montr. Protoc. 10-14 October, 2016, Kigali, Rwanda*, pp. 1–7, 2016.

[11] J. Bonin, *Heat Pump Planning Handbook*. Routlegde, 2015.

[12] J. Stene, "Ammonia as a Working Fluid in Heat Pumps and Liquid Chillers," *TEP20 NTNU*, 2019.

[13] Novema Kulde, "KULDEMEDIER- ECODESIGN - STATUS NOVEMBER 2018," no. November 2018, pp. 1–2, 2020.

[14] J. Stene and SINTEF Energy Research, "Master Module 7 - CO2 Heat Pumps," *Leonardo Proj. NARECO2*.

[15] RnLib, "Thermodynamic and Transport Properties of Refrigerants and Refrigerant Mixtures," *SINTEF Energy Res. Dep. Energy Process. Norw.*, 2009.

[16] S. M. Liao, T. S. Zhao, and A. Jakobsen, "Correlation of optimal heat rejection pressures in transcritical carbon dioxide cycles," *Appl. Therm. Eng.*, vol. 20, no. 9, pp. 831–841, 2000.

[17] P. C. Qi, Y. L. He, X. L. Wang, and X. Z. Meng, "Experimental investigation of the optimal heat rejection pressure for a transcritical CO2 heat pump water heater," *Appl. Therm. Eng.*, vol. 56, no. 1–2, pp. 120–125, 2013.

[18] Y. Chen and J. Gu, "The optimum high pressure for CO2 transcritical refrigeration systems with internal heat exchangers," *Int. J. Refrig.*, vol. 28, no. 8, pp. 1238–1249, 2005.

[19] J. Stene, "CO2 Heat Pumps and Chillers," *TEP20 NTNU*, 2019.

[20] L. I. Stensaas, *Vannbaserte oppvarmings- og kjølesystemer*. Skarlandpress, 2007.

[21] C. Guangyu, "Indoor Environment and Thermal Comfort (II)," 2018.

[22] R. W. Haines and M. E. Myers, *HVAC System Design Handbook*, Fifth. McGraw-Hill, 2010.

[23] B. Borgnes, "HVA ER EN TERMISK RESPONSTEST - OG HVORDAN SIKRE ET GODT RESULTAT," *Futur. Energi AS*, 2013.

[24] R. K. Ramstad, "Energibrønner som varmekilde for varmepumper," *Asplan Viak, NTNU*, 2017.

[25] NGU, "Varmeledningsevner målt på bergarter," p. 2000, 2000.

[26] J. Stene, "Residential CO2 Heat Pump System for Combined Space Heating and Hot Water Heating," NTNU, 2004.

[27] "Dorin Innovation." [Online]. Available: https://dorin.com/en/catalogo/.

[28] "CoolPack," *ipu.dk*. [Online]. Available: http://www.en.ipu.dk/Indhold/refrigeration-and-energy-technology/coolpack.aspx.

[29] R. Mastrullo, A. W. Mauro, A. Rosato, and G. P. Vanoli, "Carbon dioxide heat transfer coefficients and pressure drops during flow boiling: Assessment of predictive methods," *Int. J. Refrig.*, vol. 33, no. 6, pp. 1068–1085, 2010.

[30] "Overall Heat Transfer Coefficient Table Chart," *Engineers Edge*. [Online]. Available: https://www.engineersedge.com/thermodynamics/overall_heat_transfer-table.htm.

[31] F. Haugen, "The Good Gain method for PI (D) controller tuning," *TechTeach*, vol. 4, no. D, pp. 1–7, 2010.

Appendices

Appendix A - SOSCC Reference Models

Appendix B - CoolPack Reference Models

Appendix C - Setpoint Algorithms in Dymola

Appendix D - Variable High-side Pressure Simulation Graphs

Appendix E - Logging Setup Guide

Appendix F - Draft Version of Scientific Paper

Appendix A – SOSCC Reference Models

85 bar:

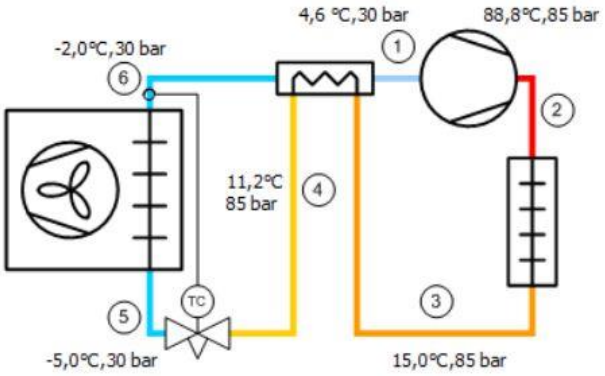

Qe = 215,69 kJ/kg
W = 57,82 kJ/kg
Qc = 267,74 kJ/kg

90 bar:

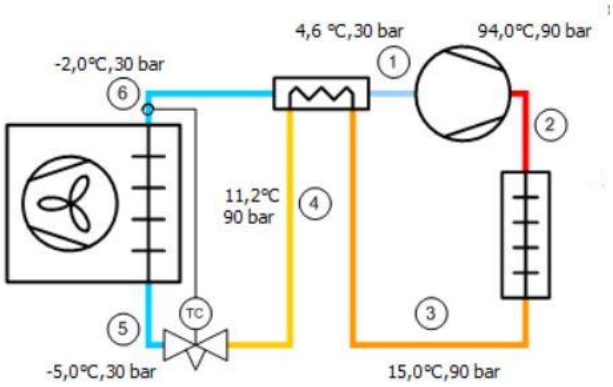

Qe = 216,43 kJ/kg
W = 61,47 kJ/kg
Qc = 271,75 kJ/kg

95 bar:

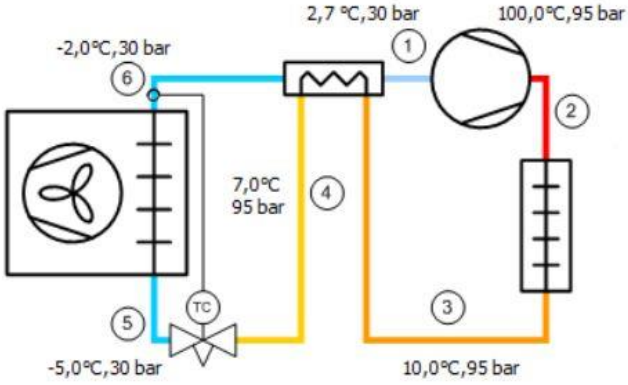

Qe = 226,53 kJ/kg
W = 63,91 kJ/kg
Qc = 289,16 kJ/kg

Appendix B – CoolPack Reference Models

85 bar:

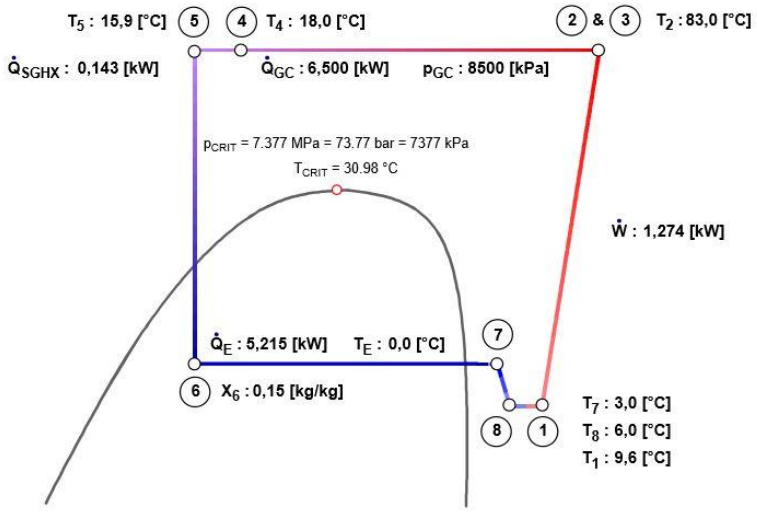

95 bar:

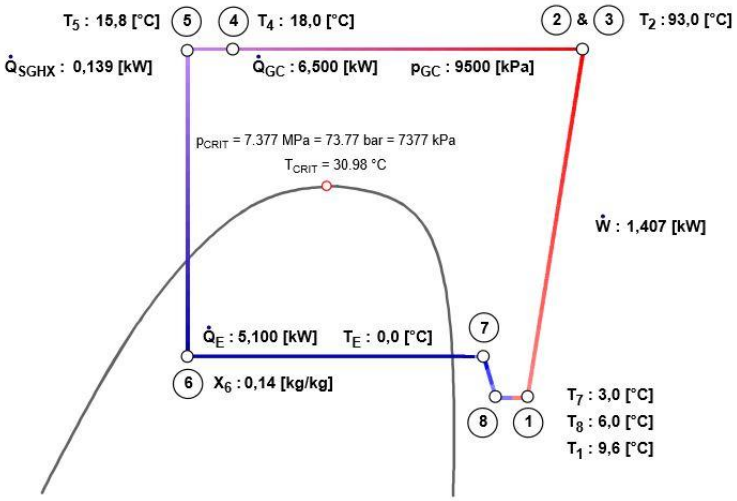

Appendix C – Setpoint Algorithms in Dymola

This section shows the algorithms for the setpoint inputs used during the different simulation scenarios.

Compressor input (Space only simulation):
Y = if(sensor_T_degC17.sensorValue>32)then 33e5 else 29e5

Compressor input (DHW only simulation):
Y = if(sensor_T_C18.sensorValue>65)then 33e5 else 29e5

Expansion valve input (Combined mode):
Y = if(sensor_Q_flowDHW.sensorValue>0)then 92e5 else 82e5

COP calculation block:
(ReheatGasCooler.summary.Q_flow+PreheatGasCooler.summary.Q_flow+SpaceheatGasCooler.summary.Q_flow)/(effCompressor.shaftPower)

High-side pressure ramp:

Parameters

height	20e5		Height of ramps
duration	30	min	Duration of ramp (= 0.0 gives a Step)
offset	80e5		Offset of output signal y
startTime	10	min	Output y = offset for time < startTime

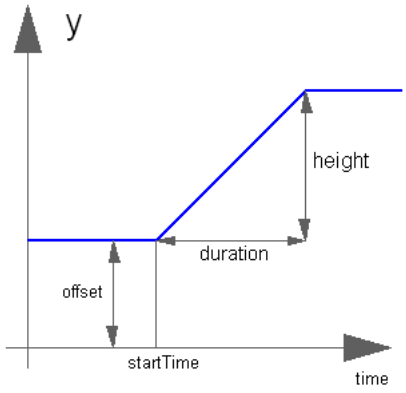

Borehole ramp:

Parameters

height	-0.5		Height of ramps
duration	60	min	Duration of ramp (= 0.0 gives a Step)
offset	273.15 + 6.0		Offset of output signal y
startTime	120	s	Output y = offset for time < startTime

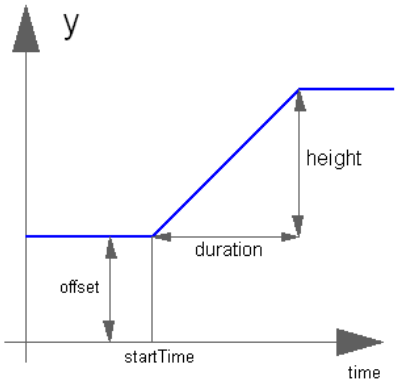

Appendix D – Variable High-side Pressure Simulation Graphs

Evaporator:

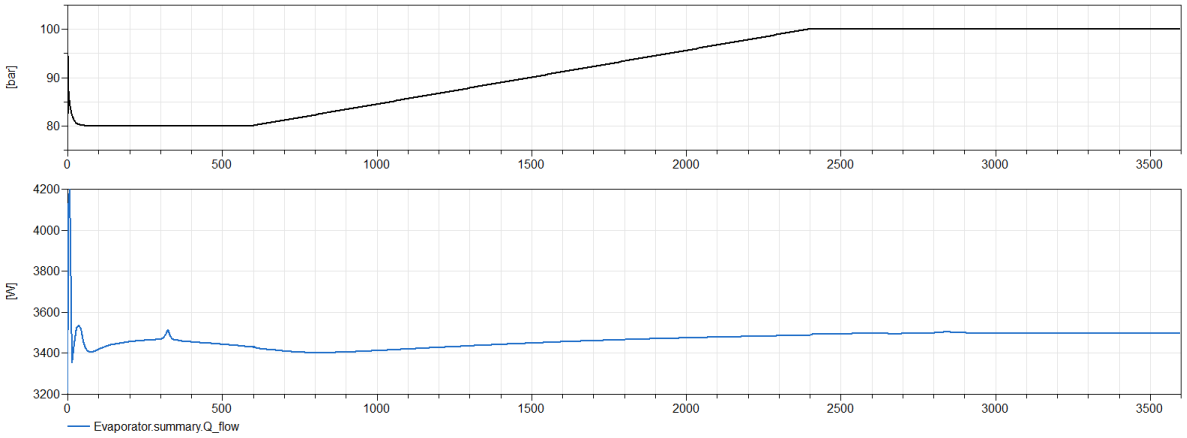

DP expansion valve:

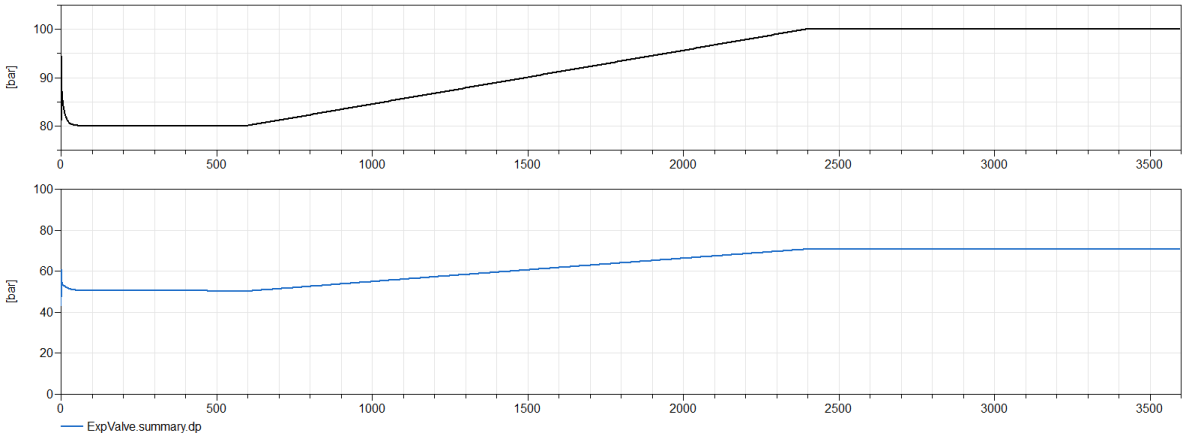

Compressor shaft power:

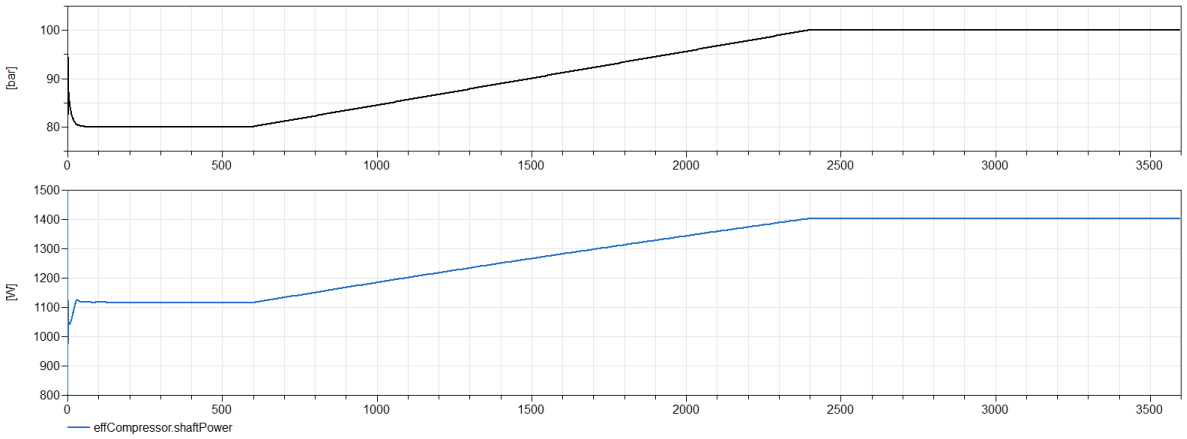

LPR filling level:

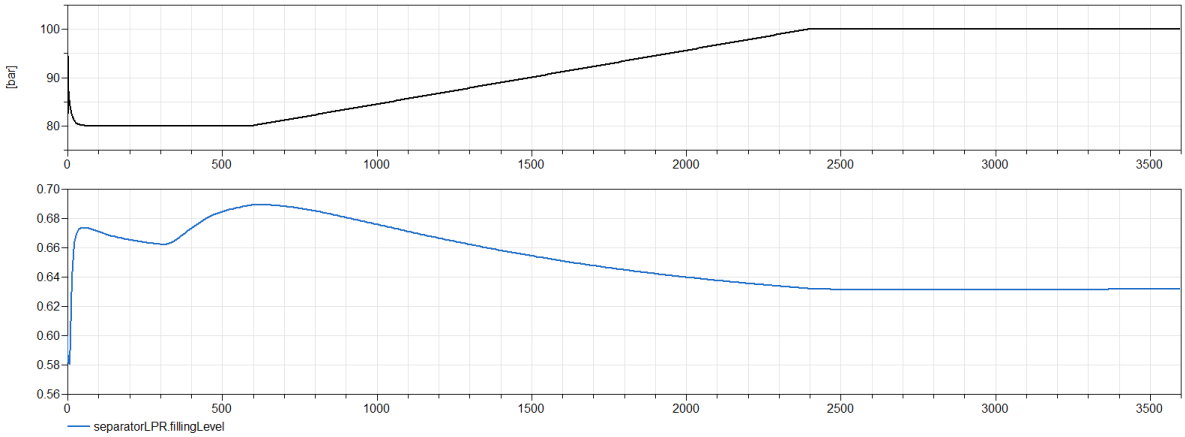

GC temperature profile CO_2 :

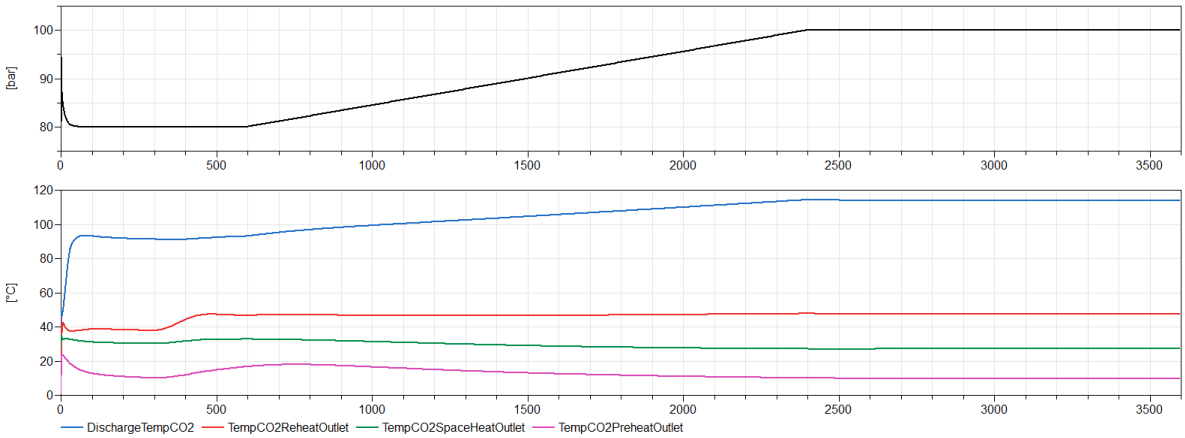

Mass flow DHW and SHW:

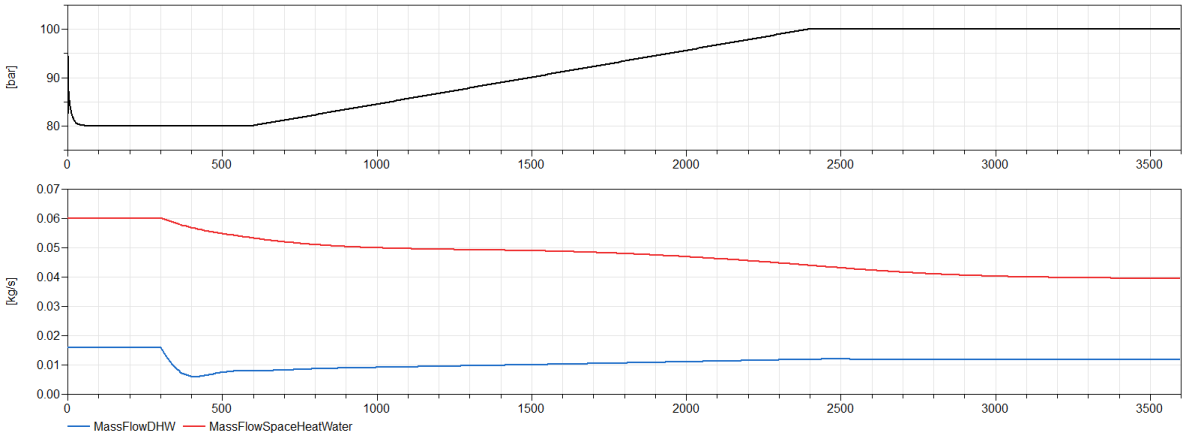

Appendix E – Logging Setup Guide

This section contains a step by step guide for the logging setup, as an assist for potential future projects.

1. Allocate an IP-address to the PLC (See separate guide in the following section).
2. Make sure the IP assignment on the logging PC is set on Automatic (DHCP)
3. Open Eaton OPC Configuration and make sure the IP-address matches with the PLC. (As long as the PLC has not been given a new IP, this step only has to be done once.)
4. Open OPCexplorer.exe and establish connection between the computer and the PLC by clicking on the chain-link symbol on top of the page. If connection is established, several folders containing all the communicating sensors, meters, alarms etc. will appear.
5. Open the Logsetup.exe. Drag the sensors, meters, alarms etc. that you want to log from the OPCexplorer.exe to the Logsetup.exe window, and select unit, format and logging time-step for the given sensor.
6. Open the Logviewersetup.exe and organize the different sensors (etc.) in folders after own desire. Define Y- and X-axis.
7. Start logging by opening the Nortend.exe.
8. To monitor the logging, open the Logviewer.exe. The setup defined in Logviewersetup.exe will appear.
9. To extract the raw data as CSV-files (Excel), right click on live graph in Logviewer.exe and click export. The exported data will appear in the "Exports" map in the Nortend map.

Allocation of IP-address:

In order for the PLC to communicate over modem, it must be set to receive IP address automatically. This is done via the touch panel.

If the process-image are inserted on the screen, they must be closed to access the settings.

Press the button labelled A in the image below:

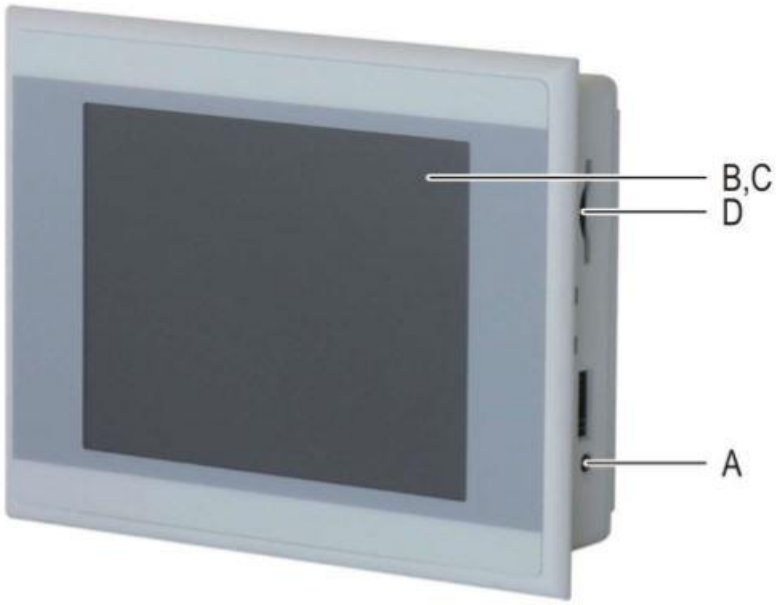

The process-image disappears, and the screen looks like the image below. The screen is pressure sensitive and can be operated only with your fingers. Press Start in the lower left corner. Continue with Programs and Control Panel.

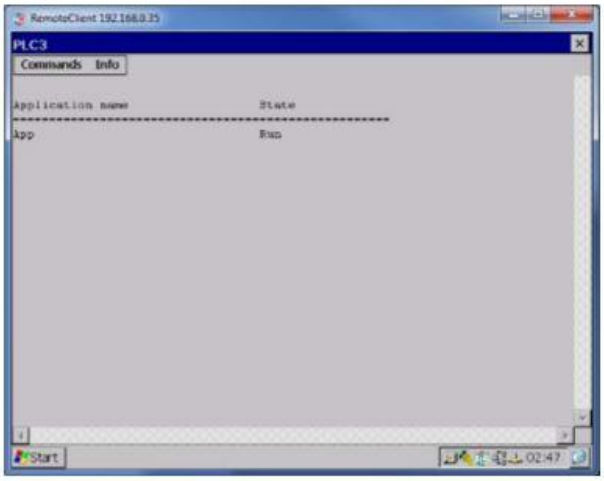

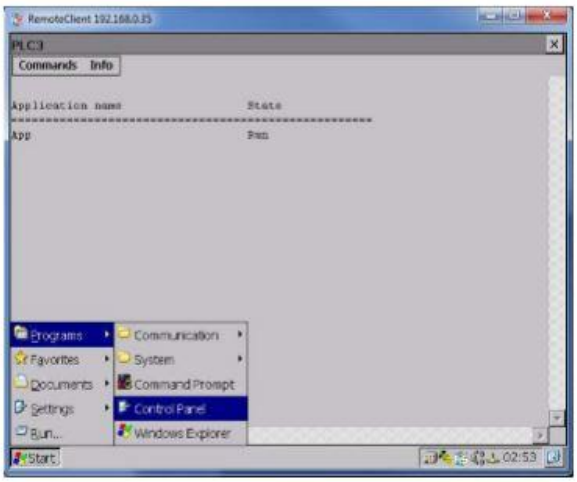

Chose “network” and “Onboard 1”, as shown below:

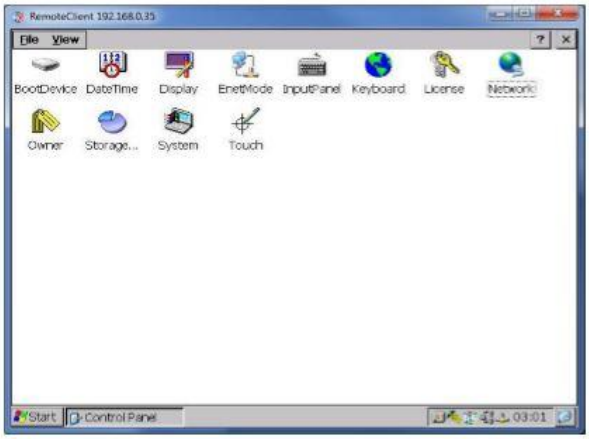

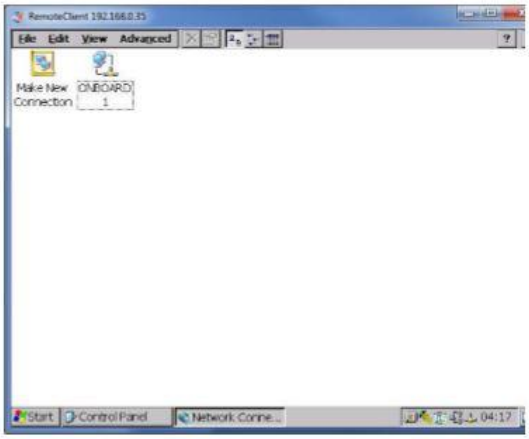

Check off on "Obtain an IP address via DHCP". Click OK.

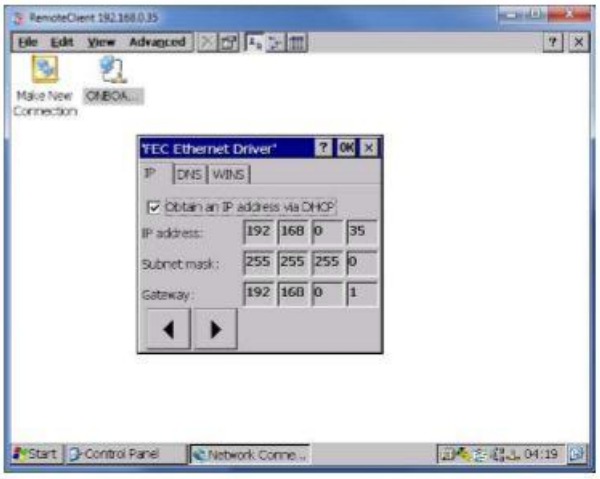

The allocation is now done. To get back to the process-image, exit your way back, drag the blue top-line that says “PLC3” to the side (see picture below). The shortcut “GRS-CE5” will appear. Double click it, and the process-image will appear.

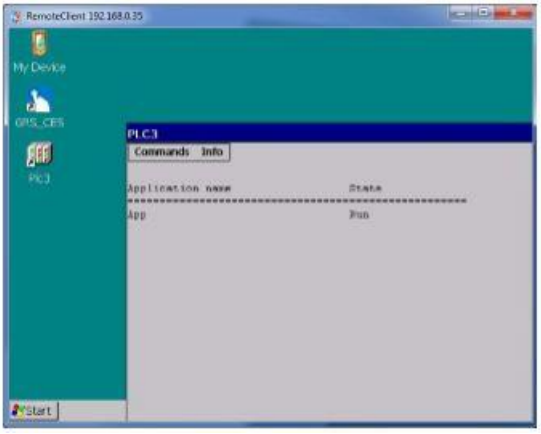

Appendix F – Draft Version of Scientific Paper

Performance Analysis of Prototype Residential CO_2 Heat Pump

Johan Christian Rømcke

Norwegian University of Science and Technology (NTNU), Department of Energy and Process Engineering (EPT). Trondheim, Norway, jcromcke@stud.ntnu.no

Abstract

Heat pumps are today rarely used for heating of domestic hot water (DHW) in Norwegian households. This is largely due to the limitations of conventional residential heat pumps, which cannot provide high enough temperatures in an effective and practical way. Heat pumps using the natural working fluid CO_2 have the potential to deliver water temperatures of 60-70 ^oC without compromising the coefficient of performance (COP). At NTNU-SINTEF, a combined mode CO_2 heat pump, for both space- and DHW heating, was developed from 2000-2004. The heat pump has since undergone several altercations and component replacements. The goal of this report is to analyse the system solutions, realistic energy/power capacity, dependability and instrumentation which enables optimized operation of the heat pump. Additionally, a dynamic computer model of the system has been developed and utilized as a tool for analysis. The findings of the analysis showed that the maximum capacity of the heat pump at its current state is at 4,5 – 5 kW. Of the three plausible operating modes; combined, space heating (SH) and DHW heating, the combined mode achieved the highest COP – 3,62. The least favourable for COP was the SH mode, with a maximum COP of 3,25. DHW heating mode achieved a maximum COP of 3,49. These findings emphasizes the importance of having sufficient cooldown of the CO_2 refrigerant in order to get the highest possible COP.

Keywords: Natural working fluids, CO_2 heat pump, DHW heating, energy analysis, dynamic modelling.

1. Introduction

The Norwegian Government has set the goal to reduce greenhouse gas emissions in Norway with at least 40 % by 2030 [1]. The building sector accounts for nearly 40 % of the total energy consumption in Norway, while about 60% of the energy use in Norwegian households is used for heating [2]. In order to reach the emission and energy goals of the future, new technology needs to be developed and implemented. The heat pump is optimal for this purpose, as it typically provides 3-4 times more thermal energy than electrical energy consumed. In the buildings of the future, zero energy buildings and power houses, a highly efficient heat pump is crucial. In the refrigeration industry, there is a vast untapped potential for natural working fluids like carbon dioxide and ammonia. Heat pumps using CO_2 as working fluid can provide temperatures high enough for heating of domestic hot water, while still having a high coefficient of performance. CO_2 heat pumps can very well be the heating technology of the future and contribute to reducing the energy consumption of the building sector.

A prototype combined mode residential CO_2 heat pump was developed at NTNU-SINTEF from 2000-2004 [3]. The heat pump has since undergone several altercations, such as new compressor and new expansion valve. During the first phase of this project, the heat pump was set up in a test rig, for instrumentation and testing. It was then moved to a residential location for operational testing and monitoring. This report contains a sensitivity analysis comparison between the model and the logged data from the residential location, as well as an overall system analysis.

2. System Description

2.1 CO_2 Heat Pump and Hydronic System

The CO_2 heat pump is a residential brine-water ground source heat pump. It is designed as a combined space heating and domestic hot water unit, originally with a capacity of 6,5 – 7 kW. The heat source is an indirect u-tube collector system, in a 150m deep bedrock borehole. The gas coolers are in a tripartite configuration, with a DHW preheating gas cooler, a hydronic floor heating gas cooler, and a DHW reheating gas cooler. The heat pump also has a suction gas heat exchanger (SGHX) and a sub cooler placed on the brine inlet at the secondary side of the evaporator. All heat exchangers are tube-in-tube counter flow type. After the evaporator, a low pressure receiver (LPR) with an oil return circuit is placed. The LPR is a 4 litre vessel. There is also an CO_2 filling line connected to the oil return. The current compressor is a semi-hermetic two-stage reciprocating compressor operated as a single-stage unit. It has a maximum capacity of 1450 RPM (35 – 60 Hz), with a displacement volume of 1,12 m^3/h. The heat pump has two expansion valves in parallel; one manual and one motor valve.

The hydronic system at the residential location consists of floor heating system and a domestic hot water system. The floor heating system supplies heat to three stories, about 280 m^2. A 100 litre buffer tank and a circulation pump distribute the warm water. An electrical peak load element is placed in the tank. The DHW system consists of four 100 litre accumulator tanks connected in series. A throttling valve controls the water mass flow accordingly to the set point temperature out of the reheating gas cooler. A three-way motor valve makes it possible to bypass the preheating gas cooler for when the inlet water temperature exceeds the CO_2 temperature out of the space heat gas cooler. *Figure 1* shows the residential heat pump system.

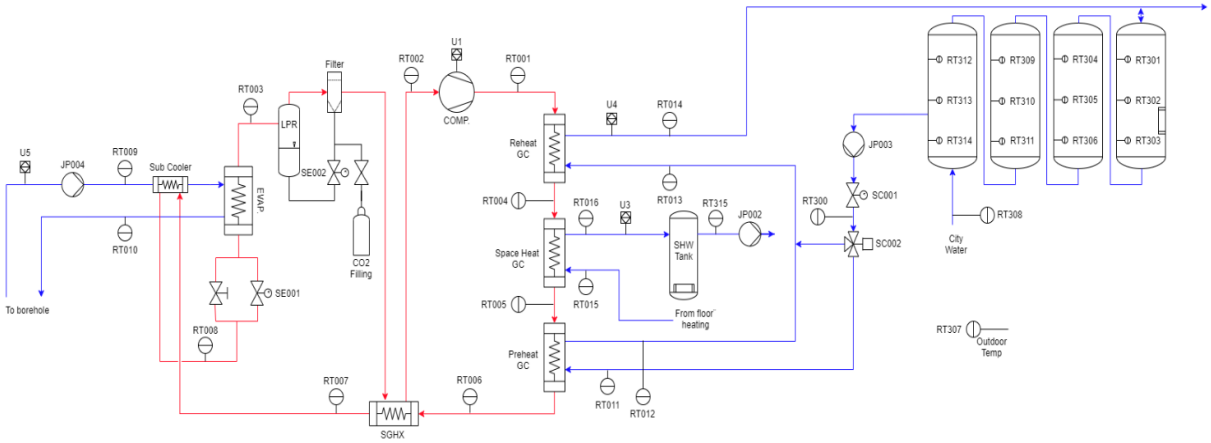

Figure 1: Process and instrumentation diagram (P&ID) of the residential heat pump system

2.2 Dynamic Computer Model

The dynamic model of the CO_2 heat pump system was developed in the simulation software Dymola, based on the Modelica programming language. In addition to the standard Dymola Library, the add-on library which offers a large selection components, has been used.

The model contains five PI-controllers to regulate the system, three on the refrigerant side and two on the hydronic side. The expansion valve is operated as a back-pressure valve, regulating the high-side pressure through throttling. A PI-controller (PI-Valve) uses a reference pressure sensor between the reheat GC and space heat GC, along with a set point element. The set point element feeds the regulator with the desired pressure level, which then regulates the back-pressure valve accordingly. A mechanical boundary which enables speed input was implemented to the compressor. The compressor is controlled through actively regulating the low side pressure within the limits of the operating frequency (35 – 60 Hz). An oil return circuit goes from the bottom of the low pressure receiver, to the main line. The task of the oil return is to regulate the refrigerant quality to ensure a desired level of superheat. A PI-controller (PI-OR) regulates the valve opening, with a reference superheat sensor placed at the compressor suction line. At the hydronic side of the space heater, a variable speed pump was implemented to enable mass flow regulation. The PI-controller (PI-SH) regulates the pump through a reference temperature sensor and an input temperature value. A volume element of 100 litres were implemented to the hydronic line to represent the buffer tank. The same control strategy was implemented for the DHW system. The PI-controller (PI-DHW) regulates the pump to achieve the desired setpoint DHW temperature. A volume element of 400 litres where added to represent the accumulator tank. Load (thermal demand) profiles were added for both space heating and DHW heating.

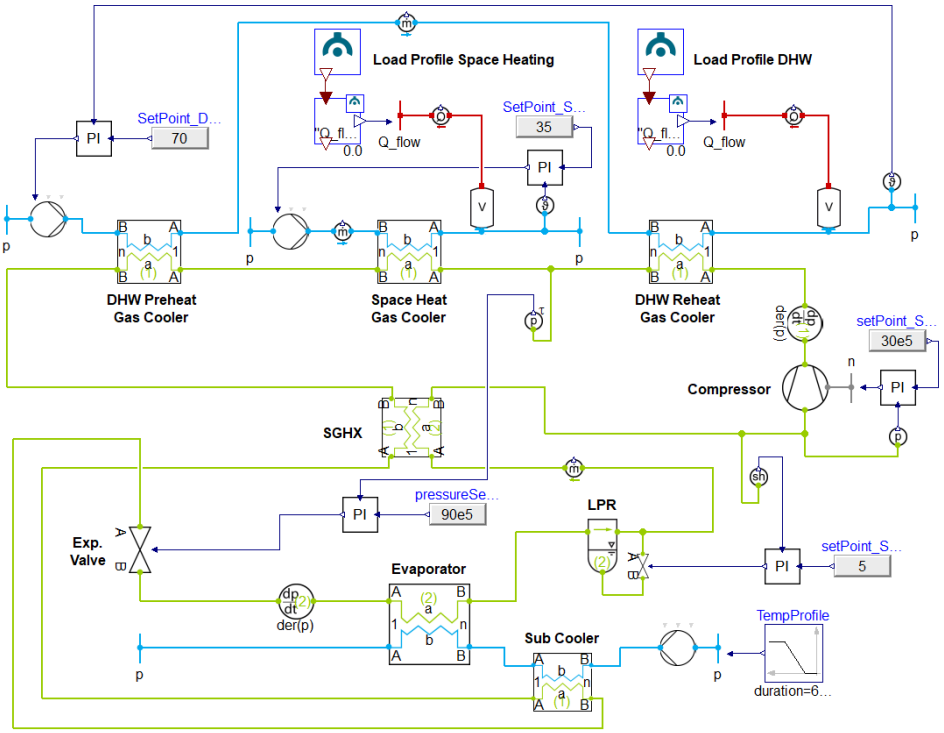

Figure 2: The dynamic Dymola model with component labelling

2.3 Load Profiles

In order to have realistic load/demand profiles to implement, a model of the residential building was developed in the simulation software IDA ICE. The model has a 70mm massive wood structure, with 200 mm isolation and a total heated area of 288 m^2 over three floors. Climate data for the Trondheim region is used. The setpoint room temperature is 21 ^oC and an occupancy of 9 people. In order to simulate the heat demand for the given building, the mode "ideal heater" has been used. This gives the necessary heat energy required to maintain the setpoint temperature of 21 ^oC in all zones. A DHW consumption schedule was made, off of experience based numbers.

Figure 3 and *4* shows the DHW- and space heating demand for a given week in late February. These load profiles were implemented to the model to test the combined mode operation.

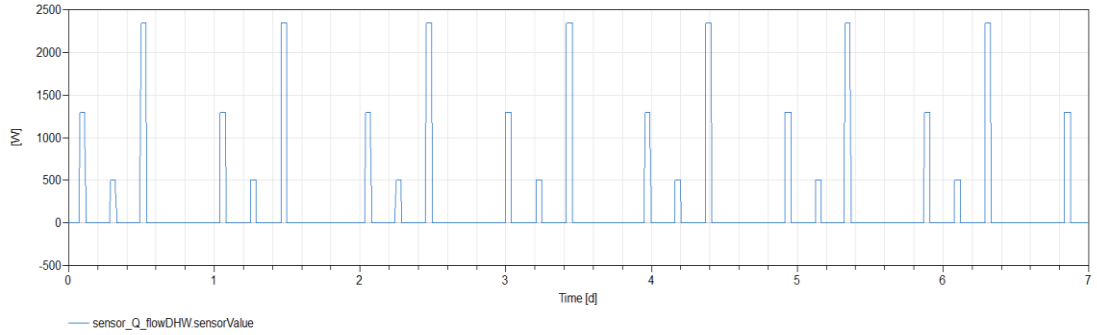

Figure 3: DHW load profile

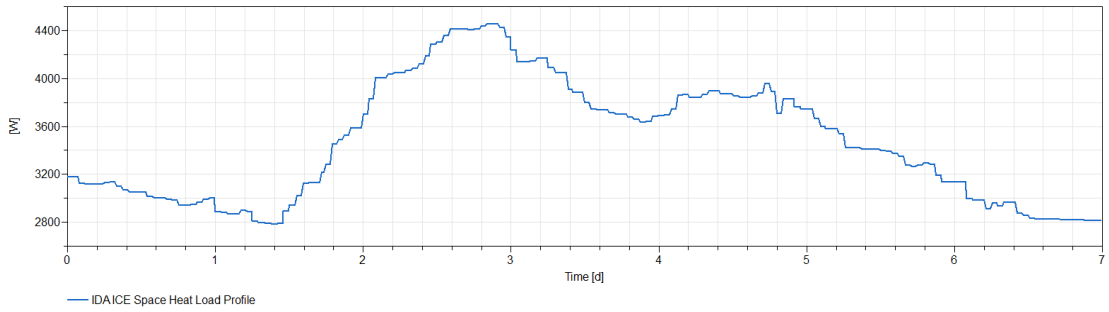

Figure 4: Space heating load profile

3. Results and Discussion

The results will be presented in three sections. First, the comparison of the sensitivity analysis between the model and the real system will be presented. The results from the model then follows, presenting simulated operational scenarios with load profiles. Lastly, the logged data from a week of operation at the residential location will be analysed.

3.1 Sensitivity Analysis Comparison

The sensitivity analysis was utilized as a tool for model validation. The secondary side conditions of the real heat pump at the residential location was recreated in the model. In order observe how the different parameters reacted, the low side pressure in both the model and the

real system was lowered until the compressor reached the maximum capacity of 60 Hz. *Figure 5* and *6* shows the comparison of the compressor speed and the corresponding low-side pressure. The model can be observed reacting quicker to the input but reaches 60 Hz almost simultaneously with the real heat pump, after about 37 minutes. The low-side pressure of the model stabilizes around 0,2 – 0,6 bar lower than the logged data from the heat pump. This could indicate that the modelled compressor is slightly bigger than the real compressor. At the high-side, the pressure was fixed at a setpoint of 92 bar. A high correlation between the model and the logged data was observed for both the high-side pressure and accordingly the discharge CO_2 temperature. Also, the CO_2 mass flow rate corresponded when compared. Overall, the correlation between the model and the real heat pump was very good, which strongly supports the validity of the model.

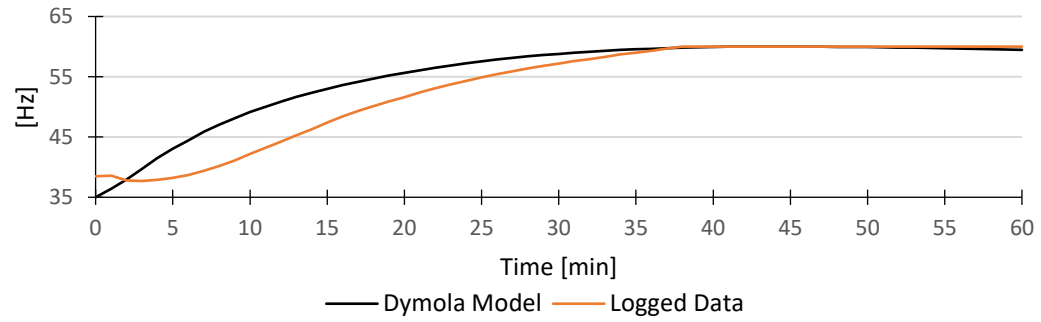

Figure 5: Compressor speed [Hz] compared

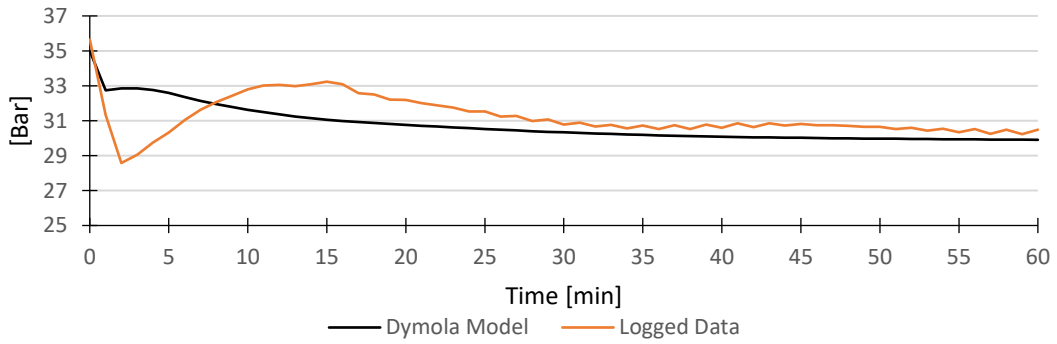

Figure 6: Low-side pressure comparison

3.2 Simulated Operating Modes

The three plausible operating modes of the heat pump has been simulated in Dymola; combined mode, SH mode and DHW mode. During the combined mode simulation, the load profiles presented in *chapter 2.3* was used. The control strategy was to regulate the high side pressure according the setpoint in the buffer tanks. If setpoint in the DHW tank was reached, the high-side pressure was decreased from 92 to 82 bar. The simulation showed that the heat pump was able to cover the DHW demand alone but had the need for peak load assistance to cover the space heating load. The average heat from the space heating gas cooler was around 2 kW, while the total DHW heating from the pre- and reheating gas cooler was about 2,5 kW. The average

COP during the combined mode operation was 3,58, peaking at 3,62. The strategy of having variable high-side pressure control proved to have only a small effect on increasing the COP, as shown in *Figure 7*. The small drops of COP observed in the graph is when the pressure increased from 82 to 92 bar.

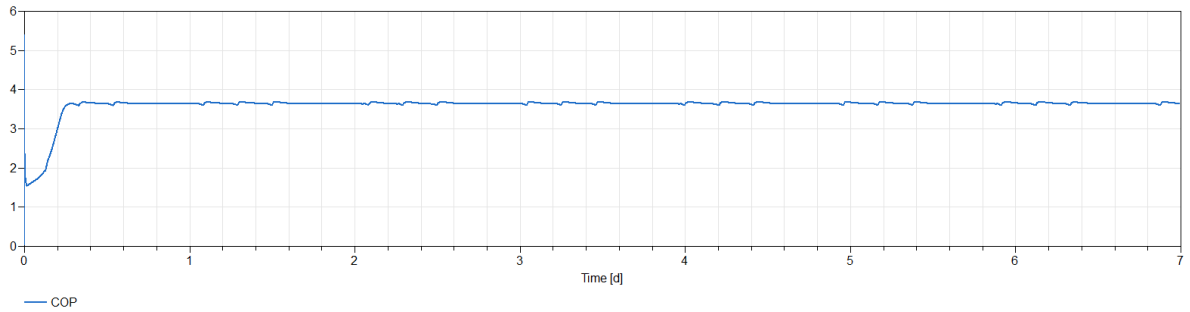

Figure 7: COP during simulated combined mode operation

During the DHW mode simulation, a load profile with higher consumption was used, to test the abilities of the heat pump. The control strategy in this simulation was fixed high side pressure of 92 bar, and variable low-side pressure through compressor speed regulation. The compressor was given a setpoint of 65 °C in the DHW tank, if reached, the speed would decrease. During this simulation, the heat from the pre- and reheating gas cooler at 60 Hz was just above 4,2 kW. The strategy of controlling the low-side pressure through compressor speed seemed to have a higher impact on increasing the COP. *Figure 8* shows the COP in relation to the compressor speed. The maximum COP observed during the DHW mode was 3,49, while the average COP at 60 Hz was 3,17.

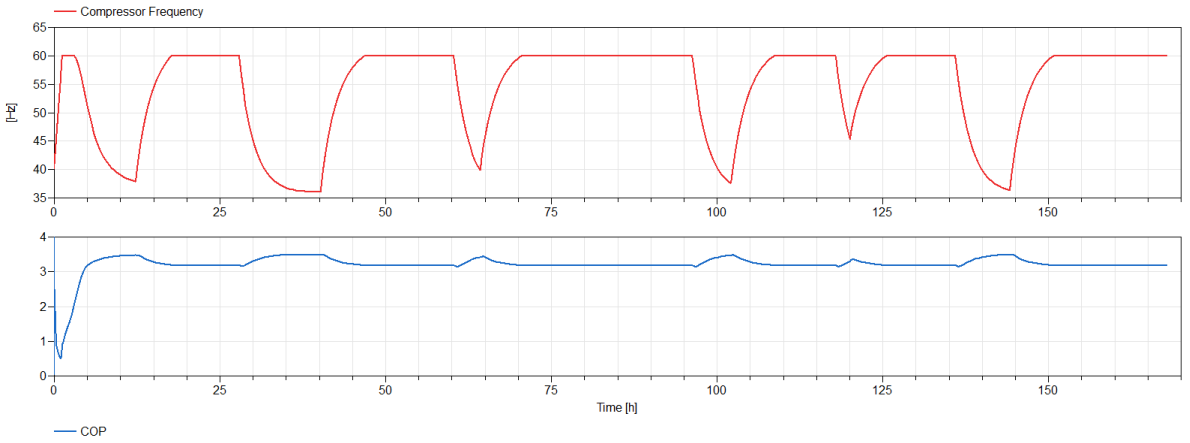

Figure 8: COP compared to compressor speed

For the last operating mode, SH mode, a load profile from a week in early October. This load profile is moderate compared to the one utilized in the first simulation. The control strategy in this simulation was fixed high side pressure, and variable low-side pressure through compressor speed regulation as well. The high-side pressure setpoint was 80 bar, while the compressor speed setpoint was 32 °C in the SHW tank. With this load profile, the heat pump was able to

cover the demand the entire week, with an average capacity of 3,4 kW. The COP for the SH mode was the lowest of the three operating modes, peaking at 3,25. On average the COP was at 2,84. *Figure 9* shows the COP in relation to the compressor speed.

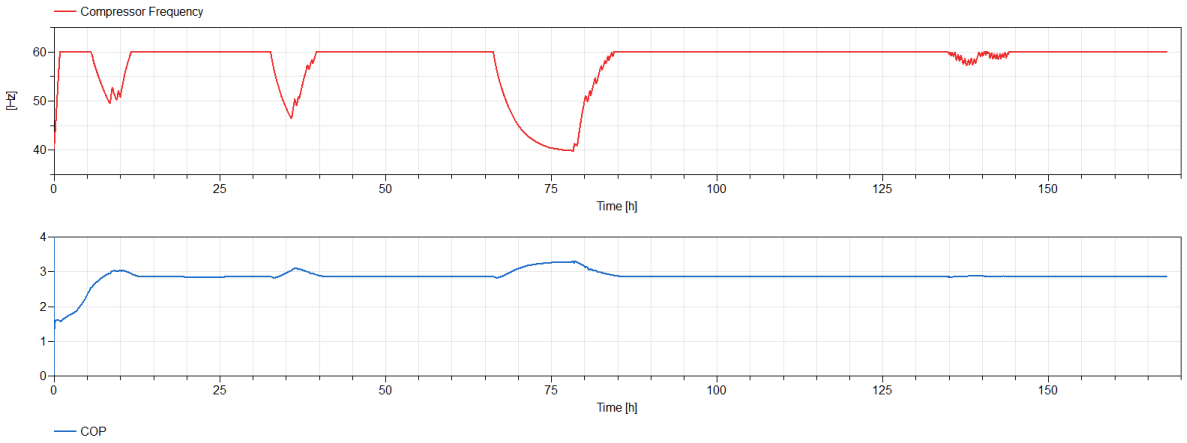

Figure 9: COP and compressor speed [Hz]

3.3 Operational Data

In this section, the logging results from the heat pump at the residential location will be presented. The logging was done during an unusually cold week in the month of May. The cold weather caused a constant space heating demand. During the week, the compressor was shut off eleven times due to an unidentified error. It was still possible to get operational data to analyse. The high side pressure was fixed at 82 bar for both SH- and combined mode, with variable low-side pressure regulation. *Figure 10* shows the heat delivered from the space heating GC and the pre- and reheating GC. During SH mode, the heat pump is delivering 4,3 kW on average. During combined mode, the peak delivery is about 4,8 kW, averaging 4,5 kW. The average COP during SH- and combined mode was calculated to be 3,07 and 3,18 respectively. The low COP value for the combined mode, compared what was found in the model, can be tied to the high DHW inlet temperature, averaging at 19 ºC in the real system.

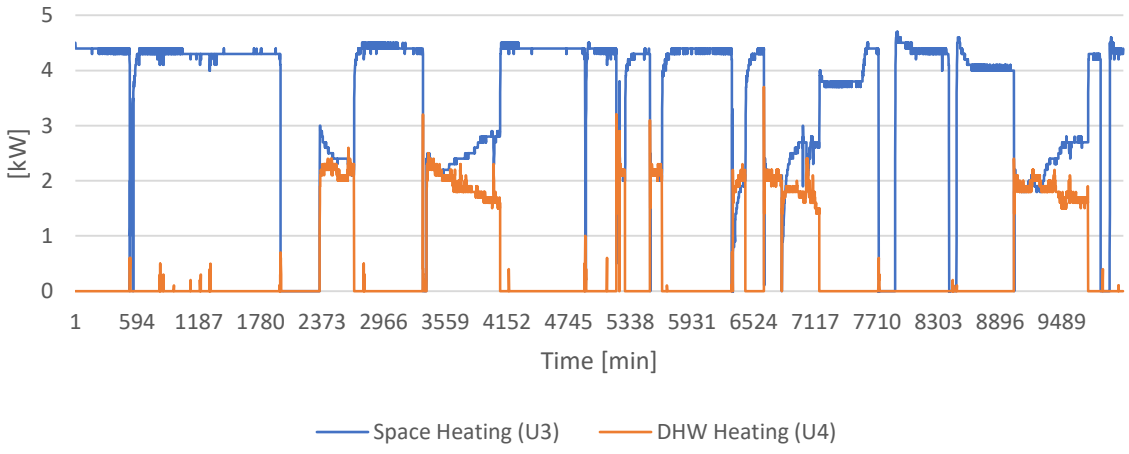

Figure 10: Logged values for energy meters U3 and U4

4. Conclusion

The performance of a prototype residential CO_2 heat pump has been investigated through testing and dynamic computer modelling. To validate the model, a sensitivity analysis comparison between the real heat pump and the model was done. The comparison showed a good correlation, and its therefore reasonable to conclude that the model is valid representation of the real system. The results from both the model and the logged data from the real system showed that the maximum capacity of the heat pump realistically is in the range of 4,5 – 5 kW. Of the three plausible operating modes; combined, space heating (SH) and DHW heating, the combined mode achieved the highest COP, at 3,62. The least favourable for COP was the SH mode, with a maximum COP of 3,25. DHW heating mode achieved a maximum COP of 3,49. The combined mode COP calculated for the real system was on average lower then what was found in the model. This is likely due to the difference in DHW inlet temperature. The average inlet temperature in the real system was 19 ^{o}C, while in the model it was 7 ^{o}C. These findings emphasize the importance of having sufficient cooldown of the CO_2 refrigerant in order to get the highest possible COP.

References

[1] “Lov om klimamål (klimaloven). 2017.” [Online]. Available: https://lovdata.no/dokument/NL/lov/2017-06-16-60.

[2] “Bygningsenergi.” [Online]. Available: https://www.standard.no/fagomrader/bygg-anlegg-og-eiendom/bygningsenergi/.

[3] J. Stene, “Residential CO2 Heat Pump System for Combined Space Heating and Hot Water Heating,” NTNU, 2004.

Johan Christian Rømcke

Master's Thesis

NTNU
Norwegian University of
Science and Technology